From Soil Aggregate to Watershed, from California's Central Valley to the Salton Sea – Agricultural Selenium Contamination across Ecosystems, Scales, and Disciplines

by

Matteo Francesco Kausch

A dissertation submitted in partial satisfaction of the

requirements for the degree of

Doctor of Philosophy

in

Environmental Science, Policy, and Management

in the

Graduate Division

of the

University of California, Berkeley

Committee in charge:

Professor Céline Pallud, Chair

Professor Ronald Amundson

Professor Yoram Rubin

Spring 2013

Abstract

From Soil Aggregate to Watershed, from California's Central Valley to the Salton Sea – Agricultural Selenium Contamination across Ecosystems, Scales, and Disciplines

by

Matteo Francesco Kausch

Doctor of Philosophy

in

Environmental Science, Policy, and Management

University of California, Berkeley

Professor Céline Pallud, Chair

Selenium (Se) is a trace element of great ecological importance whose environmental distribution is highly impacted by anthropogenic activity. In the 1980s, selenium was recognized as a major aquatic contaminant following widespread deformities and mortality among waterfowl hatchlings near the agricultural drainage evaporation ponds of the Kesterson Reservoir (CA, USA). Today, 400,000 km^2 in the Western United States are threatened by agricultural selenium contamination, as are parts of Canada, Egypt, Israel, and Mexico. From the soil aggregate to the watershed, from the soils of the Central Valley to the sediments of the Salton Sea, and from Environmental Science to Policy and Management, in this dissertation I explore agricultural selenium contamination across scales, ecosystems, and disciplines. I begin with a review of the science, policy, and management of irrigation-induced selenium contamination in California, the heart of worldwide research on the issue. I then delve into the physical and biogeochemical mechanisms that control selenium reduction and mobility within the structured surface soils that are the source of contamination, using an aggregate-scale combined experimental and reactive transport modeling approach. Finally, I present a diagenetic model for selenium incorporation into the sediment of the Salton Sea, which has been receiving seleniferous agricultural drainage over the last 100 years.

To extract lessons from the last 30 years of seleniferous drainage management and water quality regulation in California, I reviewed the history and current developments in science, policy, and management of irrigation-induced selenium contamination in California. Specifically, I evaluated improvements in the design of local attenuation methods and the development of programs for selenium load reductions at the

regional scale. On the policy side, I assessed the site-specific water quality criteria under development for the San Francisco Bay-Delta in the context of previous regulation. This approach may be a landmark for future legislation on selenium in natural water bodies and I discussed challenges and opportunities in expanding it to other locations such as the Salton Sea. By combining proven management tools with the novel, site-specific policy approach, it may be possible to avoid future events of irrigation-induced selenium contamination. However, the majority of regional selenium load reductions in California were achieved by decreasing drainage volume rather than selenium concentrations. Thus, there appear to be opportunities for additional improvements through management practices that enhance selenium retention in source soils.

Soil aggregates are the basic structural units of soil. They are mm- to cm-sized microporous assemblages of loosely bound soil particles, separated from one another by macropores. To elucidate how aggregate-scale transport and microbial reduction affect selenium retention in surface soils, I conducted a series of flow-through experiments utilizing artificial aggregate systems. These systems mimic the dual porosity of structured soils with an artificial soil aggregate (ID 2.5 cm) contained in a flow-through reactor cell. Aggregates were composed of either pure quartz sand or ferrihydrite-coated quartz sand inoculated with selenium reducing bacteria (*Thauera selenatis* or *Enterobacter cloacae* SLD1a-1). Oxic and anoxic conditions were compared, as well as various selenate (0.25-0.8 mM) and carbon source (0.3 and 1.2 mM) input concentrations. The presence of oxygen in the input solution significantly decreased selenium reduction, however, the detection of selenite in effluent samples indicates the occurrence of anoxic microzones within aggregates. Furthermore, I found that solid phase concentrations of reduced selenium increased towards the core of aggregates across all experimental conditions. A bulk model, ignoring intra-aggregate heterogeneity in reactions and transport, misrepresented the dynamics of the aggregate systems.

To quantify the likely implications of these experimental results for soils with different degrees of aggregation, I formulated a general mechanistic framework for aggregate scale heterogeneity in selenium reduction. Specifically, I constructed a dynamic 2D model of selenium fate in single idealized aggregates, in which reactions were implemented with double-Monod rate equations coupled to the transport of pyruvate, O_2, and Se-species (selenate, selenite, and elemental selenium). The spatial and temporal dynamics of the model were validated with the experimental data and predictive simulations were performed covering aggregate sizes between 1 and 2.5 cm diameters. Simulations predict that selenium retention scales with aggregate size. Depending on aeration conditions and the input concentrations of selenate and pyruvate, selenium retention was predicted to be 4-23 times higher in 2.5-cm-aggregates compared to 1-cm-aggregates. Under oxic conditions, aggregate size and pyruvate-concentrations were found to have a positive synergistic effect on selenium retention. Promoting soil aggregation on seleniferous agricultural soils may thus help decrease the impacts of selenium contaminated drainage on downstream aquatic ecosystems receiving it.

One such ecosystem is California's largest inland water body, the Salton Sea, which is maintained entirely by agricultural runoff. Whereas elevated selenium

concentrations are detected in the rivers feeding the lake, the lake's concentrations of dissolved selenium are low since most selenium entering the lake is sequestered in its sediment through microbial reduction. To predict the distribution profiles of selenium within the sediment and evaluate the factors driving them, I constructed a diagenetic model for reductive incorporation of selenate into Salton Sea sediment. The model predicts near surface (2 cm) sediment concentrations of solid phase selenium between 0.024 and 0.272 μmol/g depending on local reduction kinetics, and dissolved concentrations in the water column. This is in good agreement with the literature when considered in conjunction with the potential impact of bioturbation which according to exploratory simulations may lower near surface concentrations by around 25%. The range of modeled selenium concentrations in surface sediment crosses threshold values for which negative impacts on fish and waterfowl have been predicted or observed at other sites, suggesting that ecological impacts of selenium in the Salton Sea may depend locally on variation in the diagenetic factors here explored.

This work presents agricultural selenium contamination as a complex problem that crosses ecosystems, scales, and disciplines. From a management perspective, the tension between dispersed non-point sources and hotspots where elevated selenium concentrations and sensitive aquatic ecosystems converge is difficult to address. Differences in biogeochemical conditions and trophic transfer within food webs render traditional regulatory approaches ineffective and force regulators to engage with the science of site-specific selenium transfer between ecological compartments. At the same time, gaps still exist in our mechanistic understanding of selenium's environmental cycling and in our integration of scientific knowledge across different ecosystems and scales. Centimeter scale heterogeneity in the biogeochemical conditions within source soils may fundamentally control selenium emissions across large agricultural areas and thus determine the selenium loading of rivers, lakes, and estuaries. Within aquatic environments receiving seleniferous drainage, the first few centimeters of surface sediment may control selenium exposure for entire food webs. Improved understanding at this level holds the potential to simultaneously reduce selenium emissions and respond more effectively to pollution where it occurs. In order to preserve sensitive habitat while also meeting agricultural drainage needs in seleniferous regions we must bridge the gaps between ecosystems, scales, and disciplines.

Dedication

Alla mia Mamma, che mi ha dato le ali per volare.
Meinem Vater, der mir das Fragen beibrachte.
To Lexi, who gave me joy and motivation.

“La science dit le premier mot sur tout, le dernier mot sur rien.”
“Science says the first word on everything and the last word on nothing.”

- Victor Hugo

Curriculum Vitae

Name: Matteo Francesco Kausch

Degree and date to be conferred: Ph.D., 2013

Secondary education: Wald-Oberschule Gymnasuim, Berlin, Germany, 1998-2004

Collegiate institutions attended:

Jacobs University Bremen, Germany, B.Sc., 2004-2007

Major: Geosciences and Astrophysics

University of California, Berkeley, USA, Ph.D., 2007-2013

Major: Environmental Science, Policy, and Management

Professional Publications:

Kausch, M. and Pallud, C., 2013. Modeling the impact of soil aggregate size on selenium immobilization. *Biogeosciences* 10, *1323-1336, doi:10.5194/bg-10-1323-2013.*

VillaRomero, J.-F., Kausch, M. and Pallud, C., 2013. Selenate reduction and adsorption in littoral sediments from a hypersaline California lake, the Salton Sea. *Hydrobiologia, doi: 10.1007/s10750-013-1443-7*.

Kausch, M., Ng, P., Ha, J. and Pallud C., 2012. Soil-aggregate-scale heterogeneity in microbial selenium reduction. *Vadose Zone Journal* 11 (2), doi:10.2136/vzj2011.0101.

Kausch, M. and Pallud, C., 2011. Impact of ferrihydrite coating and aeration conditions on microbial selenium (Se) reduction and retention in artificial soil aggregates. *Mineralogical Magazine* 75, 1157.

Pallud, C., Kausch, M., Fendorf, S. and Meile, C., 2010. Patterns and spatial modeling of reductive ferrihydrite transformation observed in artificial soil aggregates. *Environmental Science & Technology* 44, 74-79.

Kausch, M., Ha, J. and Pallud, C., 2010. Heterogeneous selenium reduction in artificial soil aggregates. *Geochim. Cosmochim. Acta.* 74 (Suppl. 1): Abstract 499.

Kausch, M., Meile, C. and Pallud, C., 2008. Spatial modeling of iron transformations within artificial soil aggregates. *Eos, Transactions, AGU* 89, Fall Meeting Supplement, B11B-0357.

Professional positions held:

Cradle to Cradle Products Innovation Institute, San Francisco, USA, Research and Development Fellow, 2013 – present.

The Spark, San Francisco, USA, Co-founder and Vice President, 2011 – present.

University of California, Berkeley, USA, Graduate Student Researcher, 2007 – 2013.

University of California, Berkeley, USA, Graduate Student Instructor, 2008 – 2012.

Jacobs University Bremen, Germany, Research and Teaching Assistant, 2005 – 2007.

Table of Contents

Introduction

Since the industrial revolution, humanity has fundamentally changed the cycling of major and trace elements on Earth with drastic and often detrimental effects on the global biosphere. Fossil fuel combustion, land-use change, and industrial nitrogen fixation have increased atmospheric CO_2 concentrations by about 30% and more than doubled the nitrogen added yearly to terrestrial systems compared to pre-industrial times (Vitousek et al. 1997). These major disruptions of the carbon and nitrogen cycles have led to global climate change and widespread eutrophication of aquatic ecosystems. The human impacts on the cycling of trace elements are less widely known, but no less severe (Rauch and Pacyna, 2009). Anthropogenic mobilization of silver, chromium, nickel, lead, and zinc from the lithosphere is similar in magnitude to their natural mobilization, and for copper it is an order of magnitude greater. These large anthropogenic trace element fluxes from the lithosphere have led to contamination of air, water, soil, sediment, and increased human body burdens (Bindler, 2011; Nriagu and Pacyna, 1988; Singh et al., 2011). Selenium is among the trace elements most highly impacted by human activities (Haygarth, 1994). It is mobilized from the pedo- and lithosphere through irrigated agriculture, the mining and smelting of metal ores, as well as the refining and use of fossil fuels. In conjunction with bioaccumulation that can rapidly lead to hazardous selenium levels for fish and waterfowl, anthropogenic selenium releases to streams and water bodies have already led to numerous contamination events around the world (Lemly, 2004). Additionally, the threat of aquatic selenium contamination is expected to keep increasing in the foreseeable future, as increased demand for energy and resources drive increases in the human activities responsible for selenium release (Chapman et al., 2010; Lenz and Lens, 2009).

Selenium is heterogeneously distributed across terrestrial and marine environments (Haygarth, 1994). On land, seleniferous soils (>0.5 μg/g) and those marked by selenium deficiency (<0.1 μg/g) sometimes occur as close as 20 km from one another (Lenz and Lens, 2009). The heterogeneous terrestrial distribution of selenium gives rise not only to problems of ecological toxicity, but also deficiency. Animals and microorganisms require selenium for the synthesis of the essential seleno-amino acids selenocysteine and selenomethionine (Heider et al., 1993; Prakash et al., 2010; Stolz et al., 2006). In humans, selenium is needed as an antioxidant, for the production of active thyroid hormone, and for the proper functioning of the immune system (Rayman, 2000). However, the intake range between deficiency and toxicity is exceedingly small – the World Health Organization defines the safe dietary range as 40-400 µg/day (WHO, 1996). Therefore, selenium is of international concern with regards to food, water, and environmental concentrations (Gore et al., 2010; Lenz and Lens, 2009; Levander and Burk, 2006). Selenium bioaccumulates, with tissue concentrations in animals and plants typically 1-3 orders of magnitude above those found in water (US.EPA, 2004). Consequently, the predominant uptake pathway for humans and wildlife is through the consumption of food rather than water. Excess or insufficient human dietary selenium levels are usually connected with the consumption of crops grown on seleniferous or

selenium deficient soils (Fairweather-Tait et al., 2011). For example Keshan disease, caused by a deficiency in selenium, is endemic to certain regions of China and occurs predominantly in areas where selenium concentrations in soils are below 0.125 μg/g (Fairweather-Tait et al., 2011), whereas a major outbreak of selenium intoxication occurred in Enshi, China where soil selenium concentrations averaged 8 μg/g (Yang et al., 1983). While the impacts of selenium intake on human health remain an active area of research (Fairweather-Tait et al., 2011), cases of toxicity are exceedingly rare among humans (Lenz and Lens, 2009). The human health criterion for selenium was removed from US Clean Water Act standards in 1992, because the current federal aquatic wildlife criterion for selenium (5 μg/L) is more restrictive (US.EPA, 1992). International drinking water standards, where they exist, tend to be around 40-50 μg/L (Fawell and Combs, 2011; US.EPA, 2010a).

Selenium received global recognition as an aquatic contaminant following the unprecedented events in the 1980s at the Kesterson Reservoir in California (Marshall, 1985). Large amounts of this trace element had been mobilized through irrigation of selenium-rich soils in the western San Joaquin Valley, transported along with agricultural runoff, and accumulated at the Reservoir. This resulted in death and deformities for 64% of the wild aquatic bird hatchlings at the site and within a few years, the former wildlife refuge was classified as a toxic waste site (Presser, 1994). These events led to a shift in the global perception of selenium. While research had thus far been focused on farm-scale problems related to crop accumulation and toxicity to livestock, it became clear that excessive selenium concentrations in agricultural runoff were a watershed-scale resource protection issue that would greatly complicate irrigation management in affected regions (Engberg et al., 1998; Ohlendorf et al., 1985). The problem is not endemic to California– other nations where irrigation-induced selenium contamination has been observed include Canada, Egypt, Israel, and Mexico (Lemly, 2004). However, in the Western United States alone, nearly 400,000 km^2 of land are susceptible to irrigation-induced contamination (Presser et al., 1994; Seiler et al., 1999). Among the affected regions, California has been the hotspot for global research and management of agricultural selenium contamination (Abrams et al., 1990; Banuelos et al., 2005; Fio and Fujii, 1990; Gao and Tanji, 1996; Karlson and Frankenberger, 1989; Ohlendorf et al., 1987; Renner, 2003; Wahl et al., 1994). As selenium load management in the San Joaquin Valley has made significant progress, new major sites of concern, such as the San Francisco Bay-Delta (Presser and Luoma, 2006) and the Salton Sea (Kaiser, 1999; Moreau et al., 2007a) have emerged.

The mobility, toxicity and consequently environmental impacts of selenium depend on the element's chemical speciation driven by microbial activity and redox conditions (Dungan and Frankenberger, 1999; Hamilton, 2004; Stolz and Oremland, 1999; Stolz et al., 2006). To understand the mobility of selenium in surface soils, which are the source of agricultural selenium contamination, it is necessary to study the element's physical transport and microbially catalyzed reactions within the context of the soil's spatial structure. Soil aggregates are mm to cm sized structural units of bound soil particles (Brady and Weil, 2002) and represent the smallest systems in which the coupling of these biogeochemical processes can be studied on a well-defined scale

(Tokunaga et al., 2003). Improved mechanistic understanding of reactive selenium transport within soil aggregates may lead to the development of management techniques that will reduce selenium emissions from agricultural soils and provide reprieve for aquatic environments downstream.

The Salton Sea, California's largest inland water body, has been receiving seleniferous agricultural runoff for more than a century (Cohen and Hyun, 2006; Krants et al., 2002; Schroeder et al., 2002). Of the 66 water bodies listed on California's 303(d) list of impaired waters for concerns regarding selenium pollution, the hypersaline Salton Sea is by far the largest (US.EPA, 2010b) and arguably the one of greatest ecological significance. It has been labeled one of the most important bird habitats in the American Southwest, because it is used by more than 100,000 waterfowl pertaining to resident and migratory bird species, including endangered ones like the brown pelican (*Pelecanus occidentalis* Linnaeus) (Moreau et al., 2007a). It is home to millions of tilapia (*Oreochromis mossambicus* x *O. urolepis*) and until recently, also bairdiella (*Bairdiella icistia*) and orangemouth corvina (*Cynoscion xanthulus*) (Caskey et al., 2007; Hurlbert et al., 2007; Hurlbert, 2008). Since the Salton Sea's accidental creation in 1906, more than 90% of California's natural wetland habitat has been converted to agricultural or urban uses making the artificial lake an essential stopover for migratory waterfowl on the Pacific Flyway (Krants et al., 2002). However, periodic die-offs among Salton Sea birds are common and have been increasing in both frequency and severity over the last century (Moreau et al., 2007a). While microbial pathogens are assumed to be the main cause of observed mortality events, the cause of death of more than 150,000 eared grebes (*Podiceps nigricollis* Brehm) that perished in 1992 could not be established. The immune systems of water birds at the Salton Sea may be impaired by dietary exposure to a mix of aquatic contaminants including selenium. In fact, selenium concentrations in Salton Sea fish are elevated enough to be a reproductive and immune health threat to piscivorous birds consuming them (Moreau et al., 2007a; Moreau et al., 2007b).

In this dissertation I explore agricultural selenium contamination across a number of spatial and temporal scales and from various disciplinary perspectives. I begin with a review of the science, policy, and management of irrigation-induced selenium contamination in California. Using artificial aggregate experiments and a reactive transport model, I then delve deep into the physical and biogeochemical mechanisms that control selenium mobility at the soil aggregate scale within source soils. Finally, I present a diagenetic model for selenium incorporation into the sediment of the Salton Sea, which has been receiving seleniferous agricultural drainage over the last 100 years.

References

Abrams, M.M., R.G. Burau, and R.J. Zasoski. 1990. Organic selenium distribution in selected California soils. Soil Science Society of America Journal 54:979-982.

Banuelos, G.S., Z.Q. Lin, I. Arroyo, and N. Terry. 2005. Selenium volatilization in vegetated agricultural drainage sediment from the San Luis Drain, Central California. Chemosphere 60:1203-1213.

Bindler, R. 2011. Contaminated lead environments of man: reviewing the lead isotopic evidence in sediments, peat, and soils for the temporal and spatial patterns of atmospheric lead pollution in Sweden. Environmental Geochemistry and Health 33:311-329.

Brady, N.C., and R.R. Weil. 2002. The Nature and Properties of Soils. 13th ed. Prentice Hall, Upper Saddle River, NJ.

Caskey, L.L., R.R. Riedel, B. Costa-Pierce, J. Butler, and S.H. Hurlbert. 2007. Population dynamics, distribution, and growth rate of tilapia (Oreochromis mossambicus) in the Salton Sea, California, with notes on bairdiella (Bairdiella icistia) and orangemouth corvina (Cynoscion xanthulus). Hydrobiologia 576:185-203.

Chapman, P.M., W.J. Adams, M.L. Brooks, C.G. Delos, S.N. Luoma, W.A. Maher, H.M. Ohlendorf, T.S. Presser, and D.P. Shaw. 2010. Ecological Assessment of Selenium in the Aquatic Environment CRC Press, Boca Raton.

Cohen, M., and K. Hyun. 2006. Hazard – The future of the Salton Sea with no restoration project. Pacific Institute, Oakland, California.

Dungan, R.S., and W.T. Frankenberger, Jr. 1999. Microbial transformations of selenium and the bioremediation of seleniferous environments. Bioremediation Journal 3:171–188.

Engberg, R.A., D.W. Westcot, M. Delamore, and D.D. Holz. 1998. Federal and state perspectives on regulation and remediation of irrigation-induced selenium problems, p. 1-25, *In* W. T. Frankenberger and R. A. Engberg, eds. Environmental chemistry of selenium. Marcel Dekker, New York.

Fairweather-Tait, S.J., Y.P. Bao, M.R. Broadley, R. Collings, D. Ford, J.E. Hesketh, and R. Hurst. 2011. Selenium in human health and disease. Antioxidants & Redox Signaling 14:1337-1383.

Fawell, J.K., and G.F. Combs. 2011. Selenium in Drinking-water, pp. 14, Vol. 10.01. WHO Press, Geneva.

Fio, J.L., and R. Fujii. 1990. Selenium speciation methods and applications to soil saturation extracts from San Joaquin Valley, California. Soil Science Society of America Journal 54:363-369.

Gao, S., and D.W. Tanji. 1996. Water selenium speciation and sediment fractionation in a California flow-through wetland system. Journal of Environmental Quality 29:1275-1283.

Gore, F., J. Fawell, and J. Bartra. 2010. Too much or too little? A review of the conundrum of selenium. Journal of Water Health 8:405-416.

Hamilton, S.J. 2004. Review of selenium toxicity in the aquatic food chain. Science of the Total Environment 326:1-31.

Haygarth, P.M. 1994. Global importance and global cycling of selenium, p. 1-28, *In* W. T. Frankenberger, Jr. and S. Benson, eds. Selenium in the Environment, 1st ed. Marcel Dekker, Inc, New York.

Heider, J., A. Bock, and A.H. Rose. 1993. Selenium Metabolism in Micro-organisms, p. 71-109 Advances in Microbial Physiology, Vol. Volume 35. Academic Press.
Hurlbert, A.H., T.W. Anderson, K.K. Sturm, and S.H. Hurlbert. 2007. Fish and fish-eating birds at the Salton Sea: a century of boom and bust. Lake and Reservoir Management 23:469-499.
Hurlbert, S.H. 2008. The Salton Sea Centennial Symposium - Proceedings of symposium celebrating a century of symbiosis among agriculture, wildlife and people, 1905-2005 - San Diego, USA, March 2005 - Preface. Hydrobiologia 604:1-3.
Kaiser, J. 1999. Battle Over a Dying Sea. Science 284:28-30.
Karlson, U., and W.T. Frankenberger. 1989. Accelerated rates of selenium volatilization from California soils. Soil Science Society of America Journal 53:749-753.
Krants, T., S. Hoover, M. Diederich, M. Brenneman, K. Althiser, P. Egle, D. Guthrie, S. Huynen, E. Kena, D. Kreske, M. Karman, J. Lensch, L. Lewis, and M. Sorensen. 2002. Salton Sea Atlas Redlands Institute / ESRI Press, Redlands, California.
Lemly, A.D. 2004. Aquatic selenium pollution is a global environmental safety issue. Ecotoxicology and Environmental Safety 59:44-56.
Lenz, M., and P.N.L. Lens. 2009. The essential toxin: The changing perception of selenium in environmental sciences. Science of The Total Environment 407:3620-3633.
Levander, O., and R. Burk. 2006. Update of human dietary standards for selenium, p. 399-410, *In* D. L. Hatfield, et al., eds. Selenium: Its Molecular Biology and Role in Human Health. Springer US, New York.
Marshall, E. 1985. Selenium poisons refuge, California politics. Science 229:144-146.
Moreau, M.F., J. Surico-Bennett, M. Vicario-Fisher, R. Gerads, R.M. Gersberg, and S.H. Hurlbert. 2007a. Selenium, arsenic, DDT and other contaminants in four fish species in the Salton Sea, California, their temporal trends, and their potential impact on human consumers and wildlife. Lake and Reservoir Management 23:536-569.
Moreau, M.F., J. Surico-Bennett, M. Vicario-Fisher, D. Crane, R. Gerads, R.M. Gersberg, and S.H. Hurlbert. 2007b. Contaminants in tilapia (Oreochromis mossambicus) from the Salton Sea, California, in relation to human health, piscivorous birds and fish meal production. Hydrobiologia 576:127-165.
Nriagu, J.O., and J.M. Pacyna. 1988. Quantitative assessment of worldwide contamination of air, water and soils by trace-metals. Nature 333:134-139.
Ohlendorf, H.M., D.J. Hoffman, M.K. Saiki, and T.W. Aldrich. 1985. Embryonic mortality and abnormalities of aquatic birds: Apparent impacts of selenium from irrigation drainwater. Science of the Total Environment 52:49–63.
Ohlendorf, H.M., R.L. Hothem, T.W. Aldrich, and A.J. Krynitsky. 1987. Selenium contamination of the grasslands, a major California waterfowl area. Science of the Total Environment 66:169–183.
Prakash, D., J. Pandey, B.N. Tiwary, and R.K. Jain. 2010. Physiological adaptations and tolerance towards higher concentration of selenite (Se+4) in Enterobacter sp AR-4, Bacillus sp AR-6 and Delftia tsuruhatensis AR-7. Extremophiles 14:261-272.
Presser, T.S. 1994. "The Kesterson effect". Environmental Management 18:437-454.

Presser, T.S., and S.N. Luoma. 2006. Forecasting Selenium Discharges to the San Francisco Bay-Delta Estuary: Ecological Effects of a Proposed San Luis Drain Extension Professional Paper 1646, Vol. 1646. U.S. Geological Survey, Reston, Virginia.
Presser, T.S., M.A. Sylwester, and W.H. Low. 1994. Bioaccumulation of selenium from natural geologic sources in western states and its potential consequences. Environmental Management 18:423-436.
Rauch, J.N., and J.M. Pacyna. 2009. Earth's global Ag, Al, Cr, Cu, Fe, Ni, Pb, and Zn cycles. Global Biogeochemical Cycles 23:16.
Rayman, M.P. 2000. The importance of selenium to human health. The Lancet 356:233–241.
Renner, R. 2003. California to develop selenium standard for wildlife. Environmental Science & Technology 37:274A–275A.
Schroeder, R.A., W.H. Orem, and Y.K. Kharaka. 2002. Chemical evolution of the Salton Sea, California: nutrient and selenium dynamics. Hydrobiologia 473:23-45.
Seiler, R.L., J.P. Skorupa, and L.A. Peltz. 1999. Areas susceptible to irrigation-induced selenium contamination of water and biota in the western United States U.S. Department of the Interior.
Singh, B.R., S.K. Gupta, H. Azaizeh, S. Shilev, D. Sudre, W.Y. Song, E. Martinoia, and M. Mench. 2011. Safety of food crops on land contaminated with trace elements. Journal of the Science of Food and Agriculture 91:1349-1366.
Stolz, J.F., and R.S. Oremland. 1999. Bacterial respiration of arsenic and selenium. FEMS Microbiology Reviews 23:615-627.
Stolz, J.F., P. Basu, J.M. Santini, and R.S. Oremland. 2006. Arsenic and selenium in microbial metabolism. Annual Review of Microbiology 60:107-130.
Tokunaga, T.K., J. Wan, T.C. Hazen, E. Schwartz, M.K. Firestone, S.R. Sutton, M. Newville, K.R. Olson, A. Lanzirotti, and W. Rao. 2003. Distribution of chromium contamination and microbial activity in soil aggregates. Journal of Environmental Quality 32:541-549.
US.EPA. 1992. Water Quality Standards; Establishment of Numeric Criteria for Priority Toxic Pollutants; States' Compliances. Federal Register 57:60848 (57 FR 60848).
US.EPA. 2004. Draft Aquatic Life Water Quality Criterion for Selenium, Vol. EPA-822-D-04-00. US Environmental Protection Agency, Washington, DC.
US.EPA. 2010a. National Primary Drinking Water Regulations; Announcement of the Results of EPA's Review of Existing Drinking Water Standards and Request for Public Comment and/or Information on Related Issues. Federal Register 75:15500 (75 FR 15500).
US.EPA. 2010b. California's 2008-2010 Section 303(d) list of impaired waters. California State Water Resources Control Board, Sacramento.
Wahl, C., S. Benson, and G. Santolo. 1994. Temporal and spatial monitoring of soil selenium at Kesterson Reservoir, California. Water Air and Soil Pollution 74:345-361.
WHO. 1996. Chapter 6 - Selenium World Health Organization, Geneva.

Yang, G., S. Wang, R. Zhou, and S. Sun. 1983. Endemic selenium intoxication of humans in China. American Journal of Clinical Nutrition 37:872-881.

Chapter 1 – Science, policy, and management of irrigation-induced selenium contamination in California

Abstract – Selenium was recognized as an important aquatic contaminant following the identification of widespread deformities in waterfowl at the agricultural drainage evaporation ponds of the Kesterson Reservoir (CA, USA) in 1983. Since then, California has been the focal point for global research and management of selenium contamination. I analyzed the history and current developments in science, policy, and management of irrigation-induced selenium contamination in California. In terms of management, I evaluated the effects of improvements in the design of local attenuation methods (drainage reuse and evaporation ponds) in conjunction with the development of programs for selenium load reductions at the regional scale (namely the Grassland Bypass Project). In terms of policy, the Environmental Protection Agency is currently working on site-specific water quality criteria for the San Francisco Bay-Delta that may be a landmark for future legislation on selenium in natural water bodies. I provide a critical analysis of this approach and discuss challenges and opportunities in expanding it to other locations such as the Salton Sea. Management lessons learned in California and the novel policy approach may help prevent future events of selenium contamination.

1. Introduction

Selenium received recognition as an environmental contaminant in the 1980s, as a result of the unprecedented events at the Kesterson Reservoir in California (**Fig. 1a**), a national wildlife refuge at the time (Marshall, 1985). Large amounts of this trace element had been mobilized through irrigation of selenium-rich soils in the western San Joaquin Valley, transported along with agricultural runoff, and accumulated at the Reservoir. Toxic selenium concentrations brought about death and deformities for as much as 64% of the wild aquatic birds hatched at the reservoir, including both local migratory species. Within a few years, the habitat of a variety of fish and waterfowl was classified as a toxic waste site (Presser, 1994). Today, the Reservoir's ponds are drained and covered beneath a layer of soil fill (Wu, 2004), yet the mechanisms of selenium release now known as "the Kesterson effect" are still a threat in California and around the world (Lemly, 2004).

The environmental and management conditions creating irrigation-induced selenium contamination have been characterized in Theresa Presser's seminal work (Presser, 1994). In brief, problems arise when seleniferous soils, such as those formed from Cretaceous marine sedimentary deposits along the Western side of the San Joaquin basin are subjected to irrigated agriculture. Salts, including selenium, naturally present in such soils are mobilized through irrigation, and high evaporation rates concentrate them in the root zone. In order to avoid negative effects on plant growth, subsurface drainage systems are used to export excess salts from the soil. This is particularly necessary in places where deep percolation is inhibited by a shallow impermeable layer (such as the Corcoran clay layer that spans the San Joaquin Valley, (SJVDP, 1990)). Such subsurface runoff routinely contains selenium in concentrations that exceed the US Environmental

Protection Agency (EPA) designation of toxic waste (>1,000 µg/L) and thus poses an acute threat to aquatic ecosystems that receive it (Presser, 1994).

The irrigation runoff feeding into the evaporation ponds of the Kesterson reservoir averaged 300 µg Se/L (Wu, 2004). The discovery of widespread deformities among waterfowl hatched near these ponds in 1983 led to a shift in the perception of selenium. While research had thus far been focused on farm-scale problems related to crop accumulation and toxicity to livestock, it became clear that excessive selenium concentrations in agricultural runoff was a watershed-scale resource protection issue that would greatly complicate irrigation management throughout the Western United States (Engberg et al., 1998; Ohlendorf et al., 1985). As a result, California has been a hotspot for global research and management of environmental selenium contamination (Abrams et al., 1990; Banuelos et al., 2005; Fio and Fujii, 1990; Gao and Tanji, 1996; Karlson and Frankenberger, 1989; Ohlendorf et al., 1987; Renner, 2003; Wahl et al., 1994).

As selenium load management in the San Joaquin basin has made significant progress, new major sites of concern, such as the San Francisco Bay-Delta (Presser and Luoma, 2006) and the Salton Sea (Kaiser, 1999; Moreau et al., 2007), have emerged in California. Current regulatory standards for selenium as aquatic contaminant are insufficient to be protective of sensitive ecosystems because they do not account for amplified exposure through bioaccumulation (Luoma and Presser, 2009; Renner, 2003). There are many other pathways of anthropogenic selenium contamination – the San Francisco Bay-Delta for example receives half of its input from refineries (Presser and Luoma, 2010b). However, the diffuse (non-point) agricultural sources are particularly hard to control (Austin, 2001), are the principal source of selenium in western US surface waters (Engberg et al., 1998), and have shaped California's history like no other selenium source. This paper analyzes what can be learned from the last three decades of seleniferous drainage management and regulatory approaches developed in California. In particular I seek to answer two key questions: 1) What were the greatest achievements and shortfalls of seleniferous drainage management in California? 2) To what extent may the current development of site-specific selenium water quality criteria for the San Francisco Bay and Delta serve as a model for future regulation?

2. Background

2.1. Selenium in the environment

Selenium is a naturally occurring trace element heterogeneously distributed across terrestrial and marine environments (Haygarth, 1994). On land, seleniferous soils (>0.5 µg/g) and those marked by selenium deficiency (<0.1 µg/g) sometimes occur as close as 20 km from one another (Lenz and Lens, 2009). Selenium contamination of natural ecosystems is linked to an array of human activities including irrigated agriculture, mining and smelting of metal ores, as well as refining and combusting of fossil fuels. The biospheric enrichment factor, which is computed as the ratio of anthropogenic to estimated "natural" emissions of a substance, was found to be 17 for selenium (compared

to 1.7 for arsenic for example), highlighting the dominance of the anthropogenic component in the modern selenium cycle (Haygarth, 1994). Anthropogenic fluxes are expected to keep increasing in the foreseeable future as energy and resource demands increase (Chapman et al., 2010; Lenz and Lens, 2009). Selenium bioaccumulates, with tissue concentrations in animals and plants typically 1-3 orders of magnitude above those found in water (US.EPA, 2004). Consequently, the predominant selenium uptake pathway for animals is through the consumption of food rather than water. Bioaccumulation and biomagnification are particularly intense in aquatic ecosystems and selenium contamination of such habitats is a global concern (Lemly, 2004). In the Western United States alone, nearly 400,000 km^2 of land are susceptible to irrigation-induced contamination by the same mechanisms that led to the demise of the Kesterson Reservoir (Presser et al., 1994; Seiler et al., 1999). Other nations where irrigation-induced selenium contamination has been observed include Canada, Egypt, Israel, and Mexico (Lemly, 2004).

The environmental impacts of selenium depend on the element's chemical speciation. The element's primary dissolved forms, selenate (SeO_4^{2-}) and selenite (SeO_3^{2-}), are mobile and bioavailable (Frankenberger and Arshad, 2001). They can be sequestered in soils or sediments upon microbial reduction to solid elemental Se(0), metal selenides, or volatilized to the atmosphere upon reduction to gaseous methylated Se(-II). Both selenate and selenite are toxic at elevated concentration, selenite however was found to be more toxic than selenate in direct exposure studies involving invertebrates and fish and also to bioaccumulate more readily at the base of aquatic food chains (Hamilton, 2004). Additionally, once any dissolved form of selenium is assimilated by an organism it is converted into highly bioavailable organo-selenide species, Se(-II) (Luoma and Presser, 2009). Exposure studies comparing organo-selenides to selenite in the diets of water birds established lower toxicity thresholds for the former (Hamilton, 2004). Organo-selenides are released from decaying organisms and organic matter during decomposition and can then persist in solution or be oxidized to selenite, while the conversion back to selenate does not occur at relevant rates in aquatic environments (Luoma and Presser, 2009). Thus, recycling of selenium at the base of aquatic food webs through assimilation and decomposition usually leads to a buildup of the more bioavailable and toxic forms (selenite and organo-selenides) over time (Chapman et al., 2010; Luoma and Presser, 2009). This buildup of bioavailable selenium species may also explain why tissue concentrations in the upper trophic levels of stagnant or low-flowing ecosystems typically exceed those of fast flowing ecosystems with comparable selenium inputs, but shorter residence times (Chapman et al., 2010; Luoma and Presser, 2009; Orr et al., 2006).

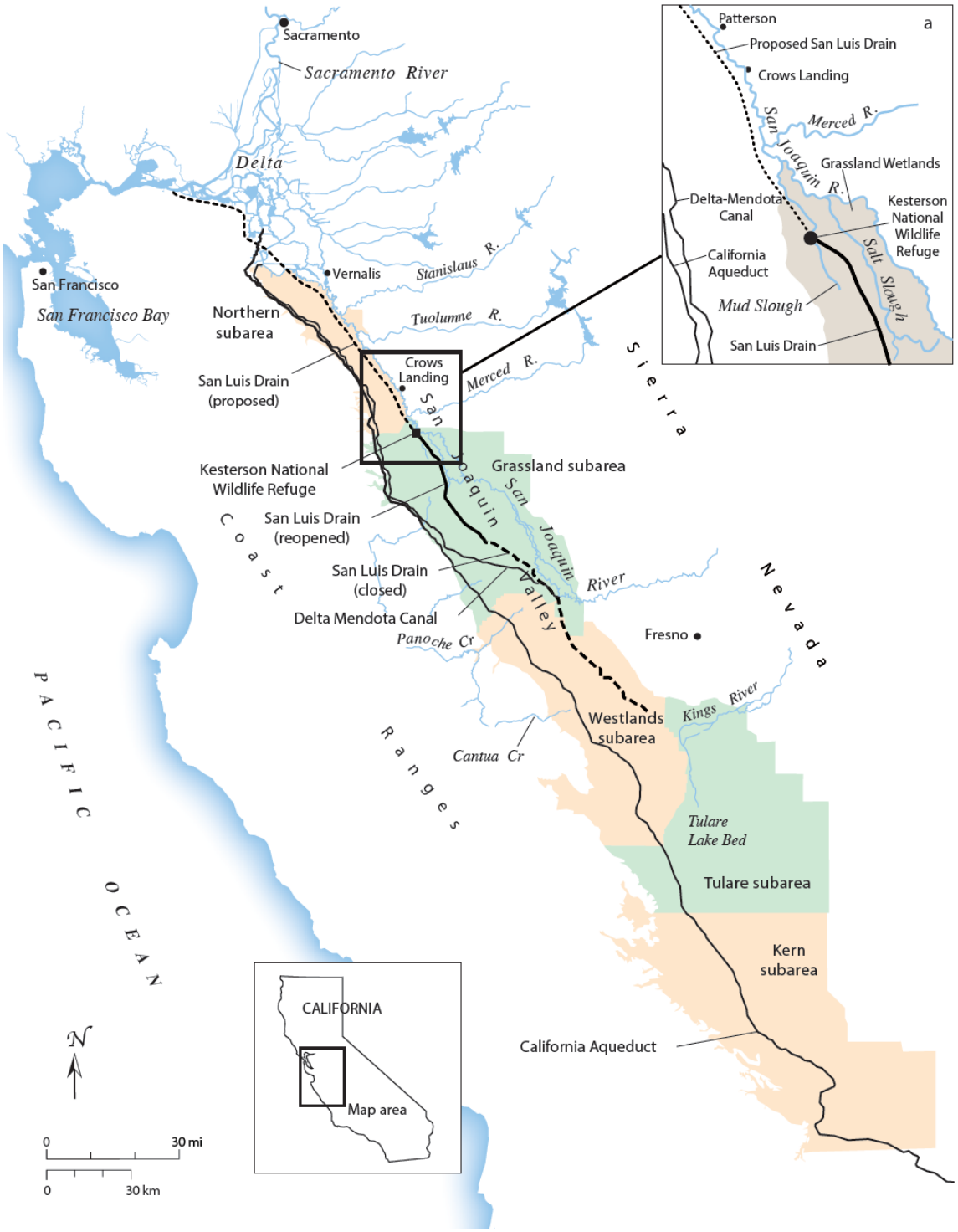

Figure 1. Map of drainage areas, rivers, and channels associated with irrigation induces selenium contamination in California's Central Valley. The drainage management subareas of the Central Valley are shown in green and beige. Adapted with permission from Presser and Luoma, 2006.

2.2. Regulation of selenium as aquatic contaminant in the US

The complex environmental cycling of selenium has been a major obstacle in creating water quality regulations for this element (US.EPA, 1987). Regulatory concentration guidelines vary widely between jurisdictions and there are significant opportunities for new regulatory approaches (Luoma and Presser, 2009). The Californian office of the EPA is currently working on site-specific water quality criteria for the protection of wildlife in the San Francisco Bay and Delta (McNaughton and Yale, personal communication). These criteria are to be based on a modeling approach developed by USGS scientists, capable of translating tissue limits to dissolved concentration limits (Presser and Luoma, 2010b). There is hope among aquatic toxicologists that California's new site-specific approach may become a model for national standards (Renner, 2003).

For all contaminants regulated since 1985, aquatic life criteria under the Clean Water Act have been defined through separate dissolved concentration limits for longer term "continuous" (CCC) and short term "maximum" (CMC) limits (US.EPA, 1992). The selenium criteria that were established in 1987 defined continuous concentration limits (measured as 4-day averages) of 5 μg/L as acid-soluble selenium with maximum concentrations (1-hour average) not exceeding 20 μg/L more than once every three years for freshwater environments, but allowed up to 71 μg/L with up to one three-year exceedance of 300 μg/L for saltwater environments. These selenium limits became legally binding for 14 states including California after promulgation with the 1992 Water Quality Standards (US.EPA, 1992). A central problem with the current criteria is that they were predominantly based on data drawn from direct exposure laboratory studies and thus failed to take into account the more ecologically relevant toxic effects due to bioaccumulation and trophic transfer. The freshwater criteria were based on field data from a contamination event (Belews Lake), while the saltwater criteria were purely based on laboratory studies which did not account for bioaccumulation. The resulting difference of more than one order of magnitude between fresh- and saltwater criteria is not supported by field data (Luoma and Presser, 2009). In fact, the saltwater criteria have widely been regarded as underprotective of wildlife, including waterfowl (Luoma and Presser, 2009). In addition, the freshwater criteria appear underproductive of particularly sensitive ecosystems and species (Engberg et al., 1998). To be protective of waterfowl in the wetlands of the Central Valley Region, a 2 μg Se/L monthly mean water quality criterion was deemed necessary by the Regional Water Quality Control Board and this objective was officially approved for the region by the EPA in 1990 (US.EPA, 2000). For the wetlands of the Central Valley Region, this criterion overrides the statewide criteria promulgated in 1992 and remains in effect today.

However, given the wide range of bioavailability between different selenium species and the complex transfer processes between environmental compartments and trophic levels, regulation based solely on dissolved or acid-soluble concentrations has been characterized as inadequate (Canton and Van Derveer, 1997; Luoma and Presser, 2009; Renner, 2003). In response to such criticism the EPA proposed in 2004 a new tissue-based criterion for selenium (US.EPA, 2004) with a 7.91 μg/g (dry weight) fish

tissue limit to supersede the previous national water quality guidelines for selenium. This limit is based on the lowest level of effect in juvenile bluegill sunfish (*Lepomis macrochirus*) under simulated overwintering conditions (Lemly, 1993) (US.EPA, 2004). Whereas there is little doubt that tissue concentrations are more representative of exposure than dissolved concentrations for individual species, it is unclear if a single fish tissue limit will be protective across entire food webs including a diversity of fish and waterfowl (Hamilton, 2004; Presser and Luoma, 2010a; Renner, 2003). The proposed tissue based criteria have to date remained at draft stage due to objection by the US Fish and Wildlife Service.

2.3. History of irrigation-induced selenium contamination and management in California

The historic developments that lead to the rise of selenium contamination in the San Joaquin Valley (**Fig. 2**) can be traced to the passage of the California Water Resources Development Act of 1960. The Act laid the financial foundation for the State Water Plan providing for the construction of the nation's largest water distribution system and including also infrastructure measures for "the removal of drainage water" (SJVDIP, 1998). The State Water Projects funded under this plan began delivering water to 4,000 km^2 in the Southern San Joaquin Valley as of 1968 (SJVDP, 1990). To prevent salinization and manage agricultural runoff, the Bureau of Reclamation constructed collector drains, a main drainage canal (the San Luis Drain), and a regulating reservoir, Kesterson (BoR, 2008). Originally, the San Luis Drain was planned to deliver drainage out of the San Joaquin Valley all the way to the San Francisco Bay Delta, however the northern part of the drain (**Fig. 1**) was never completed (SJVDP, 1990). Instead, from the time of the San Luis Drain's completion in 1975 until its temporary closure in 1986, all runoff water channeled through the drain was delivered to the evaporation ponds of the Kesterson Reservoir, which had become part of a newly created national wildlife refuge in 1970 (SJVDP, 1990). There, in the early 1980s, high rates of embryo deformity and mortality, as well as large numbers of adult deaths among waterfowl were identified as caused by the elevated selenium concentrations in the evaporation ponds (Ohlendorf et al., 1985; Wu, 2004). This led to the closure of the Reservoir to all runoff inputs in 1986 (Wu, 2004). Further measures in 1988, including drainage of evaporation ponds as well as covering of the deeper ponds with fill soil, led to the elimination of aquatic habitat at the Kesterson Reservoir, thus preventing any additional waterfowl from being exposed to selenium at the location (Wahl et al., 1994).

Despite the closure of the Kesterson Reservoir, problems of excessive selenium concentrations persisted in the greater surrounding Grassland wetland area (**Fig. 1a**), the largest freshwater wetland ecosystem in California (Yale et al., 2011). Farmers of the Grassland drainage area had historically discharged their surface and subsurface runoff through the natural channels of the Grassland wetlands to the San Joaquin River (Austin, 2001; GBP, 2009). As a result of increased scrutiny following the events at Kesterson (Ohlendorf et al., 1987), 33 km^2 of the Grasslands were added to California's Clean Water Act section 303(d) list of impaired waters due to excessive selenium concentrations in 1988. The wetland's two major flow channels Salt and Mud Slough

(**Fig. 1a**) followed in 1990 (Yale et al., 2011). In 1996, the Grassland Bypass Project (GBP) was created to amend this situation (GBP, 2009). The GBP consists of a series of measures to reduce selenium loads in the Grassland marshes and the San Joaquin River, including the reopening of a stretch of the San Luis Drain bypassing the wetlands (**Fig. 1**) (GBP, 2009). The GBP is analyzed below in the section entitled "Selenium load reduction coupled to conveyance into the San Joaquin River".

In addition to the Central Valley, the San Francisco Bay (**Fig. 1**), which receives about half of its selenium load through irrigation runoff from the Valley, has become of increasing concern with respect to selenium contamination since the 1980s (Presser and Luoma, 2006). The San Francisco Bay currently receives effluent containing about equal amounts (~500 kg/year each) of selenium from riverine input and from the effluents of five oil refineries located in the North Bay (Presser and Luoma, 2010b). Although dissolved selenium concentrations observed in the Bay and Delta have been below levels typically of concern (<1 µg/L), those measured in the tissue of sensitive avian and fish species (white sturgeon [*Acipenser transmontaus*] and surf scoter [*Melanitta perspicillata*]) since 1989 have routinely exceeded levels of toxicity (Presser and Luoma, 2006). Especially at risk are bottom feeding fish, diving ducks, and crab feeding on an invasive bivalve, *Potamocorbula amurensis*, which was found to have particularly high bioaccumulation potential for selenium in the North Bay (tissue concentrations up to 20 µg/g) (Presser and Luoma, 2006). It is in this context that the new site-specific selenium criteria for the San Francisco Bay and Delta discussed in the penultimate section of this paper are being developed (Presser and Luoma, 2010b).

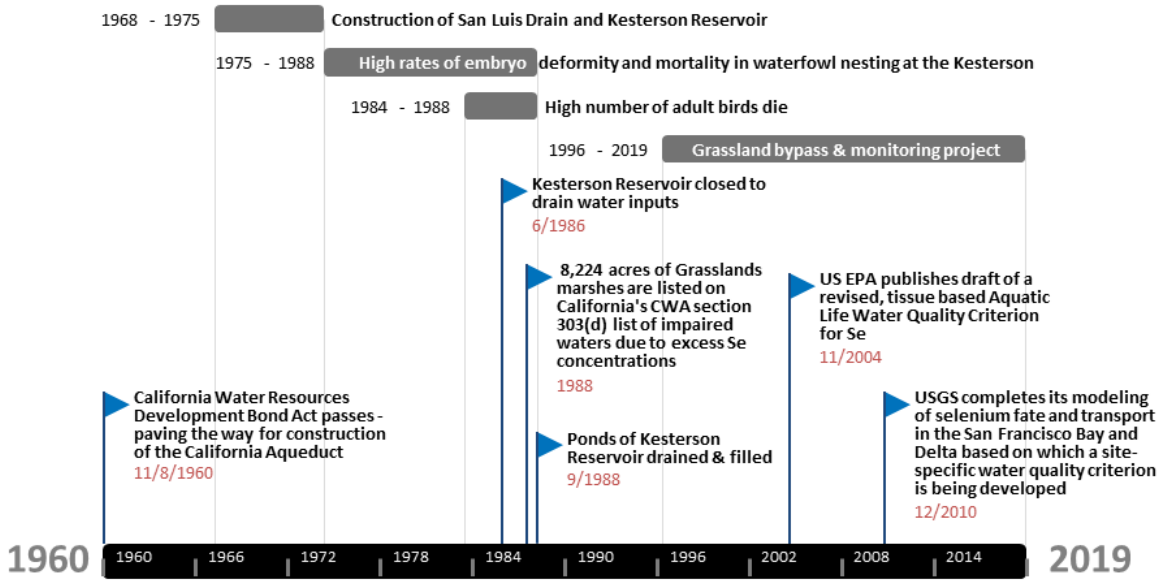

Figure 2. Timeline of landmark events: History of agricultural selenium contamination and management in California.

3. Approaches to seleniferous drainage management in California

Two fundamental approaches have been used to manage seleniferous runoff in the San Joaquin Valley: local disposal and conveyance out of the San Joaquin Valley. Geographically, the separation between these two approaches aligns with the drainage areas defined under the San Joaquin Valley Drainage Program's grand management plan (SJVDP, 1990). The southern subareas Kern, Tulare and, after the San Luis drain closure, also the Westlands subarea dispose of runoff locally, while the Northern and Grassland subareas convey drainage to the San Joaquin River (**Fig. 1**). The two approaches share common elements (**Table 1**). In either case, methods are employed to decrease the disposal load by first decreasing drainage production (**a** in **Table 1**) and then decreasing the volume and selenium concentrations of the drainage itself (**b** in **Table 1**). Fundamentally, only the final disposal step differs, with drainage either being evaporated and the salts disposed, or channeled to be diluted in a larger water body (**c** in **Table 1**).

Table 1. Overview of methods used for the remediation and disposal of seleniferous drainage with their major drawbacks. Colors correspond to development stages with green marking methods that have already been widely implemented, blue marking those which are at the pilot stage, and red marking the method of regional groundwater management for which additional research is required (Presser and Schwartzbach, 2008). Primary references: [1] SJVDIP (1999a-e), [2] Presser and Schwartzbach (2008), [3] Oster and Grattan (2002), [4] Corwin et al. (2008), [5] BoR (2006), [6] Begaliev et al. (2006), [7] GBP (2009).

Method	Major drawback	Primary references
a. Drainage source reduction		
Land retirement	impact on local agricultural economy	[1d], [2]
Reduced irrigation/improved efficiency		[1e]
Regional groundwater management		[2]
b. Volume/concentration reduction		
Re-use	potential for wildlife exposure, increases in dissolved soil Se may be unsustainable for reuse plots (>10 years)	[1a], [3], [4]
Reverse osmosis	highly saline waste	[1b], [2]
Bio-treatment	need for designated landfills for high Se bio-waste	[1b], [2]
c. Final disposal		
Evaporation ponds	potential for wildlife exposure, need for salt waste dumps	[1c]
Enhanced solar evaporators	need for salt waste dumps	[1c], [2], [6]
Conveyance out of watershed	potential for wildlife exposure	[5], [7]

The debate on how to sustainably manage selenium loads and drainage needs in the Central Valley is far from over. Mass balance analysis by the USGS reveals that the drainage needs of the Westlands subarea, the greatest near surface selenium reservoir among the subareas, cannot be met without the retirement of at least one third of the 1,200 km^2 of agricultural lands and the use of treatment methods for selenium and salt removal that are as of yet unproven (Presser and Schwartzbach, 2008). For a detailed discussion of proposed management scenarios for this subarea the reader is referred to the Final Environmental Impact Statement of the San Luis Drainage Feature Re-evaluation (BoR, 2006) and the technical analysis of proposed plans by Presser and Schwartzman (Presser and Schwartzbach, 2008). The current plans under discussion for the Westlands in terms of selenium removal include reverse osmosis and reductive precipitation in microbial bioreactors that have so far only been tested at the pilot scale (b in Table 1). It is uncertain whether the proposed bioreactors will be effective with the high salinity inputs expected to result from reverse osmosis (Presser and Schwartzbach, 2008). Given such uncertainty I focus on the proven management methods by which seleniferous drainage is actively being managed in the San Joaquin Valley (i.e. green items in Table 1).

3.1. Local disposal or remediation of seleniferous runoff

Locally, seleniferous runoff can be treated using technologies that physically, chemically or biologically remove selenium from water, reused through irrigation of designated land planted with salt tolerant crops, or disposed of in evaporation facilities. A number of removal technologies have been proposed post-Kesterson (SJVDIP, 1999b), however the physical and chemical methods are too costly and the biological methods fail to reduce selenium concentrations in treated drainage to below 2 µg/L at relevant scales (SJVDIP, 1999c). Thus, for lack of better alternatives, drainage reuse and evaporation ponds are so far the local remediation and disposal methods of choice.

The reuse of seleniferous drainage as irrigation water on designated reuse plots thus reducing the water volume requiring final disposal, has seen a marked expansion over the last decade, with areas of reuse in the Grassland subarea alone increasing from 7.4 km^2 to more than 20 km^2 (capacity to reuse up to 1.9×10^7 m^3) from 1996 to 2009 (GBP, 2009). The cost of operation can sometimes be offset through the production of commercial crops. A number of innovative approaches often involving a sequence of increasingly salt tolerant crops in either time (crop cycling) or space (sequential reuse) have been developed and tested in the San Joaquin Valley (Oster and Grattan, 2002; SJVDIP, 1999a). Of the 2,600 kg selenium produced in the Grassland subarea in 2009, about half were disposed through drainage reuse (GBP, 2009). The exact fate of this selenium is as of yet unclear. In particular, there are concerns about the long term (>10 years) sustainability of drainage reuse, after increasing concentrations of dissolved selenium were observed at all monitored soil depths (0-1.2 m) in the only study monitoring soil selenium for an extended time period (5 years) on a reuse plot in the San Joaquin Valley (Corwin et al., 2008). Additionally, there are concerns that endangered wildlife such as the San Joaquin kit fox (*Vulpes macrotis mutica*), the kangaroo rat

(*Diplodomys sp.*), and the blunt-nosed leopard lizard (*Gambelia sila*) may be adversely affected if their ranges overlap with reuse areas (Beckon and Maurer, 2008).

Evaporation ponds, which are shallow basins used for the evaporative disposal of drainage water, are deployed primarily in the Tulare and Kern subareas (SJVDIP, 1998). Since there are no drainage channels or rivers to convey drainage out of these two subareas, evaporation is the only option for final disposal (c in Table 1). The design of evaporation ponds has been optimized post-Kesterson to reduce wildlife use and thus the risk of exposure to elevated selenium concentrations in pond water (SJVDIP, 1999c). Specifically, steep levee slopes, elimination of windbreaks, and a minimum water depth of 0.6 m are used to deter waterfowl. Enhanced solar evaporator designs that use sprinklers to ideally eliminate standing water altogether have been tested at the pilot scale, but have not seen wide-spread deployment to date (Begaliev et al., 2006; Presser and Schwartzbach, 2008). Evaporation ponds are currently exempt from water quality guidelines that apply to natural waters, however management needs to include active and continuous measures to limit wildlife use through hazing and removal of pond vegetation. Additionally, the provision of nearby alternative habitat for waterfowl is recommended when selenium concentrations exceed 2 µg/L (SJVDIP, 1999c). While these management procedures are necessary during the operation of evaporation ponds to avoid ecological damage, they also greatly increase the cost of operation. In fact, the owners of many of the privately operated evaporation ponds in the San Joaquin Valley have decided to cease operation as a result of imposed requirements (SJVDIP, 1998). Another drawback of this method of local disposal is that the evaporate needs to be stored at dedicated disposal sites. This is particularly problematic if evaporation is chosen to continuously dispose drainage from large source areas. For example, it has been estimated that if the drainage program in the Westlands district is expanded as planned, up to 400,000 tons of salt may need to be disposed yearly, which would require dedicated dumpsites covering an area of around 1 km^2 (at 20 m depth) every 50 years (Presser and Schwartzbach, 2008).

3.2. Selenium load reduction coupled to conveyance into the San Joaquin River

The Northern and the Grassland subareas (**Fig. 1**) channel a large portion of their runoff to the San Joaquin River. Among the two, only the Grassland subarea has been marked by problematic selenium loads (SJVDP, 1990). Due to the Grassland Bypass Project (GBP), it is also the subarea in which management of seleniferous runoff has made the greatest progress over the last 20 years (**Table 2**).

The GBP was created in 1996 through an agreement between the U.S. Bureau of Reclamation and the regional drainage entity of the Grassland Area Farmers (GAF) under the legal umbrella of the San Luis and Delta-Mendota Water Authority. It consists of three central measures. First, a 45 km stretch of the San Luis drain was opened to convey subsurface drainage from the GAF to Mud Slough, thereby bypassing most of the wetlands (**Fig. 1a**). Second, limits were imposed on the total allowable selenium discharge by the GAF and these limits were set to decrease over time (15% in the original 5 year agreement 1996-2001). Finally, ongoing monitoring of water quality and quantity was initiated across the project area to enforce limits and gage impact (Austin, 2001;

GBP, 2009). The original 5 year project was extended by 8 years in 2001 and then by 10 years in 2009 (GBP, 2009; Yale et al., 2011). Whereas the use agreement specified load-dependent incentive fees for exceedance of the specified selenium load limits, the true innovation consisted in enabling the GAF to develop an internal selenium load trading program (Austin, 2001). This trading program represents the first ever cap-and-trade style program for any pollutant allowing trades directly between nonpoint sources. It is also the first instance in which "total maximum daily load" (TMDL) requirements under the Clean Water Act have been successfully enforced against a nonpoint source (Austin, 2001). Since 2001 the drainage management efforts of the GAF have shifted away from the load trading program and towards centralized management for the region (McGahan, personal communication), however the overall strategy has remained consistent (McGahan, 2011). Funds obtained as part of the GBP are used to support programs and actions aimed at reducing selenium loads (GBP, 2009; McGahan, 2011), such as the local drainage reuse measures described above.

The direct aid provided by the GBP as well as the economic incentives for load reduction and conservation initially created by its load trading program have led to an overall reduction in selenium loads (Austin, 2001; McGahan, 2011). In fact, the total annual loads of selenium discharged through the San Luis Drain have decreased continuously over the course of the project, from 3,110 kg in 1997 to 560 kg in 2009. This has been reflected in a reduction of selenium loads in the San Joaquin River from a pre-project annual average of 3,690 kg to 690 kg in 2009 (below the confluence with the Merced) (GBP, 2009). Weekly selenium concentration monitoring data collected below the confluence with the Merced between 1996 and 2012, reveal seasonality in selenium loads (concentrations peak in the high flow winter months), but reaffirm the overall load reductions reported by the GBP (**Fig. 3**). However, the reduction is primarily due to a reduction in total discharge from 6.1×10^7 (pre-project annual average) to 1.6×10^7 m^3 in 2009. Average selenium concentrations of discharge decreased from 67 to 33 μg/L in the same time period (GBP, 2009) and were still significantly above the water quality criterion of 5 μg/L.

Much of the reduction in selenium loads can be credited directly to the impact of the projects and measures implemented as part of the GBP. For example, through the San Joaquin River Water Quality Improvement Project, more than 20 km^2 of land have been purchased and planted with salt tolerant crops providing the capacity to reuse up to 1.9×10^7 m^3 of drainage water (1,700 kg of selenium) per year (GBP, 2009). A GBP unrelated factor in the successful load reduction was the prevalence of drought during the early 1990s which incentivized investments in efficient irrigation technology and other conservation measures on the side of the GAF (Austin, 2001). Therefore, considerations of best management practices and technology aside, the creation of quantitative economic incentives for selenium load reduction should be a priority of any seleniferous drainage management program. Unfortunately, comprehensive incentive programs such as the GAF load trading program remain the exception rather than the rule, for selenium as they do for many other pollutants.

Table 2. Key metrics of successes and failure of the Grasslands Bypass Project. Successes are listed with '+'-sings and failures with '–'-signs.

Institutional:

+ 16 years of data on selenium loads and concentrations collected in drainage channels, wetland habitats, and the San Joaquin River

+ first ever cap-and-trade program implemented entirely between non-point sources; first instance in which TMDLs have been successfully enforced against a nonpoint source

+ more than 20 km^2 of land have been purchased and planted with salt tolerant crops providing the capacity to reuse up to 1.9×10^7 m^3 (compared to 1.6×10^7 m^3 being discharged through the San Luis Drain)

– still dependent on out-of-valley discharge pathway, San Luis Drain contract twice extended

Load reduction:

+ global annual loads of Se discharged through the San Luis Drain have decreased continuously over the course of the project from 3,110 kg in 1997 to 560 kg in 2009.

– Se load reduction primarily due to a reduction in total discharge from 6.1×10^7 (pre-project annual average) to 1.6×10^7 m^3 in 2009; average Se concentrations of discharge decreased from 67 to 33 μg/L (still significantly above the water quality criterion of 5 μg/L)

Habitat protection:

+ removed all seleniferous drainage water from 145 km of channels that supply water to more than 650 km^2 of sensitive wetlands and wildlife; 65 km stretch of the San Joaquin River removed from California's 303(d) list of impaired waters

+ Se concentrations in Salt Slough dropped from 16 μg/L in 1996 to below 2 μg/L for most of the project duration; Se concentrations in fish tissue dropped from toxic levels (~10 μg/g) to below concern (<5 μg/g) between 1992 and 1995; Salt Slough was removed from California's 303(d) list of impaired waters

– Se concentration in 10 km stretch of Mud Slough through drainage is delivered have increased and usually exceed the 5 μg/L water quality criterion; rise in concentrations is likely to endanger local sensitive species

– Se concentrations in the stretch of the San Joaquin River between the confluence with Mud Slough and the confluence with the Merced River still seasonally exceed 5 μg/L water quality criterion; seasonal peaks may endanger sensitive juvenile live-stage of Chinook salmon

– 2 μg/L wetland criterion was still exceeded in parts of the Grassland marshes in 2002, due to project unrelated high flow input not captured by the bypass; Grassland marshes still listed in on California's 303(d) list of impaired waters

The primary motivation of the GBP was the protection of the sensitive wetland habitat in the Grassland area. Through circumvention, the GBP has effectively removed all seleniferous drainage water from 145 km of channels that supply water to more than 650 km^2 of sensitive wetlands and wildlife areas (GBP, 2009). This led to a rapid decrease in selenium concentrations at the monitoring stations in this area after the GBP's implementation in 1996. In Salt Slough for example (**Fig. 1a**), concentrations have dropped from 16 µg/L in water year 1996 to below 2 µg/L for most of the project duration (GBP, 2009). In addition, selenium concentrations monitored in the tissue of various fish species collected at the slough (mosquito fish (*Gambusia affinis*), minnows (*Pimephales promelas*), and others) have dropped from toxic levels (~10 µg/g) between 1992 and 1995 to below levels of concern (<5 µg/g) after 1998 (GBP, 2009). Accordingly, the slough was removed from California's 303(d) list of impaired waters in 2008 (Yale et al., 2011). A 65 km stretch of the San Joaquin River upstream of Mud Slough was delisted in 2010 (Yale et al., 2011).

On the other hand, selenium loads in the 10 km stretch of Mud Slough through which selenium-rich drainage is being delivered from the San Luis Drain to the San Joaquin River (**Fig. 1a**) have increased since the start of the GBP and usually exceed 5 µg/L (GBP, 2009). This rise in concentrations is likely to endanger local sensitive species including juvenile Chinook salmon (*Oncorhynchus tshawytscha*) and Steelhead trout (*Oncorhynchus mykiss*) (Beckon and Maurer, 2008). For the Chinook salmon in particular, seasonally elevated selenium concentrations in the stretch of the San Joaquin River between the confluence with Mud Slough and the confluence with the Merced River (**Fig. 1a**) may prove problematic. Selenium concentrations have exceeded 10 µg/L in 6 of 24 months during the most recently published monitoring period, typically during the rainy season, i.e. between September and February (GBP, 2009). The seasonality of these peaks (compare **Fig. 3**) coincides with the emergence of the Chinook salmon's sensitive juvenile live-stage, and the concentrations are in a range were increased mortality of up to 20% can be expected for juveniles (Beckon and Maurer, 2008). Thus selenium input through Mud Slough in this particular stretch of the San Joaquin River may represent an obstacle for ongoing efforts to restore salmon above the Merced, where they have been extirpated due to water diversions (Beckon and Maurer, 2008). Additionally, whereas selenium concentrations in most of the marshes have decreased, the 2 µg/L criterion was still exceeded in parts of the wetlands as recently as 2002, due to high flow input originating from the Delta-Mendota Canal (US.FWS, 2002), which was not captured by the bypass (**Fig. 1a**). As a result, the Grassland marshes listed in 1988 remain on California's 303(d) list of impaired waters today (US.EPA, 2010). Two key challenges facing future attempts to bypass sensitive ecosystems emerge. First, caution needs to be exercised in preventing ecological damage in locations to which seleniferous runoff is being diverted. Second, circumvented locations may still receive selenium inputs due to other sources in the watershed. Consequently thorough monitoring of both circumvented and receiving water bodies is essential, especially during periods of high flow.

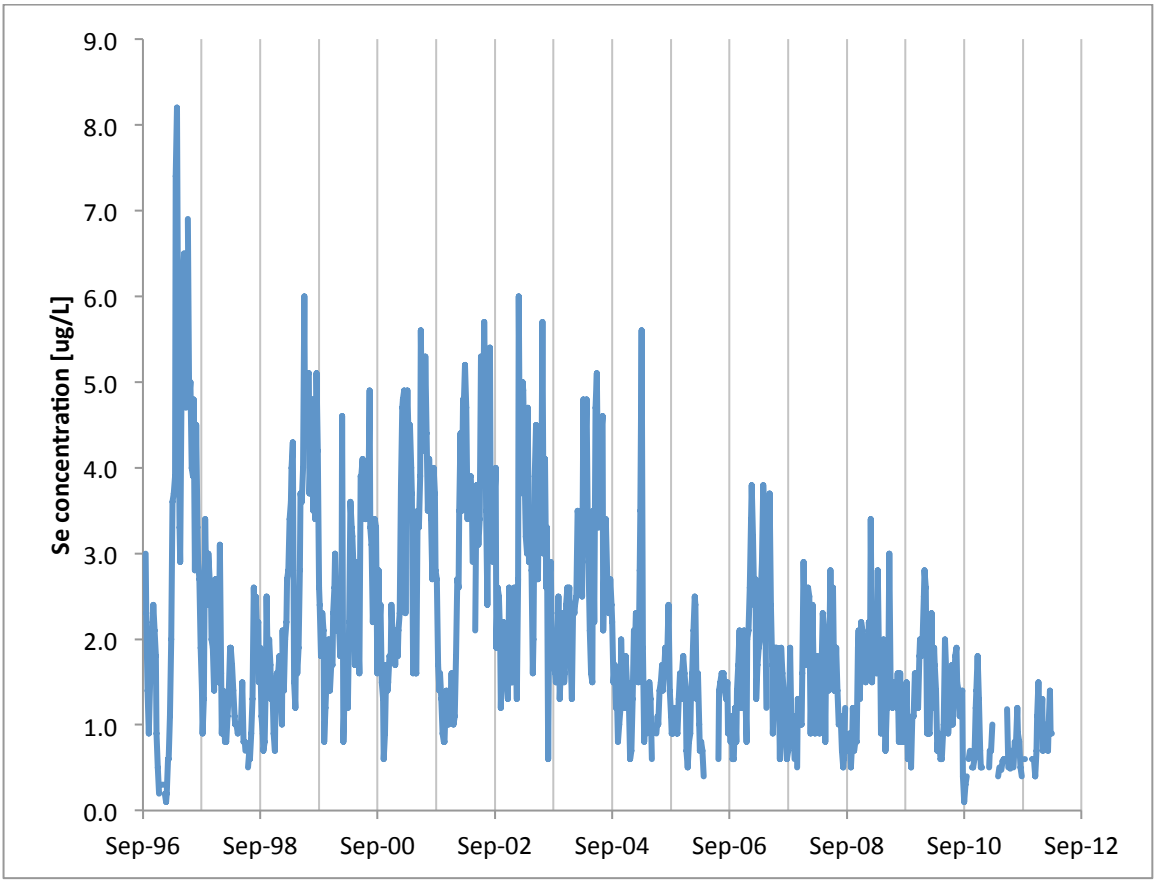

Figure 3. Selenium concentrations in the San Joaquin River below the confluence with the Merced River (Fig. 1). Concentrations are shown for the period from the beginning of the GBP (1996) to the most recent 2012 monitoring data provided by the US Bureau of Reclamation. Selenium concentrations can be seen to decrease on an annual average basis with seasonal peaks in the winter months.

4. Site-specific modeling and regulation of selenium contamination

In 2010, USGS scientists Theresa Presser and Samuel Luoma completed an ecosystem-scale selenium modeling effort in support of site-specific fish and wildlife criteria development for the San Francisco Bay and Delta (Presser and Luoma, 2010b). In brief, the model consists of three key components. First, the partitioning between dissolved selenium concentrations and the "particulate/planktonic" concentrations at the base of the food web is simulated using site-specific partitioning coefficients ("K_ds"). Second, the local food web is resolved around target predator species of concern, including separate compartments for prey species or groups of species these predators feed on that differ significantly with respect to their selenium accumulation potential. Finally, the model comprises trophic transfer factors (TTFs) that correlate the concentration in the tissue of each species or trophic compartment with that of its diet. The model thus allows the calculation of tissue concentration estimates for all species

that are part of the food web by simply multiplying dissolved concentrations by the K_d and then by the TTF for each lower connecting link in the food web. The model can also be used to convert tissue concentration limits for a target species to limits in solution. This approach is unique in that it captures critical trophic transfer steps relevant to the toxicological effects of selenium on individual species, while being generic enough to remain applicable to a wide array of aquatic ecosystems with diverse biogeochemical conditions. The main requirement is the availability of site-specific field data on the partitioning between dissolved concentrations and those at the local base of the food chain as well as information on the local food web, and on trophic transfer factors for key species present at a location.

The specific application of this approach to the San Francisco Bay and Delta lead to the capability of realistically translating tissue-based criteria for the protection of desired fish and bird species into dissolved or particulate concentration limits (Presser and Luoma, 2010b). In addition, the model was used to predict the ecosystem impacts of selenium in the Bay and Delta under various management scenarios (Presser and Luoma, 2006). The California (Region 9) office of the EPA is now in the process of developing site-specific selenium criteria for the Bay and Delta based on the model results. In the future, the same modeling approach is to be used to develop site-specific criteria for other Californian ecosystem in which problems with selenium contamination occur (McNaughton and Yale, personal communication). Such regulation would allow the protection of the most sensitive ecosystems without imposing an unnecessary regulatory burden in areas with less sensitive ecosystems and also the targeted protection of critical species. This approach would thus represent a landmark in the regulation of aquatic contaminants in the US and a significant improvement over regulation that traditionally has taken the form of state or nationwide criteria based on dissolved or acid soluble concentrations.

Whereas the use of the model to determine site-specific dissolved selenium criteria or TMDLs is well warranted, its application to predict ecosystem impacts under changing environmental or management conditions may be limited to environments with relatively stable biogeochemical conditions. The reason is that the model does not explicitly account for selenium speciation nor does it separate environmental compartments such as sediments and the water column. Transformation between chemical species and transfer between environmental compartments are far more dynamic and less linear than transfer through food webs and thus necessitate a dynamical model for adequate representation. Such transfer could be of great importance in predicting selenium exposure under changing environmental conditions, especially for shallow stagnant water bodies with a high sediment-water interface to volume ratio, such as the Salton Sea. Fortunately, a dynamic model extension for water-sediment interactions could be integrated with Presser and Luoma's approach, since mathematically this approach represents a simple multiplication of concentrations by partitioning and trophic transfer factors. Without such extensions, the models predictive power is limited to the geochemical steady-state and site-specific regulatory limits derived from it need to be coupled to ongoing monitoring and periodic revisions.

5. Outlook

The last three decades have seen significant progress with respect to the management and regulation of irrigation-induced selenium contamination in California. Among local remediation methods, sequential drainage reuse ending in well-designed evaporation facilities can be a viable option limited primarily by the scalability of the operation cost and the disposal of produced salts. Much can be learned from the integrated approach pursued as part of the Grassland Bypass Project (GBP). In particular, the project provides a blueprint of the framework necessary to establish and enforce load limits in an agricultural non-point context. As long as the means to track discharge quantities and concentrations are available, this approach can be translated to other agricultural sources of selenium or other pollutants (Austin, 2001). Given that a majority of selenium load reductions to date have been achieved by a reduction in drainage loads rather than selenium concentrations, there appear to be opportunities for additional reductions through management practices that enhance selenium retention in the source soils. Recent research suggests that unexplored options remain in this area, such as the management of soil structure to enhance microbial selenium reduction (Kausch et al., 2012; Kausch and Pallud, 2013), or the addition of organic matter amendments to enhance reduction, retention, and volatilization (Darcheville et al., 2008; Dhillon et al., 2010). A better understanding of the factors controlling selenium speciation in soils would also help evaluate the long-term sustainability of drainage reuse schemes.

The site-specific regulation currently under development for the San Francisco Bay and Delta represents an appropriate and timely update to federal selenium water quality criteria, which as discussed in the background section, have proven inadequate in light of scientific findings over the last two decades. In this context, scientists and resource managers should think ahead about the needs that will arise as the approach is expanded to other sites of concern with respect to selenium contamination. California's 303(d) list of impaired waters currently includes more than 60 water bodies polluted by selenium (US.EPA, 2010). By far the largest of these is the Salton Sea with an estimated 944 km^2 affected (US.EPA, 2010). Like the Kesterson Reservoir in the 1980s, the Salton Sea has long been the receiving body of seleniferous irrigation drainage (May et al., 2007). It is also one of the most important bird habitats in the American Southwest, used by hundreds of thousands of waterfowl pertaining to resident and migratory bird species, including endangered ones like the brown pelican (*Pelecanus occidentalis* Linnaeus) (Moreau et al., 2007). Whereas the Salton Sea is an obvious target for the expansion of the site-specific regulatory approach, matters may be complicated by the Sea's uncertain management future (Kaiser, 1999). For example, management choices that expose sediment to oxic conditions may lead to the local release of reduced selenium accumulated in sediments, creating ecological hazard beyond that due to ongoing seleniferous irrigation-drainage inputs. In this case, the development of site-specific selenium criteria would need to be coupled to a detailed understanding not only of the trophic transfer processes in the local food web, but also the local biogeochemical transformations in the shallow basin. Thus, the promise of the site-specific approach to the regulation of selenium as contaminant creates renewed urgency for the improvement

of biogeochemical models of selenium cycling and the acquisition of field data at sites of concern.

6. Acknowledgements

The author thanks Carolyn Yale and Eugenia McNaughton, US EPA Region 9 for insightful discussion and commentary during manuscript preparation, and Charlotte Smith, Charlotte Smith & Associates, Inc. for her review and comments. I thank Joseph McGahan, Drainage coordinator for the Grassland Area Farmers for providing information regarding the current state of the GBP.

7. References

Region 9 EPA website [Online] http://www.epa.gov/region9/water/ctr/ (verified 05/01/2012).

Abrams, M.M., R.G. Burau, and R.J. Zasoski. 1990. Organic selenium distribution in selected California soils. Soil Science Society of America Journal 54:979-982.

Austin, S.A. 2001. Designing a nonpoint source selenium load trading program. Harvard Environmental Law Review 25:337-391.

Banuelos, G.S., Z.Q. Lin, I. Arroyo, and N. Terry. 2005. Selenium volatilization in vegetated agricultural drainage sediment from the San Luis Drain, Central California. Chemosphere 60:1203-1213.

Beckon, W.N., and T.C. Maurer. 2008. Potential effects of selenium contamination on federally-listed species resulting from delivery of federal water to the San Luis Unit, *In* US.DOI, (ed.). US Fish and Wildlife Service, Sacramento.

Begaliev, A., V. Cervinka, K. Buchnoff, J. Cooper, M. Delamore, J. Diener, and J. Lopez. 2006. Solar Evaporator for Integrated on-Farm Drainage Management System at Red Rock Ranch, San Joaquin Valley, California. Department of Water Resources, Sacramento.

BoR. 2006. San Luis Drainage feature re-evaluation - Final Environmental Impact Statement, *In* US.DOI, (ed.). Bureau of Reclamation, Sacramento.

BoR. 2008. San Luis Drainage feature re-evaluation - Feasibility report, *In* US.DOI, (ed.). Bureau of Reclamation, Sacramento.

Canton, S.P., and W.D. Van Derveer. 1997. Selenium toxicity to aquatic life: An argument for sediment-based water quality criteria. Environmental Toxicology and Chemistry 16:1255-1259.

Chapman, P.M., W.J. Adams, M.L. Brooks, C.G. Delos, S.N. Luoma, W.A. Maher, H.M. Ohlendorf, T.S. Presser, and D.P. Shaw. 2010. Ecological Assessment of Selenium in the Aquatic Environment CRC Press, Boca Raton.

Corwin, D.L., S.M. Lesch, J.D. Oster, and S.R. Kaffka. 2008. Short-Term Sustainability of Drainage Water Reuse: Spatio-Temporal Impacts on Soil Chemical Properties. J. Environ. Qual. 37:S-8-S-24.

Darcheville, O., L. Fevrier, F.Z. Haichar, O. Berge, A. Martin-Garin, and P. Renault. 2008. Aqueous, solid and gaseous partitioning of selenium in an oxic sandy soil

under different microbiological states. Journal of Environmental Radioactivity 99:981-992.

Dhillon, K.S., S.K. Dhillon, and R. Dogra. 2010. Selenium accumulation by forage and grain crops and volatilization from seleniferous soils amended with different organic materials. Chemosphere 78:548–556.

Engberg, R.A., D.W. Westcot, M. Delamore, and D.D. Holz. 1998. Federal and state perspectives on regulation and remediation of irrigation-induced selenium problems, p. 1-25, *In* W. T. Frankenberger and R. A. Engberg, eds. Environmental chemistry of selenium. Marcel Dekker, New York.

Fio, J.L., and R. Fujii. 1990. Selenium speciation methods and applications to soil saturation extracts from San Joaquin Valley, California. Soil Science Society of America Journal 54:363-369.

Frankenberger, W.T., and M. Arshad. 2001. Bioremediation of selenium-contaminated sediments and water. Biofactors 14:241-254.

Gao, S., and D.W. Tanji. 1996. Water selenium speciation and sediment fractionation in a California flow-through wetland system. Journal of Environmental Quality 29:1275-1283.

GBP. 2009. Grassland Bypass Project Annual Report 2008-2009. The San Francisco Estuary Institute for the Grasslands Bypass Project Oversight Comittee, San Francisco.

Hamilton, S.J. 2004. Review of selenium toxicity in the aquatic food chain. Science of the Total Environment 326:1-31.

Haygarth, P.M. 1994. Global importance and global cycling of selenium, p. 1-28, *In* W. T. Frankenberger, Jr. and S. Benson, eds. Selenium in the Environment, 1st ed. Marcel Dekker, Inc, New York.

Kaiser, J. 1999. Battle Over a Dying Sea. Science 284:28-30.

Karlson, U., and W.T. Frankenberger. 1989. Accelerated rates of selenium volatilization from California soils. Soil Science Society of America Journal 53:749-753.

Kausch, M., P. Ng, J. Ha, and C. Pallud. 2012. Soil-Aggregate-Scale Heterogeneity in Microbial Selenium Reduction. Vadose Zone Journal DOI:10.2136/vzj2011.0101.

Kausch, M.F., and C.E. Pallud. 2013. Modeling the impact of soil aggregate size on selenium immobilization. Biogeosciences 10:1323–1336.

Lemly, A.D. 2004. Aquatic selenium pollution is a global environmental safety issue. Ecotoxicology and Environmental Safety 59:44-56.

Lemly, D.A. 1993. Metabolic stress during winter increases the toxicity of selenium to fish. Aquatic Toxicology 27:133-158.

Lenz, M., and P.N.L. Lens. 2009. The essential toxin: The changing perception of selenium in environmental sciences. Science of The Total Environment 407:3620-3633.

Luoma, S.N., and T.S. Presser. 2009. Emerging Opportunities in Management of Selenium Contamination. Environmental Science & Technology 43:8483–8487.

Marshall, E. 1985. Selenium poisons refuge, California politics. Science 229:144-146.

May, T.W., M.J. Walther, and W.G. Brumbaugh. 2007. Selenium concentrations in irrigation drain inflows to the Salton Sea, California, October 2006 and January 2007. U.S. Geological Survey.

McGahan, J.C. 2011. Waste discharge requirement order No. 5-01-234, Update of long term drainage management plan (letter to the CVRWQCB). GAF, Rancho Cordova.

Moreau, M.F., J. Surico-Bennett, M. Vicario-Fisher, R. Gerads, R.M. Gersberg, and S.H. Hurlbert. 2007. Selenium, arsenic, DDT and other contaminants in four fish species in the Salton Sea, California, their temporal trends, and their potential impact on human consumers and wildlife. Lake and Reservoir Management 23:536-569.

Ohlendorf, H.M., D.J. Hoffman, M.K. Saiki, and T.W. Aldrich. 1985. Embryonic mortality and abnormalities of aquatic birds: Apparent impacts of selenium from irrigation drainwater. Science of the Total Environment 52:49–63.

Ohlendorf, H.M., R.L. Hothem, T.W. Aldrich, and A.J. Krynitsky. 1987. Selenium contamination of the grasslands, a major California waterfowl area. Science of the Total Environment 66:169–183.

Orr, P.L., K.R. Guiguer, and C.K. Russel. 2006. Food chain transfer of selenium in lentic and lotic habitats of a western Canadian watershed. Ecotoxicology and Environmental Safety 63:175-188.

Oster, J.D., and S.R. Grattan. 2002. Drainage water reuse. Irrigation and Drainage Systems 16:297-310.

Presser, T.S. 1994. "The Kesterson effect". Environmental Management 18:437-454.

Presser, T.S., and S.N. Luoma. 2006. Forecasting Selenium Discharges to the San Francisco Bay-Delta Estuary: Ecological Effects of a Proposed San Luis Drain Extension Professional Paper 1646, Vol. 1646. U.S. Geological Survey, Reston, Virginia.

Presser, T.S., and S.E. Schwartzbach. 2008. Technical analysis of in-valley drainage management strategies for the western San Joaquin Valley, California *In* US.DOI, (ed.), Vol. Open-File Report 2008-1210. U.S. Geological Survey, Reston, Virginia.

Presser, T.S., and S.N. Luoma. 2010a. A Methodology for Ecosystem-Scale Modeling of Selenium. Integrated Environmental Assessment and Management 6:685–710.

Presser, T.S., and S.N. Luoma. 2010b. Ecosystem-Scale Selenium Modeling in Support of Fish and Wildlife Criteria Development for the San Francisco Bay-Delta Estuary U.S. Geological Survey, Menlo Park, California.

Presser, T.S., M.A. Sylwester, and W.H. Low. 1994. Bioaccumulation of selenium from natural geologic sources in western states and its potential consequences. Environmental Management 18:423-436.

Renner, R. 2003. California to develop selenium standard for wildlife. Environmental Science & Technology 37:274A–275A.

Seiler, R.L., J.P. Skorupa, and L.A. Peltz. 1999. Areas susceptible to irrigation-induced selenium contamination of water and biota in the western United States U.S. Department of the Interior.

SJVDIP. 1998. Drainage Management in the San Joaquin Valley - A Status Report. San Joaquin Valley Drainage Implementation Program, Sacramento.
SJVDIP. 1999a. Drainage Reuse - Final Report. San Joaquin Valley Drainage Implementation Program, Sacramento.
SJVDIP. 1999b. Drainage Water Treatment - Final Report. San Joaquin Valley Drainage Implementation Program, Sacramento.
SJVDIP. 1999c. Evaporation Ponds - Final Report. San Joaquin Valley Drainage Implementation Program, Sacramento.
SJVDIP. 1999d. Land Retirement - Final Report. San Joaquin Valley Drainage Implementation Program, Sacramento.
SJVDP. 1990. A management plan for agricultural subsurface drainage and related problems on the westside San Joaquin Valley, pp. 183, Vol. Final Report. San Joaquin Valley Drainage Program, US Department of the Interior & California Resource Agency.
US.EPA. 1987. Ambient Water Quality Criteria for Selenium, Vol. EPA-440/5-87-006. US Environmental Protection Agency, Washington, DC.
US.EPA. 1992. Water Quality Standards; Establishment of Numeric Criteria for Priority Toxic Pollutants; States' Compliances. Federal Register 57:60848 (57 FR 60848).
US.EPA. 2000. Water Quality Standards; Establishment of Numeric Criteria for Priority Toxic Pollutants for the State of California Federal Register 65:31686 (65 FR 31686).
US.EPA. 2004. Draft Aquatic Life Water Quality Criterion for Selenium, Vol. EPA-822-D-04-00. US Environmental Protection Agency, Washington, DC.
US.EPA. 2010. California's 2008-2010 Section 303(d) list of impaired waters. California State Water Resources Control Board, Sacramento.
US.FWS. 2002. Exceedances of Water Quality Objective for Grassland Wetland Supply Channels (letter to the CVRWQCB), pp. 7. Central Valley Regional Water Quality Control Board, Sacramento.
Wahl, C., S. Benson, and G. Santolo. 1994. Temporal and spatial monitoring of soil selenium at Kesterson Reservoir, California. Water Air and Soil Pollution 74:345-361.
Wu, L. 2004. Review of 15 years of research on ecotoxicology and remediation of land contaminated by agricultural drainage sediment rich in selenium. Ecotoxicology and Environmental Safety 57:257-269.
Yale, C., T. Ditto, and R. Schnagl. 2011. Grasslands Bypass Project Reduces Selenium in the San Joaquin Basin [Online]. Available by US Environmental Protection Agency, Office of Water (posted September 2011; verified 03/28/2012).

Chapter 2 – Soil-aggregate-scale heterogeneity in microbial selenium reduction

Abstract – Given selenium's role as both an environmental contaminant and a micronutrient, the microbial reduction and subsequent sequestration of bioavailable selenium in soils are of great ecological interest. Primary particles in surface soils are typically bound into loosely packed, microporous aggregates and these aggregates may be critical spatial units in determining the fate of selenium in soils. Surrounded by macropores where preferential flow rapidly advects dissolved compounds, soil aggregates are domains of slow diffusive transport, where spatial variations in chemical concentrations and biogeochemical reactions can prevail. To investigate how aggregate-scale transport affects microbial selenium reduction rates and sequestration, to assess the impact of rate limiting factors, and to quantify emergent chemical gradients, we conducted a series of controlled flow-through experiments utilizing three-dimensional, artificial soil aggregates (ID 2.5 cm) surrounded by a macropore. Aggregates were composed of either pure quartz sand or ferrihydrite-coated quartz sand inoculated with one of two selenium reducing bacteria (*Thauera selenatis* or *Enterobacter cloacae* SLD1a-1). Oxic and anoxic conditions were compared, as well as various selenate (0.25-0.8 mM) and carbon source (0.3 and 1.2 mM) input concentrations. In the absence of ferrihydrite the majority of reduced selenium was exported from aggregates in the form of selenite. Selenite export rates varied between 0.02±0.01 and 3.4±0.2 nmol/h/$g_{aggregate}$ as a function of aeration condition and input solution composition (higher selenate or C-source concentrations led to higher selenite export). The presence of oxygen in the input solution significantly decreased selenium reduction, however, the detection of selenite in effluent samples indicates the occurrence of anoxic microzones within aggregates. Furthermore, we found that solid phase concentrations of reduced selenium increased towards the core of aggregates and are estimated to at least double within the first mm into the aggregate under all conditions investigated. This indicates that concentrations of reduced selenium may generally be expected to increase with distance from the advection boundary (macropore) inside aggregates, which would imply that soils with larger aggregates retain more selenium.

1. Introduction

Selenium (Se) is an essential micronutrient for animals and microorganisms used in the synthesis of the seleno-amino acids selenocysteine and selenomethyonine (Prakash et al., 2010; STOLZ et al., 2006). Selenium is also known to bioaccumulate within the base of the food chain, and then biomagnify to elevated concentrations that can be toxic to birds, fish, and mammals (Dungan and Frankenberger, 1999; Muscatello et al., 2008). Humans, for example, need between 30 and 85 μg day^{-1} of selenium, while chronic toxicity ensues for intakes of 400 μg day^{-1} (Lenz and Lens, 2009). Due to the narrow

intake range between selenium toxicity and deficiency, ecosystems affected by both phenomena occur globally (Haygarth, 1994).

Selenium is heterogeneously distributed across terrestrial landscapes, with seleniferous soils (>0.5 mg/kg) and those marked by selenium deficiency (<0.1 mg/kg) sometimes occurring as close as 20 km from one another (Lenz and Lens, 2009). On top of this natural heterogeneity, human interventions play a critical role in mobilizing selenium through the mining of coal, gold, silver and nickel, combustion of fossil fuels, and smelting operations (Lemly, 2004). Humans also play a major role in releasing selenium from soils to fragile aquatic and wetland ecosystems through agricultural irrigation practices. Selenium contamination of aquatic habitats is of global concern (Lemly, 2004), and in the Western United States alone, more than 150,000 square miles are susceptible to irrigation-induced Se contamination (Seiler et al., 1999).

The mechanisms leading to ecological toxicity of selenium are inextricably linked with the element's complex biogeochemical behavior. Selenium occurs naturally in four oxidation states: Se(-II), Se(0), Se(IV) and Se(VI) that vary widely with respect to their solubility, sorptive behavior and toxicity/bioavailability. The primary oxidation states associated with environmental Se toxicity, Se(VI) and Se(IV), occur as bioavailable oxyanions: selenate (SeO_4^{2-}) and selenite (SeO_3^{2-}) (Dungan and Frankenberger, 1999). Selenate sorbs weakly, while selenite forms strong stable complexes on the surfaces of minerals including ferrihydrite, goethite, hematite, apatite and manganese dioxide (Balistrieri and Chao, 1990; Catalano et al., 2006; Duc et al., 2003; Su and Suarez, 2000). Selenite is thus less mobile than selenate.

The reduction of selenate to selenite, insoluble elemental Se(0), and organic Se(-II) (including gaseous, methylated forms) takes place primarily via microbial dissimilatory reduction (Stolz and Oremland, 1999). Abiotic reduction has also been observed, but only under highly reducing conditions atypical of surface and shallow subsurface environments (Charlet et al., 2007; Myneni et al., 1997). Microbial reduction of bioavailable selenium oxyanions to solid Se(0) is thus widely viewed as one of the primary attenuation pathways for selenium in surface soils (Dungan and Frankenberger, 1999; Frankenberger and Arshad, 2001; Losi and Frankenberger, 1997a; Wu, 2004).

Selenium-reducing microorganisms are found across many bacterial genera (Stolz et al., 2006; Stolz and Oremland, 1999) and even among Archaea (Huber et al., 2000). Among the bacterial strains of selenium-reducers isolated to date, *Thauera selenatis* and *Enterobacter cloacae* SLD1a-1 have been studied most extensively (Cantafio et al., 1996; Leaver et al., 2008; Losi and Frankenberger, 1997b; Ma et al., 2007; Ma et al., 2009; Macy, 1994; Maher and Macy, 2002; Maher et al., 2003; Rech and Macy, 1992 Yee and Kobayashi, 2008; Yee et al., 2007). Both are known to reduce selenate *via* selenite to elemental Se (Dungan and Frankenberger, 1999). The selenate reductases for both organisms have been purified and analyzed exhibiting very different values in their half-saturation constant K_m (10 μM for *T. selenatis* and 2,000 μM for *E. cloacae* SLD1a-1) and maximum reaction rate V_{max} (40 μmol/min/mg for *T. selenatis* and 0.5 μmol/min/mg for *E. cloacae* SLD1a-1) (Ridley et al., 2006; Schröder et al., 1997). Both organisms are

facultative anaerobes (Losi and Frankenberger, 1998). However, whereas *T. selenatis* can grow with selenate as the sole electron acceptor for anaerobic respiration (Macy, 1994; Macy and Lawson, 1993; Macy et al., 1989; Macy et al., 1993), *E. cloacae* will not grow in the absence of other electron acceptors (Watts et al., 2003). E. cloacae can carry out selenium reduction in the presence of oxygen, though at lower rates than in the absence of oxygen (Losi and Frankenberger, 1997c), while *T. selenatis* is not known to reduce selenium in the presence of oxygen.

Within the physically complex matrix of a soil, microbial reduction is dictated by the local chemical conditions and thus subject to the soil's physical, chemical and biological heterogeneity. Aggregates, which are mm to cm sized structural units of clay, silt and sand particles bound by roots, hyphae, and organic matter (Brady and Weil, 2002), represent the smallest systems in which the spatial coupling of transport with biogeochemical reactions can be studied on a well-defined scale (Tokunaga et al., 2003). While advective solute transport is prevalent in the inter-aggregate macropores, transport in the intra-aggregate micropores is dominated by diffusion (Tokunaga et al., 2003). In conjunction with local microbial metabolic activity this often leads to the formation of strong chemical gradients within aggregates.

The importance of aggregate-scale heterogeneity in particular for local redox levels has long been recognized (Kaurichev and Tararina, 1972; Tyagny-Ryadno, 1958). Full anoxic to oxic gradients have been observed within aggregates as small as 4 mm in diameter (Sexstone et al., 1985). Tokunaga et al. (1994) showed that anoxic microzones within flat synthetic soil aggregates (1-3 cm in diameter) are likely to support localized sites of Se reduction and documented transport-controlled reduction of soluble Cr(VI) to solid Cr(III) taking place exclusively within the surface layer of natural soil aggregates (9 to 15 cm dimensions) immerged in a Cr(VI) solution (Tokunaga et al., 2003). Pallud et al. (2010a; 2010b) recently investigated ferrihydrite reduction in anoxic flow-through experiments utilizing novel artificial aggregate systems that closely mimic field transport conditions in structured soils and found strong radial gradients in secondary mineralization products as a result of mass-transfer limitations. Utilizing the same artificial aggregate systems, Masue-Slowey et al. (2011) investigated arsenic reduction and release in artificial aggregates surrounded by oxic solution and found through reactive transport modeling that the development of an anoxic region within the aggregate best described their experimental results. Given the valuable insights that these novel aggregate reactors systems have shed on the dynamics of iron and arsenic redox chemistry at the aggregate-scale an application to selenium reduction appears consequential. The dynamics of selenium cycling at the aggregate-scale are expected to differ drastically from those investigated so far in these systems, since unlike arsenic, selenium is an example of a contaminant that can be reductively immobilized from solution in soils.

In this study I present data on selenium reduction from a series of flow-through reactor experiments utilizing these novel aggregate reactor systems that mimic the dual porosity of structured soils with a microporous artificial soil aggregate contained in a flow-through reactor macropore. Our guiding hypothesis was that aggregate-scale

transport coupled to microbial selenium reduction will lead to systematic spatial concentration gradients within aggregates. Similarly to what has been observed for iron minerals and arsenic (Pallud et al., 2010a, 2010b; Masue-Slowey et al., 2011), we expected the Se reduction rates and emergent gradients to depend on the bulk chemical concentrations of carbon source and electron acceptor, aeration conditions, microbial activity, and the presence of sorptive phases in the solid matrix of aggregates. Our objective was thus to assess the impact of these factors on aggregate-scale selenium reduction and transport as well as to characterize emergent chemical gradients. Aggregates were made of sand or ferrihydrite-coated sand, to assess the impact of sorption on selenium reduction and transport, and initially contained a homogenous distribution of either *Thauera selenatis* or *Enterobacter cloacae* SLD1a-1 as model selenium-reducer. Experiments were performed under oxic and anoxic conditions to constrain the influence of oxygen on Se reduction. Different concentrations of organic carbon sources and selenate were examined since they are key limiting factors for microbial Se reduction. Temporally resolved data on selenate and selenite concentrations at the reactor outflow and spatially resolved data on solid phase Se species within the aggregates was collected. We show that the coupling between physical and biogeochemical factors in our systems leads to increasing concentrations of reduced selenium in the solid phase towards the core of aggregates under a diverse set of conditions and that the investigated experimental factors have a predictable yet aggregate dynamics specific (i.e. not captured by bulk dynamics) impact on reduction rates. Insights gained here have the potential to improve our capacity to predict Se transport and attenuation in structured soils, thereby facilitating the management of selenium contaminated soils.

2. Materials and Methods

2.1. Artificial aggregate construction

Spherical (2.5 cm diameter) aggregates were constructed in the laboratory using the protocol developed by Pallud et al. (2010b). Aggregates were composed of either pure fine quartz sand (IOTA® 4 pure quartz powder, grain size of 150-250 μm, Unimin Corporation) or ferrihydrite-coated quartz sand (8-10 $g_{Fe}/kg_{aggregate}$, synthesis (Schwertmann and Cornell, 2000) and coating (Pallud et al., 2010b) as previously described), and contained a homogenous distribution of either *E. cloacae* or *T. selenatis.* The purpose of these simple solid matrices is to control the physics and chemistry of aggregate systems, perform reproducible experiments, and isolate effects of aggregate scale transport with a well constrained set of biogeochemical reactions. Before constructing aggregates, sand was inoculated with one bacterial strain to a density of approximately 10^8 cells/g dry aggregate mass (confirmed *via* colony forming unit (CFU) plate counts on 30 g/L tryptic soy broth or minimal medium (Macy et al., 1989) agar, 15 g/L, for *E. cloacae* and *T. selenatis* respectively). No carbon source or selenium was present in the aggregates at time of synthesis. The inoculated sand, mixed with hydrogel agarose to promote particle aggregation (150 g of 0.5 wt % agarose, 30 mL of bacterial

suspension and 300 g of sand), was molded into aggregates using a spherical press. Physical similarity of constructed and natural soil aggregates has previously been confirmed by Hg-porosimetry measurements (performed on ferrihydrite coated sand aggregates): Their apparent dry bulk density is 1.19 g/cm^3, they have an average pore diameter of approximately 39 μm, and a porosity of 0.58 (Pallud et al., 2010b).

2.2. Flow-through reactor experimental set-up and input solutions

Each aggregate was placed at the center of a cylindrical reactor cell (5.1 cm ID, 3.7 cm long) filled with either oxic or anoxic input solution. The input solution consisted of artificial groundwater medium (prepared in 10 mM PIPES and containing (in mg/L): NaCl, 30; NH_4Cl, 0.95; KCl, 5; $MgSO_4$, 50; KH_2PO_4, 0.950 and 1 mL/L mineral Wolfe's solution) with a final selenate concentration of 0.25, 0.4, 0.5 or 0.8 mM and a final pyruvate or acetate (for *E. cloacae* and *T. selenatis* experiments, respectively) concentration of 0.3 or 1.2 mM (from a filtered-sterile stock solution) to investigate the impact of reactant concentrations. The pH was adjusted to 7.2. The composition of input solutions remained constant throughout. Constant flow rates of 1 mL/h were imposed at the reactor's lower boundary (±0.1 mL/h for series involving *E. cloacae* and ±0.3 mL/h for series involving *T. selenatis*) using a peristaltic pump and effluent samples were collected in 8 hour increments for 160-192 hours. For aggregate-reactor systems like the ones employed in this study these flow rates result in diffusion-dominated transport within aggregates (Pallud et al., 2010a). **Table 1** summarizes the experimental conditions of performed series.

Table 1: Overview of experimental conditions and measurements. The symbol + indicates that measurements were performed, whereas the symbol – indicates that measurements were not obtained. All listed experiments consisted of two separate aggregate-reactor systems with a C-source concentration of either 0.3 mM or 1.2 mM respectively (pyruvate for E. cloacae, acetate for T.selenatis). b.d. (below detection) marks series with no detectable selenite export.

Experimental conditions				Measurements		
Bacterial strain	Ferrihydrite coating	Aeration condition	Input selenate concentration (mM)	Selenite export	Solid phase concentration	
					Selenate	Reduced Selenium
E. cloacae	no	oxic	0.25, 0.4, 0.5, 0.8	+	+	+
E. cloacae	no	anoxic	0.25, 0.4, 0.5, 0.8	+	+ (0.4, 0.8)	+ (0.4, 0.8)
E. cloacae	yes	oxic	0.25, 0.5	+ (b.d.)	+	+
T. selenatis	no	oxic	0.25, 0.5	+	+	–
T. selenatis	no	anoxic	0.25, 0.5	+	–	–
T. selenatis	yes	oxic	0.25, 0.5	+ (b.d.)	+	–

Anoxic experiments were fully contained within an anaerobic chamber with palladium catalysts and N_2/H_2 headspace (Coy Laboratories, Inc., Grass Lake, MI), and the input solutions were made anoxic by purging with O_2-free N_2 for 15 minutes. For oxic experiments, thorough aeration of the solution surrounding aggregates was achieved by using oxic input solutions and continuously bubbling air into the reactor cells. At the end of experiments aggregates were manually shaved using a sterile stainless razor blade into three concentric sections (core: radius 0-5 mm, mid-section: radius 5-9 mm, and exterior: radius 9-12.5 mm, corresponding to relative volumes of 6.4%, 30.9% and 62.7%, respectively) for solid phase Se extractions. Bacterial counts (see section 2.1) were conducted with solid material from dissected aggregate sections from a series of 4 oxic and 4 anoxic aggregates, but no significant differences between sections were found.

2.3. Selenium speciation analysis in liquid samples and selenite export rates

Effluent samples and solid phase extraction products from flow-through experiments were analyzed for total Se and selenite concentrations using a Perkin Elmer 5300 DV inductively coupled plasma-optical emission spectrometer (ICP-OES). Total Se was determined using the ICP-OES operating in regular mode and selenite concentrations were measured *via* ICP-OES coupled to a hydride generation set-up based on the phase separator set-up described by Bosnak and Davidowski (2004) and with flow rates as those used by Brooks (1991) in manifold 2 (HG-ICP-OES). A sample injection time of 120 seconds prior to optical emission reading and a rinse time of at least 30 seconds with an additional 100 seconds following samples exceeding 150 ppb were used, due to a significant memory effect. Elemental and speciation standards were prepared from certified reference stock solutions (VHG Labs, Inc.) in a matrix matching the composition of measured samples (standards used for the measurement of extraction products thus contained the same nitric acid concentrations as the diluted extraction products, namely 3.2 or 1.6 mM HNO_3). Selenate concentrations were computed as the difference between total selenium and selenite concentrations. All selenite concentrations measured in effluent samples were corrected from trace concentrations in the input solutions (impurities of approximately 0.005 moles of selenite per mole of selenate). Selenite export rates for each reactor were then computed by multiplying effluent concentrations at quasi-steady-state by the flow-rate and normalizing by aggregate dry mass. These quasi-steady-state concentrations were obtained by averaging across a time-span of at least 64 h, or eight consecutive 8 h samples.

2.4. Solid phase extraction

Solid phase extraction was performed using a modified version of the nitric acid extraction as performed by Antanaitis et al. (2008). The method was modified by lowering the extraction temperature to 26°C to avoid volatilization (Bem, 1981) and by increasing the extraction time to 16h. With such method, we obtained adequate recoveries in quality control samples, while also preserving the speciation of selenate and selenite. After thorough grinding of samples in a quartz mortar, solid phase extractions were performed on 0.5 g (dry weight) sub-samples in 5 mL of 16 M HNO_3 in sealed Teflon vessels placed on a rotary shaker inside an incubator set at 26°C for 16-24h. Triplicate

extractions were performed for the exterior and mid sections of each aggregate and duplicate extractions for the core sections, due to limited sample amount. After extraction, selenate and selenite concentrations in the extraction products from aggregate sections were determined using ICP-OES/HG-ICP-OES (see section 2.3). The average recoveries for quality control samples spiked with various amounts of selenate and selenite (between 0.05 and 10 μmol/g) were 98±15% for selenite (from 10 samples) and 97±5% for total selenium (from 17 samples). No difference in recoveries was observed between the quality control samples for the ferrihydrite coated sand and the pure sand. Both Se(IV) and total Se were below the detection limit in control (non-spiked) samples. Due to the possible production of solid elemental selenium in our systems, we also tested our method with known amounts of elemental selenium (Alfa Aesar®, Ward Hill, MA) to determine its chemical fate during extraction. It resulted that any elemental selenium was oxidized to selenite during extraction: the recoveries of triplicate quality control samples containing 2, 5, and 50 μg of elemental selenium were 103±16%, 94±5%, and 102±2% measured as selenite *via* HG-ICP-OES. We consequently cannot distinguish between selenite and elemental selenium in our solid phase extracts and are reporting measures of the "reduced selenium" fraction (selenite and elemental selenium) and selenate in analyzed solid phase samples.

2.5. Statistical Analysis

All statistical analyses were performed using IBM®SPSS® Statistics v.19. The threshold for statistical significance used was $P<0.01$ for all tests. Statistical difference between groups of selenite export rates was tested using one-way ANOVA with post-hoc comparison *via* the least significant difference (LSD) method. Impact of experimental conditions and sample type on solid phase selenate concentrations was assessed using hierarchical ANOVA with the factor sequence (degrees of freedom): aeration conditions (df=1), bacterial strain (df=1), solid matrix type (df=1), input selenate concentration (df=3), input carbon source concentration (df=1), and aggregate section (df=2).

3. Results

Results are expressed as the mean of measurements ±1 standard deviation unless otherwise stated.

3.1. Selenite export rates and estimated reduction rates

Selenite export rates represent the fraction of reduced selenium that is exported from aggregates in the form of selenite. While not equivalent to bulk reduction rates due to the retention of reduced selenium in the solid phase, they are a lower bound for bulk selenium reduction and are expected to scale with bulk reduction in the absence of an adsorbent such as ferrihydrite. No selenite was detected in the outflow from reactors containing ferrihydrite-coated sand aggregates, hence selenite export rates were not obtained. For reactors containing pure sand aggregates, selenite export rates varied between 0.02±0.01 and 3.4±0.2 nmol of selenite/h/$g_{aggregate}$ (**Fig. 1**).

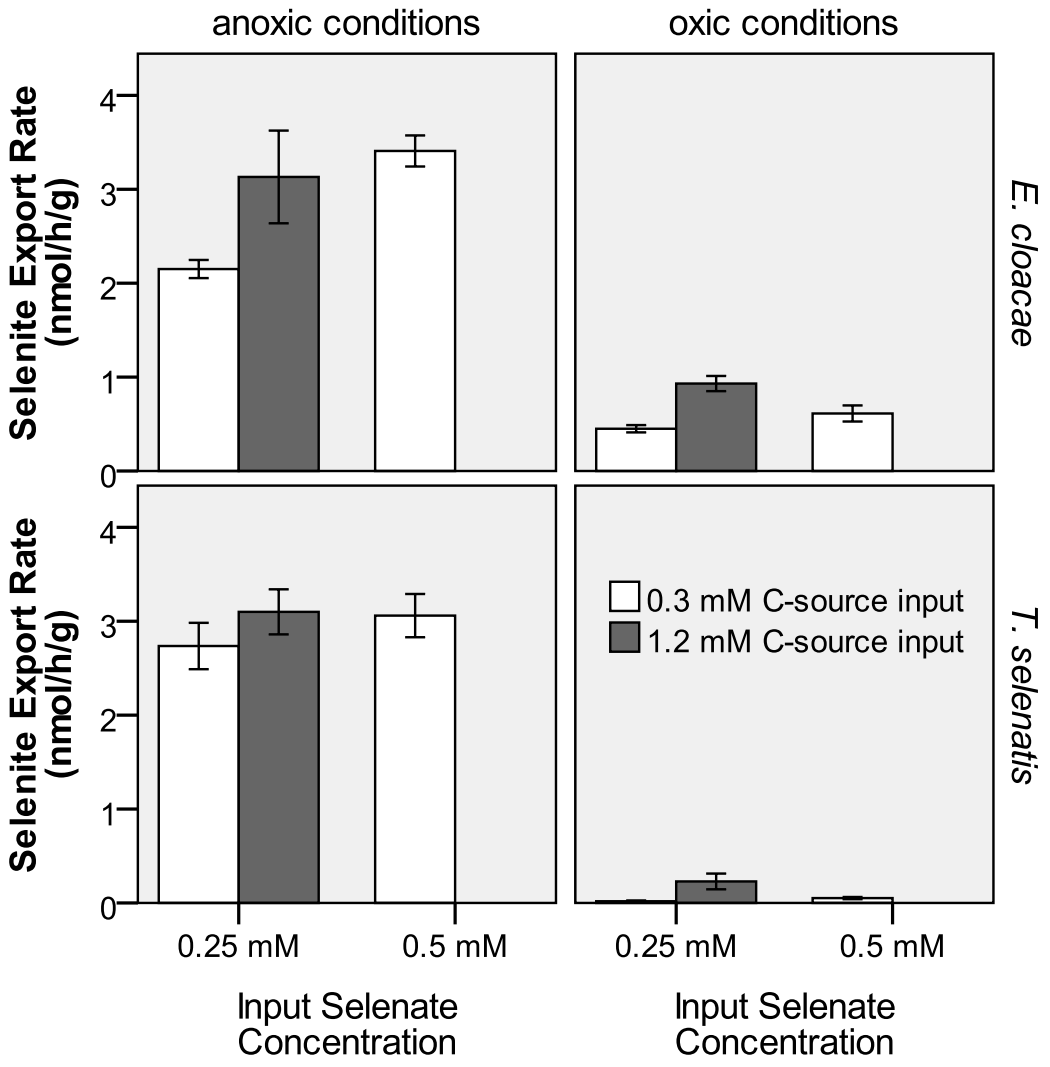

Figure 1: Selenite export rates averaged across time points measured at quasi-steady state (as described in section 2.3) as a function of input solution concentration, anoxic vs. oxic conditions and the bacterial strain for experiments run with pure sand aggregates. Selenite export rates were below detection limit for experiments with ferrihydrite-coated sand aggregates. Error bars represent standard deviations around the mean of averaged time points ($8 \leq n \leq 17$).

Under anoxic conditions, selenite export rates ranged between 2.2±0.1 and 3.4±0.2 nmol of selenite/h/$g_{aggregate}$. While the export rates for *E. cloacae* and *T. selenatis* were numerically similar under anoxic conditions we discuss them separately given the different carbon sources used and the differences between the metabolisms of the two strains. Both higher input concentrations of the C-source and of selenate resulted in

higher selenite export rates. Doubling the input concentrations of selenate from 0.25 to 0.5 mM resulted in an increase in the selenite export rate from 2.2±0.1 to 3.4±0.2 nmol of selenite/h/$g_{aggregate}$ for *E. cloacae* and from 2.7±0.3 to 3.1±0.2 nmol of selenite/h/$g_{aggregate}$ for *T. selenatis* (P<0.01). Quadrupling the C-source concentration from 0.3 mM to 1.2 mM led to an increase in selenite export rates from 2.2±0.1 to 3.2±0.5 nmol of selenite/h/$g_{aggregate}$ for *E. cloacae* and from 2.7±0.3 to 3.1±0.2 nmol of selenite/h/$g_{aggregate}$ for *T. selenatis* (P<0.01).

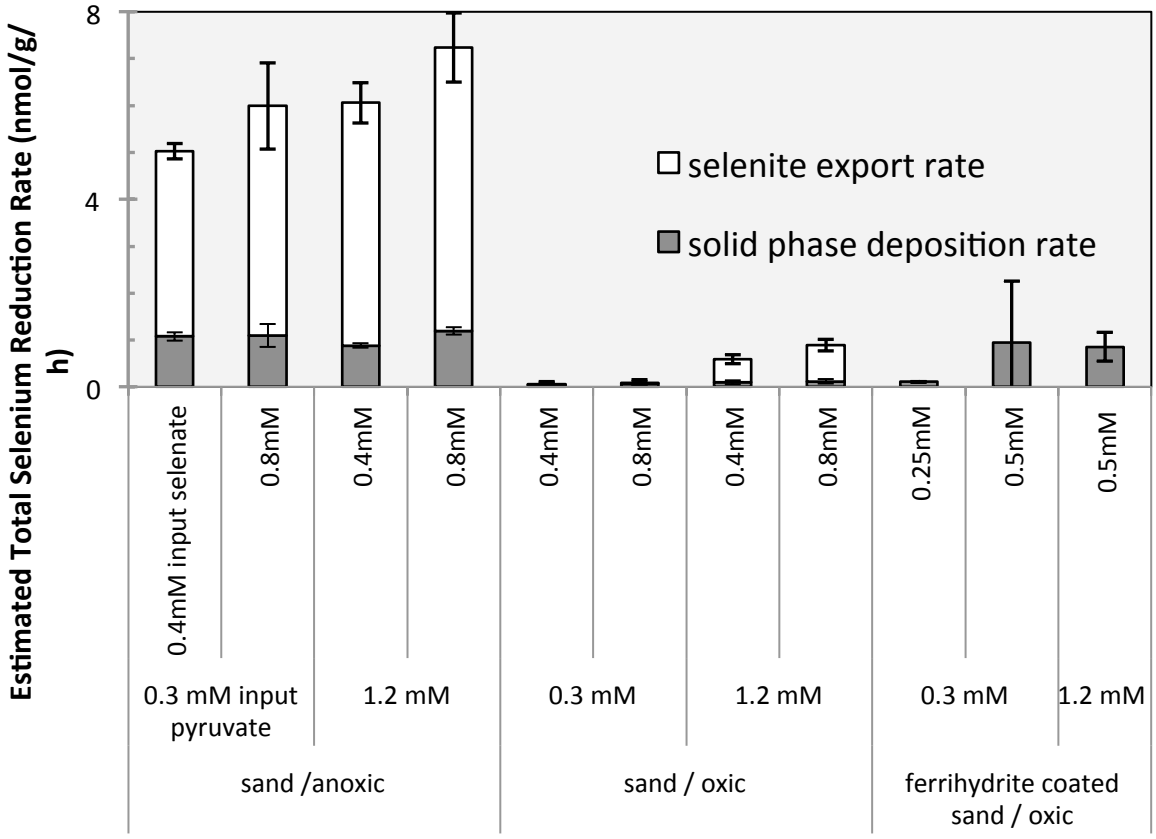

Figure 2: Estimated total selenium reduction rates from experiments with *E. cloacae* as a function of experimental conditions (selenate input concentrations, pyruvate input concentrations, and solidphase composition / aeration conditions). Lower error bars represent the standard deviation of solid phase measurements divided by experiment duration and upper error bars represent this standard deviation plus the standard deviation of the mean steady-state selenite export rate.

Overall, selenite export rates were lower by a factor of about 5 and 10-100 under oxic conditions than under anoxic conditions (**Fig. 1**) for *E. cloacae* and *T. selenatis* respectively. Under oxic conditions, selenite export rates were consistently lower for *T. selenatis* (0.02±0.01 to 0.2±0.1 nmol/h/$g_{aggregate}$) than for *E. cloacae* (0.45±0.04 to 0.9±0.1 nmol/h/$g_{aggregate}$). Higher input concentrations of the C-source resulted in

increased selenite export rates. Quadrupling the C-source concentration increased selenite export rates from 0.45±0.04 to 0.9±0.1 nmol/h/$g_{aggregate}$ for *E. cloacae* and from 0.02±0.01 to 0.2±0.1 nmol/h/$g_{aggregate}$ for *T. selenatis* (P<0.01).

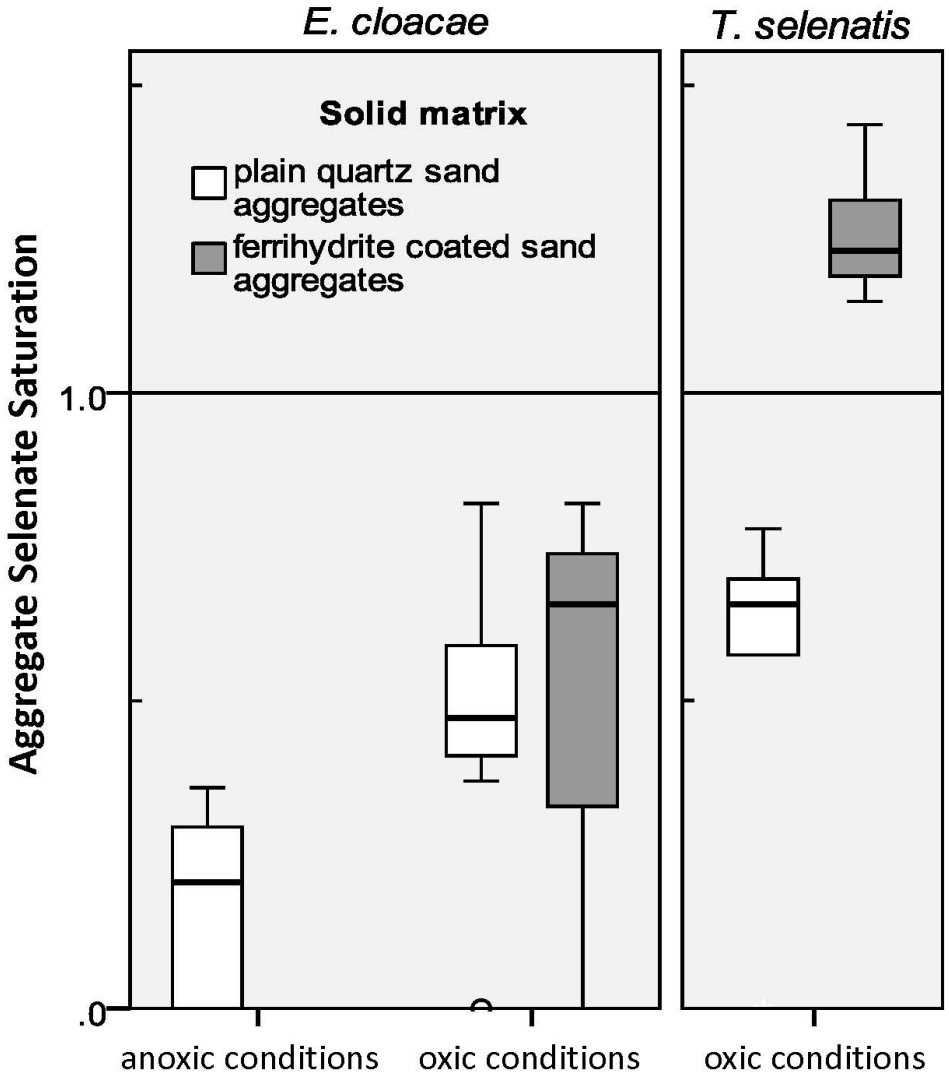

Figure 3: Ratio of aggregate to input solution selenate concentrations by solid matrix and aeration conditions. Values higher than 1 indicate, that selenate partitioned to the solid phase from the solution (i.e. sorption), and values lower than 1 indicate that consumption of selenate inside aggregates exceeded diffusive supply from the surrounding solution. Values below the detection limit where set to zero. The boxplot shows the full range of measurements (fences), the range between first and third quartile (bar), and the median value (horizontal line inside bar). A single outlier is shown as a circle (*E. cloacae*, plain quartz sand matrix, oxic conditions).

Total selenium reduction rates were estimated for the eleven aggregates for which solid phase selenite data was available (*E. cloacae*) (**Fig. 2**). Any selenium reduced inside the aggregate must either have been exported in the form of dissolved selenite or retained within the aggregate solid phase. We used the solid phase reduced selenium measurements in conjunction with selenite export rates to estimate total selenium reduction rates. Assuming that reduced selenium was deposited in the solid phase at a constant rate throughout the course of experiments, we determined the rate of deposition by dividing the solid phase concentrations (determined at experiment conclusion) by the duration of experiments. It is possible that solid phase deposition rates were in fact higher (due to increased selenite concentrations in solution) or lower (due to solid phase saturation) at the time at which pseudo steady-state was reached in selenite export, but this represents the best estimate available to us. It can be seen that in the absence of ferrihydrite most reduced selenium is exported as selenite rather than deposited in the solid phase.

3.2. Selenate solid phase concentrations

Solid phase selenate concentrations ranged from below detection limit to 0.35±0.04 $\mu mol/g_{aggregate}$ for all experiments and aggregate sections (data not shown). Solid phase selenate concentrations did not differ significantly between sections of the same aggregate or aggregates run with different C-source concentrations but otherwise identical conditions (hierarchical ANOVA P=0.35 and 0.09 respectively).

To isolate reactive transport effects on solid phase selenate from those due to different selenate input concentrations, solid phase selenate concentrations were normalized with respect to the concentrations expected in an unreactive porous medium (i.e. in a solid matrix with pore spaces fully saturated with input solution). This value, here referred to as aggregate selenate saturation, was obtained by multiplying the input selenate concentration by 0.49 mL/g, which is the ratio of the porosity and the bulk density of the aggregate material used, and ranged from 0.12 to 0.39 $\mu mol/g_{aggregate}$ for selenate input concentrations ranging between 0.25 and 0.8 mM. The ranges of aggregate selenate saturations categorized according to aeration condition, bacterial strain, and solid matrix are shown in **Fig. 3**. Values higher than 1 indicate that selenate partitioned to the solid phase from the solution (i.e. sorption), and values lower than 1 indicate that consumption of selenate inside aggregates exceeded diffusive supply from the surrounding solution. The aggregate selenate saturation varied from below detection limit for solid phase samples from pure sand aggregates run under anoxic conditions utilizing *E. cloacae* to 129±9% for solid phase samples from ferrihydrite coated sand aggregates run under oxic conditions utilizing *T. selenatis*. Hierarchical ANOVA revealed that aeration conditions, bacterial strain, solid matrix and input selenate concentrations all had a significant impact ($P<0.01$) on aggregate selenate saturation (in order of decreasing importance). F-values were 54, 44, 24 and 7.8 for aeration conditions, bacterial strain, solid matrix and input selenate concentrations respectively. Increasing concentrations of selenate in the input generally led to increasing aggregate selenate saturation. Ferrihydrite coating and oxic conditions generally led to increased saturation, while inoculation with

E. cloacae generally led to lower selenate saturation as compared to inoculation with *T. selenatis* (**Fig. 3**).

3.3. Reduced selenium solid phase concentrations

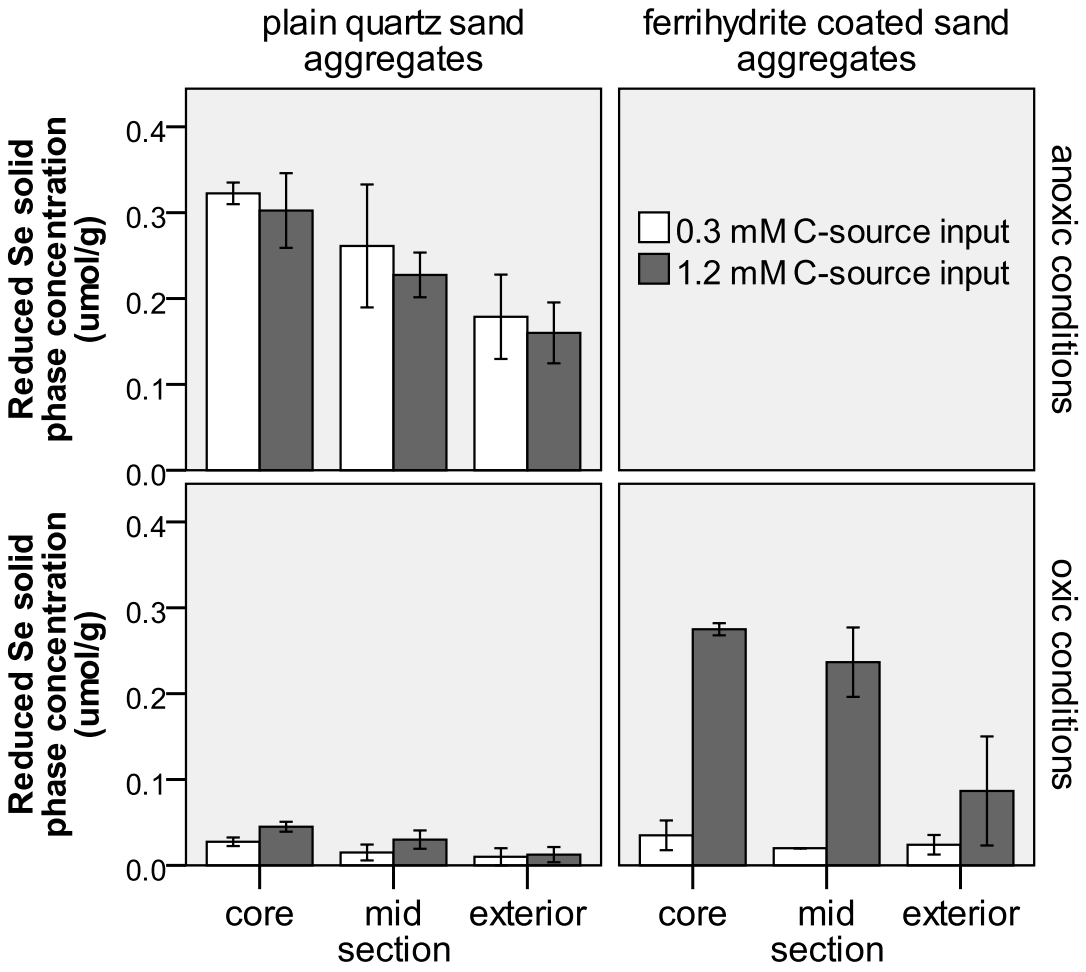

Figure 4: Reduced selenium solid phase concentrations from *E. cloacae* experiments categorized by aggregate section. Each bar represents the mean of six extractions/measurements (four for core sections) from two aggregates run with 0.4 and 0.8 mM selenate input solution respectively (0.25 and 0.5 mM for ferrihydrite experiments). Error bars reflect standard deviations around the mean.

Reduced selenium solid phase concentrations in the aggregate exterior, mid-section and core ranged from 0.01±0.01 to 0.34±0.01 μmol/$g_{aggregate}$ (**Fig. 4**). There is a consistent trend for reduced selenium solid phase concentrations to increase from the exterior to the interior of aggregates. The lowest concentrations were observed for the exterior sections of pure sand aggregates run under oxic conditions. The highest reduced selenium solid phase concentrations were observed for the core sections of pure sand

aggregates run under anoxic conditions (anoxic experiments with ferrihydrite coated sand aggregates were not performed).

Reduced selenium solid phase concentrations in pure sand aggregates were significantly higher under anoxic conditions as compared to oxic conditions, while for both sets of conditions neither the input concentration of selenate nor that of pyruvate had a significant effect. The solid phase concentrations of reduced selenium in ferrihydrite coated sand aggregates from oxic experiments displayed particularly large variation (0.017 ± 0.002 to 0.27 ± 0.01 $\mu mol/g_{aggregate}$) but were on average higher than those in pure sand aggregates. The aggregate run with the highest selenate (0.5 mM) and pyruvate (1.2 mM) input concentrations stands out as having significantly higher reduced selenium solid phase concentrations as compared with the two ran with 0.3 mM pyruvate (one at 0.25 and the other at 0.5 mM selenate).

4. Discussion

4.1. Impact of aeration conditions on solid phase selenate concentrations and selenium reduction rates

We used selenite export rates as a proxy for bulk selenium reduction. While as discussed in section 3.1 total reduction rates are expected to be somewhat higher then selenite export rates due to solid phase deposition inside the aggregate (**Fig. 2**), the export rates do provide a hard lower bound for reduction rates. Selenite export rates were lower under oxic than under anoxic conditions, indicating lower selenium reduction rates in the presence of oxygen. Lower selenium reduction rates reflect the ability of *E. cloacae* to reduce selenate in the presence of oxygen, but at lower rates than in anaerobic conditions (Losi and Frankenberger, 1997b; Yee and Kobayashi, 2008). However, since there is no evidence that *T. selenatis* can carry out selenate reduction in the presence of oxygen, the observed selenite export for the oxic experiments is an indication of the existence of anoxic micro-zones within the aggregate. Anoxic zones may arise if the consumption of oxygen by *T. selenatis via* oxic respiration exceeds diffusive supply of oxygen into the aggregate from the surrounding solution. These zones enable selenium reduction within the aggregate, similar to what has long been known in the context of denitrification within natural soil aggregates (Sexstone et al., 1985). Reactive transport modelling conducted for analogous systems investigating arsenic desorption (Masue-Slowey et al., 2011) demonstrates that anoxic zones arise from aerobic respiration in artificial aggregates of this size and composition.

The lower solid phase selenate concentrations observed under anoxic conditions as compared to oxic conditions indicate that transport of selenate from the surrounding solution into the aggregate is slower than consumption within the aggregate *via* reduction. This is further evidence that soil structure and diffusion-dominated transport within aggregates can impact selenium reduction. Aggregates may thus promote selenium reduction and retention in a soil by creating anoxic environments conducive to the process and drawing mobile, bioavailable selenium from the surrounding soil solution.

4.2. Impact of input solution composition on selenium reduction rates

The impact of input solution composition on selenite export rates is in accordance with expectations about the reaction kinetics of microbially-mediated selenate reduction. The observed decrease of the export rates with decreasing input concentrations of selenate and C-source can be understood in the context of a simple model based on Monod kinetics. The classical Monod relationship is still the most widely used expression for microbial reaction kinetics and where the possibility that both the electron donor and acceptor are controlling reaction kinetics exists, the so called double-Monod is usually the tool of choice (Rittman and VanBriesen, 1996):

$$\frac{1}{n}\frac{d[\mathrm{SeO_4^{2-}}]}{dt} = -v_{\max}\cdot\frac{[\mathrm{SeO_4^{2-}}]}{K_m^{\mathrm{SeO_4^{2-}}}+[\mathrm{SeO_4^{2-}}]}\cdot\frac{[DOC]}{K_m^{\mathrm{SeO_4^{2-}}}+[DOC]} \qquad (1)$$

where n is the local cell density of the selenate reducers (cells/µL), $[\mathrm{SeO_4^{2-}}]$ and $[DOC]$ are the local concentrations of selenate and C-source respectively (mM), $v_{\max}$ is the maximal cellular selenate reduction rate (nmol/h/cell), and $K_m^{\mathrm{SeO_4^{2-}}}$ and K_m^{DOC} are the half-saturation constants for selenate and C-source respectively (mM). In the absence of other selenite sources or sinks we can write:

$$\frac{d[\mathrm{SeO_3^{2-}}]}{dt} = -\frac{d[\mathrm{SeO_4^{2-}}]}{dt} = n\cdot v_{\max}\cdot\frac{[\mathrm{SeO_4^{2-}}]}{K_m^{\mathrm{SeO_4^{2-}}}+[\mathrm{SeO_4^{2-}}]}\cdot\frac{[DOC]}{K_m^{DOC}+[DOC]} \qquad (2)$$

Ignoring intra-aggregate transport/heterogeneity of selenate, selenite and C-source in the aggregate reactor system would lead to the expectation that selenite export rates depend on input concentrations in roughly the same fashion:

$$E \approx E_{\max}\cdot\frac{[\mathrm{SeO_4^{2-}}]}{K_m^{\mathrm{SeO_4^{2-}}}+[\mathrm{SeO_4^{2-}}]}\cdot\frac{[DOC]}{K_m^{DOC}+[DOC]} \qquad (3)$$

where E and $E_{\max}$ are the selenite export rate and the maximum selenite export rate respectively. To investigate where the assumption of aggregate homogeneity breaks down, we have applied this simple model to our selenite export rate data from pure quartz sand aggregate experiments and obtained a set of best-fit half-saturation constants, as well as estimates for maximum selenite export rates (**Table 2**). Whereas the limited number of data points available for model fitting, in particular with *T. selenatis*, prevents us from drawing quantitative conclusions, the model application reveals two noteworthy points.

Firstly, it becomes evident that the response of the aggregate reactor systems to input selenate and C-source concentrations adheres fairly closely to Monod kinetics under anoxic conditions, but not at all under oxic conditions: Estimated maximum selenite export rates ($E_{\max}$) under anoxic conditions displayed relative standard

deviations (RSD) of 12.4% and 0.4% for *E. cloacae* and *T. selenatis* respectively, as compared to 38.1% and 107.6% under oxic conditions. While increases of selenate or C-source in the input concentration still lead to increased selenite export under oxic conditions, the introduction of oxygen into the solution surrounding the aggregates appears to have a non-linear effect on selenium reduction kinetics in the aggregate-reactor system. This shows that ignoring aggregate-scale heterogeneity under bulk oxic condition is likely to yield inaccurate predictions in models.

Secondly, the difference in response to increasing selenate concentrations in the input solution for the two bacterial strains is in agreement with information available about the kinetic properties of their selenate reductases. *E. cloacae*'s selenate reductase was found to have a half saturation constant (K_m) of 2 mM (Ridley et al., 2006), while that of *T. selenatis* was found to have a K_m of 0.01 mM (Schröder et al., 1997). We observed effective K_m of 0.5 mM and 0.07 mM for *E. cloacae* and *T. selenatis* respectively and can thus confirm that the enzymatic differences between the two selenate reducers manifest at the aggregate scale. The authors are aware of only one study in which cellular kinetic parameters from a batch experiment were published for *E. cloacae* (Ma et al., 2007) and none for *T. selenatis*. Ma et al. (2007) found the K_m of *E. cloacae* to be 3.1 mM. Given the increased complexity of our aggregate systems and the fact that we are ignoring transport and fitting selenite export rates (i.e. eqn. 3) rather than reduction rates (i.e. eqn. 2) in this analysis, the difference with the K_m obtained here *via* model fitting (0.5 mM) appears modest. Both the K_m for *E. cloacae* and for *T. selenatis* aggregate systems reported here fall in the range of values observed for a diverse set of sediments in the literature (0.008-0.72 mM) (Steinberg and Oremland, 1990). Thus the differences between different selenium reducing microbes are reflected at the aggregate scale.

Table 2: Results obtained by fitting average selenite export rates with a Michaelis-Menten based model (Eq. 3). Error ranges represent standard deviations from the mean of estimates based on data obtained with the same bacterial culture and aeration condition, but different input solution concentrations.

	Best fit half-saturation constants, K_m		Estimated maximum selenite export rate, E_{max}					
			anoxic conditions			oxic conditions		
	C-source	selenate	data points	[nmol/h/g]	relative st.dev.	data points	[nmol/h/g]	relative st.dev.
	[mM]	[mM]						
E. cloacae	0.2	0.5	7	12.3±1.5	12.4%	6	2.0±0.7	38.1%
T. selenatis	0.06	0.07	3	4.1±0.0	0.4%	3	0.1±0.1	107.6%

4.3. Impact of ferrihydrite coating on selenium reduction and retention in aggregates

Aggregates composed of ferrihydrite-coated sand showed elevated solid phase concentrations of both selenate and reduced selenium and had no detectable selenite in effluent samples. In order to obtain a quantitative view of sorption to ferrihydrite we can compare experiments performed under oxic conditions for both bacterial strains with and without ferrihydrite coating, but under identical input solution compositions (i.e. 0.25 and 0.5 mM selenate).

There was no significant difference between selenate solid phase concentrations in pure quartz sand and ferrihydrite-coated sand aggregates in *E. cloacae* experiments, but this is likely due to the fact that selenate concentrations in the aggregates were limited by diffusion constraints as evidenced by the low overall solid phase selenate saturations (below 50% for pure sand aggregates) in the respective experiments. For *T. selenatis* experiments, where reduction was slower, solid phase selenate concentrations were on average 0.13±0.03 $\mu mol/g_{aggregate}$ higher in ferrihydrite coated sand aggregates as compared to pure sand aggregates. With ferrihydrite coating of 9±1 $g_{Fe}/kg_{aggregate}$ this corresponds to a surface excess of 14±2 $\mu mol/g_{Fe}$.

With regards to selenite adsorption, we compare experiments containing ferrihydrite with analogous ferrihydrite-free experiments that had selenite in the outflow. It follows from the absence of selenite in the outflow of experiments containing ferrihydrite-coated sand aggregates that selenite was sorbed by the ferrihydrite. By dividing the time integrated selenite export from ferrihydrite-free experiments by aggregate mass we can thus obtain estimates between 60–110 $nmol/g_{aggregate}$ of sorbed selenite for *E. cloacae* and between 3–25 $nmol/g_{aggregate}$ for *T. selenatis* in ferrihydrite-coated sand experiments. Since sorption of selenite was limited by production rather than sorption capacity and no kinetic sorption data can be extracted from our experiments these values cannot be compared with the literature. For *E. cloacae*, however, for which direct reduced selenium solid phase measurements are available we can see that the estimates of sorbed selenite obtained from comparing experiments with and without ferrihydrite agree with measured solid phase values of reduced selenium (20–140 $nmol/g_{aggregate}$ volume average for ferrihydrite coated sand aggregates). The observations from solution and solid phase data thus appear internally consistent across experimental conditions.

4.4. Spatial gradients of selenium retention in aggregates

Reduced selenium solid phase concentrations, which are available exclusively from *E. cloacae* experiments, increased from the exterior to the core of the aggregates under oxic as well as anoxic conditions within both pure sand and ferrihydrite-coated sand aggregates. Given the significant impact that aeration conditions and ferrihydrite coating have on total aggregate selenite export and reduced selenium retention it is remarkable how consistent this spatial trend is across investigated conditions. Reduced selenium solid phase concentrations increase with distance from the aggregate surface and linear regression between the two variables using the least-squares method yield R^2

values ranging between 0.98-1.00 for the four pure sand aggregates run under anoxic conditions, 0.92-1.00 for those run under oxic conditions, and between 0.88-1.00 for the three ferrihydrite coated sand aggregates run under oxic conditions. The slopes of the linear regression lines ranged between 1-26 nmol/g/mm, but were strictly positive. Average slopes were 21±1, 8±9, and 12±11 nmol/g/mm for pure quartz sand aggregates run under anoxic conditions, pure quartz sand aggregates run under oxic conditions, and ferrihydrite coated sand aggregates run under oxic conditions respectively. Intercepts ranged from 0.04 to 10 nmol/g and were numerically strictly smaller than the corresponding slope values, meaning that solid phase concentrations are predicted to at least double within the first mm from an aggregate surface towards its core under all investigated conditions. This indicates that concentrations of reduced selenium may generally be expected to show increases towards the core of aggregates, which would have important implications for selenium retention at a larger scale. If we generalize the result to a functional form for solid phase concentrations of reduced selenium (C_{Se}, in nmol/g):

$$C_{Se}(d) = md + b \tag{4}$$

where $d = R - r$, is the radial distance from the aggregate surface, R is the aggregate radius, r is the radial distance from the aggregates center, and m and b are positive slope and intercept constants depending on soil conditions (aeration, soil, solution, microbial community composition, time,…). An idealized spherical aggregate of constant density (ρ) and radius R would thus have an average reduced selenium concentration proportional to its size:

$$\overline{C}_{Se}(R) = \frac{\int_V C_{Se}(d)\rho \cdot dV}{\rho \cdot V} = \frac{4\pi\rho\int_0^R C_{Se}(R-r)r^2 dr}{\rho\frac{4}{3}\pi R^3} = b + \frac{mR}{4} \tag{5}$$

Consequently, under conditions that favor microbial selenium reduction, soils with larger aggregates are expected to retain larger amounts of reduced selenium as compared to soils that are composed of small aggregates.

The consistently observed trend that reduced selenium concentrations increase towards the core of our soil aggregates across oxic and anoxic conditions as well as within pure sand and ferrihydrite-coated sand aggregates rules out oxygen inhibition of selenium reduction and sorption of selenite as mechanisms causing this trend. The observed trend is in line with transport limitations: Since the flow of selenite free input solution around the aggregate acts as a sink for selenite that is produced inside the aggregate, we would expect the concentration of reduced selenium products to increase with the length of the diffusion path (i.e. towards the core of aggregates) assuming variations in the source term inside the aggregate are either insignificant or increase with the length of the diffusion path. Significant impact of mass-transfer limitations on biogeochemical transformations of ferrihydrite within aggregates has been observed and quantified in a similar system (Pallud et al., 2010a).

5. Conclusion

In this work we have shown that aggregate scale heterogeneity arising from microbial selenium reduction can be observed within simple artificial systems. Spatial heterogeneity comes into play in creating anoxic microzones that enable selenium reduction under conditions that are otherwise unfavorable and spatial heterogeneity can be observed in the increasing concentrations of the reduced product towards the core of aggregates. Aggregates may thus improve selenium retention in a soil by creating anoxic environments conducive to the reduction process and by accumulating reduced selenium at their cores. Promoting soil aggregation on seleniferous agricultural soils, through the addition of organic matter and reduction of tillage, may be an effective management practice to reduce the impacts of selenium contaminated drainage water on downstream ecosystems. This result may also be useful in the development of treatment systems designed to remove selenium from waste water, since they suggest that the usage of a dual-porosity flow-through system may be fruitful approach. The application of aggregate-reactor systems to microbial selenium reduction was thus successful in shedding light on the dynamics that control reduction in structured soils and led to the discovery of a gradient in reduced selenium concentrations at the aggregate scale that is likely to also occur in aggregates under field conditions.

We have also shown that while reduction rates at the aggregate scale depend on the same controlling factors that have been found to be important in bulk (i.e. aeration conditions, reactant concentrations, etc.), a simple bulk model (ignoring intra-aggregate scale model) misrepresents aggregate scale dynamics of selenium reduction under oxic conditions. Finally we showed that metabolic differences (enzyme kinetics) between different selenium reducing microbes (enzyme kinetics) are reflected at the aggregate scale.

While these results highlight the need to consider aggregate scale processes when discussing selenium mobility in soils, it is not evident how they will translate into the elevated complexity of natural systems. This question needs to be attacked on three fronts: (1) The complexity of model systems needs to be incrementally increased to approach that of the field. We used 3D aggregate systems rather than simple flow-through columns or 2D systems and added a level of complexity by including a sorbent phase (ferrihydrite) in select experiments. Future work however, could focus on variations in aggregate size and shape, mixed microbial communities and unsaturated flow. (2) Field measurements need to be conducted to test results obtained with model systems. We derived a simple relationship from our results that predicts an increase of reduced selenium concentrations with aggregate size in structured soils undergoing selenium reduction. This represents a testable hypothesis that could guide future field investigations. (3) Reactive transport modeling must be employed to help interpret experimental results and bridge the gap between lab and field. The persistence of the radial solid phase gradients in reduced selenium here observed across all conditions tested (oxic/anoxic, plain sand/ferrihydrite coated sand) is striking. A reactive transport model could help clarify whether diffusive intra-aggregate transport of selenate, selenite

and electron donors coupled with microbial reduction would generally be expected to produce the observed pattern in a spherical geometry. If so, the model could be modified to test a broader range of geometries, scales, and biogeochemical processes that are expected under field conditions.

6. Acknowledgements

Funding for this project was provided by the Kearney Foundation of Soil Science, by the UC Berkeley Agricultural Experiment Station, and by the Committee on Research (COR) faculty grant from UC Berkeley. I thank Christof Meile, Sharon Bone, and Melody Nocon for discussion and feedback on the manuscript; Peter Ng, Walter Mayeda, Eden Macaroy, and Eduardo Ruiz for help in sample preparation and in conducting experiments; Juyoung Ha for collecting preliminary data and providing manuscript feedback; and Paul Brooks for his assistance in developing the analytical method on the ICP-OES. I also thank anonymous referees and the editors at the Vadose Zone Journal, where a prior version of this manuscript was published.

7. References

Antanaitis, A., Lubyte, J., Antanaitis, S., Staugaitis, G., and Viskelis, P., 2008. Selenium concentration dependence on soil properties. Journal of Food, Agriculture & Environment 6, 163 - 167.

Bem, E. M., 1981. Determination of selenium in the environment and in biological material. Environmental Health Perspectives 37, 183-200.

Balistrieri, L. S. and Chao, T. T., 1990. Adsorption of selenium by amorphous iron oxyhydroxide and manganese-dioxide. Geochimica et Cosmochimica Acta 54, 739-751.

Bosnak, C. P. and Davidowski, L., 2004. Continuous flow hydride generation using the Optima ICP Field Application Reports. Perkin Elmer Life and Analytical Sciences, Shelton, CT 06484-4794 USA.

Brady, N. C. and Weil, R. R., 2002. The Nature and Properties of Soils. Prentice Hall, Upper Saddle River, NJ.

Brooks, P. D., 1991. Simplified, inexpensive, and easily constructed hydride generator for ICP analysis. Atomic Spectroscopy 12, 1-3.

Cantafio, A. W., Hagen, K. D., Lewis, G. E., Bledsoe, T. L., Nunan, K. M., and Macy, J. M., 1996. Pilot-scale selenium bioremediation of San Joaquin drainage water with Thauera selenatis. Applied and Environmental Microbiology 62, 3298-3303.

Catalano, J. G., Zhang, Z., Fenter, P., and Bedzyk, M. J., 2006. Inner-sphere adsorption geometry of Se(IV) at the hematite (100)-water interface. Journal of Colloid and Interface Science 297, 665-671.

Charlet, L., Scheinost, A. C., Tournassat, C., Greneche, J. M., Gehin, A., Fernandez-Martinez, A., Coudert, S., Tisserand, D., and Brendle, J., 2007. Electron transfer at the mineral/water interface: Selenium reduction by ferrous iron sorbed on clay. Geochimica et Cosmochimica Acta 71, 5731-5749.

Duc, M., Lefevre, G., Fedoroff, F., Jeanjean, J., Rouchaud, J. C., Monteil-Riviera, F., Dumonceau, J., and Milonjic, S., 2003. Sorption of selenium anionic species on apatites and iron oxides from aqueous solutions. Journal of Environmental Radioactivity 70, 61-72.

Dungan, R. S. and Frankenberger, W. T., Jr., 1999. Microbial transformations of selenium and the bioremediation of seleniferous environments. Bioremediation Journal 3, 171–188.

Frankenberger, W. T. and Arshad, M., 2001. Bioremediation of selenium-contaminated sediments and water. Biofactors 14, 241-254.

Haygarth, P. M., 1994. Global importance and global cycling of selenium. In: Frankenberger, W. T., Jr. and Benson, S. Eds.), Selenium in the Environment. Marcel Dekker, Inc, New York.

Huber, R., Sacher, M., Vollmann, A., Huber, H., and Rose, D., 2000. Respiration of arsenate and selenate by hyperthermophilic archaea. Systematic and Applied Microbiology 23, 305-314.

Kaurichev, I. S. and Tararina, L. F., 1972. Oxidation-reduction conditions within and outside aggregates of grey forest soil. Pochvovedenie 10, 39-42.

Leaver, J. T., Richardson, D. J., and Butler, C. S., 2008. Enterobacter cloacae SLD1a-1 gains a selective advantage from selenate reduction when growing in nitrate-depleted anaerobic environments. Journal of Industrial Microbiology and Biotechnology 35, 867-873.

Lemly, A. D., 2004. Aquatic selenium pollution is a global environmental safety issue. Ecotoxicology and Environmental Safety 59, 44-56.

Lenz, M. and Lens, P. N. L., 2009. The essential toxin: The changing perception of selenium in environmental sciences. Science of The Total Environment 407, 3620-3633.

Losi, M. E. and Frankenberger, W. T., 1997a. Bioremediation of selenium in soil and water. Soil Science 162, 692-702.

Losi, M. E. and Frankenberger, W. T., 1997b. Reduction of selenium oxyanions by Enterobacter cloacae SLD1a-1: Isolation and growth of the bacterium and its expulsion of selenium particles. Applied and Environmental Microbiology 63, 3079-3084.

Losi, M. E. and Frankenberger, W. T., 1997c. Reduction of selenium oxyanions by Enterobacter cloacae strain SLD1a-1: Reduction of selenate to selenite. Environmental Toxicology and Chemistry 16, 1851-1858.

Losi, M. E. and Frankenberger, W. T., 1998. Reduction of selenium oxyanions by Enterobacter cloacae strain SLD1a-1. In: Frankenberger, W. T. and Engberg, R. A. Eds.), Environmental Chemistry of Selenium. Marcel Dekker, New York.

Ma, J., Kobayashi, D. Y., and Yee, N., 2007. Chemical kinetic and molecular genetic study of selenium oxyanion reduction by Enterobacter cloacae SLD1a-1. Environmental Science & Technology 41, 7795-7801.

Ma, J. C., Kobayashi, D. Y., and Yee, N., 2009. Role of menaquinone biosynthesis genes in selenate reduction by Enterobacter cloacae SLD1a-1 and Escherichia coli K12. Environmental Microbiology 11, 149-158.

Macy, J. M., 1994. Biochemistry of selenium metabolism by Thauera selenatis gen. nov. sp. nov. and use of the organism for bioremediation of selenium oxyanions in San Joaquin Valley drainage water. In: Frankenberger, W. T., Jr and Benson, S. Eds.), Selenium in the environment. Marcel Dekker, Inc, New York.

Macy, J. M. and Lawson, S., 1993. Cell yield (YM) of Thauera selenatis grown anaerobically with acetate plus selenate or nitrate. Archives of Microbiology 160, 295-298.

Macy, J. M., Michel, T. A., and Kirsch, D. G., 1989. Selenate reduction by a Pseudomonas species: a new mode of anaerobic respiration. FEMS microbiology letters 61, 195-198.

Macy, J. M., Rech, S., Auling, G., Dorsch, M., Stackebrandt, E., and Sly, L. I., 1993. Thaurea selenatis gen. nov. sp. nov., a member of the beta sub-class of Proteobacteria with a novel type of respiration. International Journal of Systematic Bacteriology 43, 135-142.

Maher, M. J. and Macy, J. M., 2002. Crystallization and preliminary X-ray analysis of the selenate reductase from Thauera selenatis. Acta Crystallographica Section D-Biological Crystallography 58, 706-708.

Maher, M. J., Santini, J. M., and George, G. N., 2003. Structural studies on the selenate reductase from Thauera selenatis. Journal of Inorganic Biochemistry 96, 185-185.

Masue-Slowey, Y., Kocar, B. D., Jofré, S. A. B., Mayer, K. U., and Fendorf, S., 2011. Transport implications resulting from internal redistribution of arsenic and iron within constructed soil aggregates. Environmental Science & Technology 45, 582-588.

Muscatello, J. R., Belknap, A. M., and Janz, D. M., 2008. Accumulation of selenium in aquatic systems downstream of a uranium mining operation in northern Saskatchewan, Canada. Environmental Pollution 156, 387-393.

Myneni, S. C. B., Tokunaga, T. K., and Brown, G. E., 1997. Abiotic selenium redox transformations in the presence of Fe(II,III) oxides. Science 278, 1106-1109.

Pallud, C., Kausch, M., Fendorf, S., and Meile, C., 2010a. Spatial patterns and modeling of reductive ferrihydrite transformation observed in artificial soil aggregates. Environmental Science & Technology 44, 74–79.

Pallud, C., Masue-Slowey, Y., and Fendorf, S., 2010b. Aggregate-scale spatial heterogeneity in reductive transformation of ferrihydrite resulting from coupled biogeochemical and physical processes. Geochimica et Cosmochimica Acta 74, 2811-2825.

Prakash, D., Pandey, J., Tiwary, B. N., and Jain, R. K., 2010. Physiological adaptations and tolerance towards higher concentration of selenite (Se+4) in Enterobacter sp AR-4, Bacillus sp AR-6 and Delftia tsuruhatensis AR-7. Extremophiles 14, 261-272.

Rech, S. A. and Macy, J. M., 1992. The terminal reductases for selenate and nitrate respiration in Thauera selenatis are 2 distinct enzymes. Journal of Bacteriology 174, 7316-7320.

Ridley, H., Watts, C. A., Richardson, D. J., and Butler, C. S., 2006. Resolution of distinct membrane-bound enzymes from Enterobacter cloacae SLD1a-1 that are

responsible for selective reduction of nitrate and selenate oxyanions. Applied and Environmental Microbiology 72, 5173-5180.
Rittman, B. E. and VanBriesen, J. M., 1996. Microbial processes in reactive modeling. In: Lichtner, P. C., Steefel, C. I., and Oelkers, E. H. Eds.), Reactive transport in porous media. Mineralogical Society of America, Washington, D.C.

Schröder, I., Rech, S., Krafft, T., and Macy, J. M., 1997. Purification and characterization of the selenate reductase from Thauera selenatis. Journal of Biological Chemistry 272, 23765-23768.
Schwertmann, U. and Cornell, R. M., 2000. Iron Oxides in the Laboratory: Preparation and Characterization. Wiley VCH Publishers, New York.
Seiler, R. L., Skorupa, J. P., and Peltz, L. A., 1999. Areas susceptible to irrigation-induced selenium contamination of water and biota in the western United States U.S. Geological Survey Circular. U.S. Department of the Interior.
Sexstone, A. J., Revsbech, N. P., Parkin, T. B., and Tiedje, J. M., 1985. Direct measurement of oxygen profiles and denitrification rates in soil aggregates. Soil Science Society of America Journal 49, 645-651.
Steinberg, N. A. and Oremland, R. S., 1990. Dissimilatory selenate reduction potentials in a diversity of sediment types. Applied and Environmental Microbiology 56, 3550-3557.
Stolz, J. F., Basu, P., Santini, J. M., and Oremland, R. S., 2006. Arsenic and selenium in microbial metabolism. Annual Review of Microbiology 60, 107-130.
Stolz, J. F. and Oremland, R. S., 1999. Bacterial respiration of arsenic and selenium. FEMS Microbiology Reviews 23, 615-627.
Su, C. M. and Suarez, D. L., 2000. Selenate and selenite sorption on iron oxides: An infrared and electrophoretic study. Soil Science Society of America Journal 64, 101-111.
Tokunaga, T. K., Sutton, S. R., and Bajt, S., 1994. Mapping of selenium concentration in soil aggregates with synchrotron X-ray fluorescence microprobe. Soil Science 158, 421-434.
Tokunaga, T. K., Wan, J., Hazen, T. C., Schwartz, E., Firestone, M. K., Sutton, S. R., Newville, M., Olson, K. R., Lanzirotti, A., and Rao, W., 2003. Distribution of chromium contamination and microbial activity in soil aggregates. Journal of Environmental Quality 32, 541-549.
Tyagny-Ryadno, M. G., 1958. Aggregate biophysical-chemical analysis of soils. Pochvovedenie 12, 76-84.
Watts, C. A., Ridley, H., Condie, K. L., Leaver, J. T., Richardson, D. J., and Butler, C. S., 2003. Selenate reduction by Enterobacter cloacae SLD1a-1 is catalysed by a molybdenum-dependent membrane-bound enzyme that is distinct from the membrane-bound nitrate reductase. FEMS Microbiology Letters 228, 273-279.
Wu, L., 2004. Review of 15 years of research on ecotoxicology and remediation of land contaminated by agricultural drainage sediment rich in selenium. Ecotoxicology and Environmental Safety 57, 257-269.

Yee, N. and Kobayashi, D. Y., 2008. Molecular genetics of selenate reduction by Enterobacter cloacae SLD1a-1. Advances in Applied Microbiology 64, 107-123.
Yee, N., Ma, J., Dalia, A., Boonfueng, T., and Kobayashi, D. Y., 2007. Se(VI) reduction and the precipitation of Se(0) by the facultative bacterium Enterobacter cloacae SLD1a-1 are regulated by FNR. Applied and Environmental Microbiology 73, 1914-1920.

Chapter 3 – Modeling the impact of soil aggregate size on selenium immobilization

Abstract – Soil aggregates are mm- to cm-sized microporous structures separated by macropores. Whereas fast advective transport prevails in macropores, advection is inhibited by the low permeability of intra-aggregate micropores. This can lead to mass transfer limitations and the formation of aggregate-scale concentration gradients affecting the distribution and transport of redox sensitive elements. Selenium (Se) mobilized through irrigation of seleniferous soils has emerged as a major aquatic contaminant. In the absence of oxygen, the bioavailable oxyanions selenate, Se(VI), and selenite, Se(IV), can be microbially reduced to solid, elemental Se, Se(0), and anoxic microzones within soil aggregates are thought to promote this process in otherwise well aerated soil. To evaluate the impact of soil aggregate size on selenium retention, we developed a dynamic 2D reactive transport model of selenium cycling in a single idealized aggregate surrounded by a macropore. The model was developed based on flow-through-reactor experiments involving artificial soil aggregates (diameter: 2.5 cm) made of sand and containing *Enterobacter cloacae* SLD1a-1 that reduces Se(VI) via Se(IV) to Se(0). Aggregates were surrounded by a constant flow providing Se(VI) and pyruvate under oxic or anoxic conditions. In the model, reactions were implemented with double-Monod rate equations coupled to the transport of pyruvate, O_2, and Se-species. The spatial and temporal dynamics of the model were validated with data from experiments and predictive simulations were performed covering aggregate sizes between 1-2.5 cm diameters. Simulations predict that selenium retention scales with aggregate size. Depending on O_2, Se(VI), and pyruvate concentrations, selenium retention was 4-23 times higher in 2.5-cm-aggregates compared to 1-cm-aggregates. Under oxic conditions, aggregate size and pyruvate-concentrations were found to have a positive synergistic effect on selenium retention. Promoting soil aggregation on seleniferous agricultural soils, through organic matter amendments and conservation tillage, may thus help decrease the impacts of selenium contaminated drainage water on downstream aquatic ecosystems.

1. Introduction

Selenium is a trace element of great ecological significance, due to its dual role as both an essential nutrient and environmental contaminant. The intake range between deficiency and toxicity of selenium for most animals is exceedingly small (Lenz and Lens, 2009). For example, humans need around 40 µg/day for optimal health; however, an intake of more than 400 µg/day can cause selenosis (WHO, 1996). Selenium is heterogeneously distributed across terrestrial landscapes, with seleniferous (>0.5 mg/kg) and selenium-deficient soils (<0.1 mg/kg) sometimes occurring as close as 20 km from one another (Lenz and Lens, 2009). The irrigation of seleniferous soils can lead to the production of sub-surface drainage water containing high selenium concentrations that cause ecological damage in downstream aquatic ecosystems. This process was first recognized in the late 1980s after the occurrence of numerous deaths and embryonic

deformities in waterfowl populations near the agricultural evaporation ponds of the Kesterson reservoir, a former wildlife refuge in California (Presser, 1994). In the Western United States alone, nearly 400,000 km^2 may be at risk of irrigation-induced selenium contamination (Seiler et al., 1999) and similar problems have also been observed in Canada, Egypt, Israel, and Mexico (Lemly, 2004). Enhanced understanding of selenium transport and retention in surface soils will improve the management of seleniferous soils to diminish the risk of contamination for downstream ecosystems.

The transport and biogeochemical behavior of selenium depend greatly on its chemical speciation. Whereas selenium occurs naturally in four oxidation states: Se(-II), Se(0), Se(IV) and Se(VI), the primary oxidation states associated with irrigation-induced contamination, Se(VI) and Se(IV), occur as bioavailable oxyanions: selenate (SeO_4^{2-}) and selenite (SeO_3^{2-}) (Dungan and Frankenberger, 1999). Elemental selenium (Se(0)) is solid and immobile, whereas Se(-II) occurs in soluble and bioavailable organo-selenides or in gaseous methylated forms (Hamilton, 2004; Stolz and Oremland, 1999). Transformations between these various species are kinetically hindered and thus the speciation of selenium is poorly predicted by thermodynamic models (Luoma and Presser, 2009). Redox reactions are catalyzed primarily by microorganisms, the transformation of Se(VI) to Se(IV) and Se(0) for example, is driven predominantly by microbial dissimilatory reduction (Stolz and Oremland, 1999). This reduction reaction yielding solid Se(0) is an important attenuation pathway for selenium in surface environments (Darcheville et al., 2008; Dungan and Frankenberger, 1999; Strawn et al., 2002; Oremland et al., 1991; Steinberg and Oremland, 1990).

The known microorganisms capable of selenium reduction are scattered across a very diverse set of prokaryotic taxa (including Crenarchaeota [Domain: Archaea], low and high GC gram-positive bacteria, β-, γ-, and ε-Proteobacteria) (Stolz et al., 2006). We chose *Enterobacter cloacae* SLD1a-1 as the benchmark organism for the reactive transport model presented in this paper. Since its original isolation from seleniferous agricultural drainage water, this γ-Proteobacterium has received a particularly large amount of research attention (Losi and Frankenberger, 1998). *E. cloacae* is known to grow both aerobically and anaerobically using a variety of electron donors, including pyruvate (Losi and Frankenberger, 1997b). It can reduce selenate via selenite to solid elemental Se (Losi and Frankenberger, 1997a) and its membrane-bound selenate reductase has been identified (Watts et al., 2003) and purified (Ridley et al., 2006). Furthermore, it has been used as a model organism in several studies investigating the molecular genetics of selenium reduction (Ma et al., 2007; Ma et al., 2009; Yee and Kobayashi, 2008; Yee et al., 2007) and has been considered as a candidate for bioremediation schemes (Losi and Frankenberger, 1998). *E. cloacae* can carry out selenium reduction under oxic conditions, though at rates that are an order of magnitude lower than under anoxic conditions (Losi and Frankenberger, 1997b). This inhibition is in accordance with thermodynamic expectations, since at neutral pH reduction of selenate to selenite is not energetically favored above a pE of 7.5 placing it generally between nitrate and manganese oxide on the redox ladder (Sposito et al., 1991). Unsurprisingly, oxygen inhibition of microbial selenium reduction has also been observed in environmental

samples (Oremland et al., 1989). Selenium reduction rates are thus sensitive to local redox potential.

Redox conditions in soils are known to display a large amount of spatial heterogeneity, owing to the heterogeneous size and distribution of pore spaces in a soil's physical structure (Arah and Vinten, 1995; Sexstone et al., 1985). A common approach to model this spatial heterogeneity in mechanistic biogeochemical models has been to represent the soil matrix as a series of spherical microporous structures or aggregates (Arah and Vinten, 1995). Soil aggregates are mm- to cm-sized structural units of mineral particles bound by roots, fungal hyphae, and organic matter that naturally occur in most soils (Brady and Weil, 2002). Whereas a variety of different shapes exist in nature, granular (approximately spherical) aggregates are particularly common in surface soils (A horizons) (Brady and Weil, 2002). Aggregates represent well-defined natural systems in which to study the impact of mm- to cm-scale spatial heterogeneity on biogeochemical reactions (Tokunaga et al., 2003).

Dissolved chemical concentrations within aggregates depend on the local coupling of reactions and transport. Whereas fast advective solute transport is prevalent in the inter-aggregate macropores, transport inside aggregates is mostly diffusive, due to the low permeability of the microporous structures. In conjunction with local microbial metabolic activity this often leads to the formation of steep chemical gradients within aggregates (Arah and Vinten, 1995; Sexstone et al., 1985; Kaurichev and Tararina, 1972), as the consumption (or production) of a chemical species inside an aggregate outpaces the diffusive supply from (or export to) the surrounding macropore (Tokunaga et al., 2003). Full transitions from oxic to anoxic have been observed in aggregates as small as 4 mm in diameter (Sexstone et al., 1985). Tokunaga et al. demonstrated that such anoxic zones can influence the mm-scale distribution and mobility of selenium based on synthetic, flat aggregate no-flow systems (Tokunaga et al., 1994). We previously developed a system of saturated-flow reactors containing single idealized soil aggregates, for the investigation of aggregate-scale gradients in the microbial reduction and secondary mineral formation of iron (Pallud et al., 2010b) and a mathematical model describing the coupled transport and reactions of iron within the system (Pallud et al., 2010a). This unique experimental approach, emulating field-like transport conditions at the aggregate-scale while allowing for controlled experiments, was later applied to investigations of arsenic mobility (Masue-Slowey et al., 2011) and heterogeneity in microbial selenium reduction (Kausch et al., 2012). In the latter study, we found increasing concentrations of reduced selenium towards the core of aggregates containing E. cloacae under both oxic and anoxic conditions independent of selenate or carbon concentrations in solution. This was hypothesized to be due to limitations in the transport rate of reduced selenium products out of the aggregate, which may imply a general role of aggregate size in selenium reduction and retention (Kausch et al., 2012).

In this study we formally tested this hypothesis by constructing a mechanistic mathematical model of the coupled transport and transformations of selenium species inside an aggregate containing selenium reducing bacteria (*E. cloacae*) and in the surrounding solution. The objectives were to evaluate the theoretical impact of variations

in aggregate size on selenium retention within a comprehensive mechanistic framework and to assess implications for the management of seleniferous soils that can be a source of water contamination. Furthermore we wanted to disentangle the roles of heterogeneity in reaction rates and chemical fluxes in producing the experimentally observed concentration gradients and resolve the production and distribution of elemental selenium in aggregates (which could not be directly measured in experiments). To this end, we reproduced our experimental results (Kausch et al., 2012) to validate the model, and then simulated selenate and selenite reduction in aggregates ranging from 1-2.5 cm in diameter.

2. Materials and Methods

2.1. Overview of experimental data used

In developing and validating our reactive transport model we used data obtained from flow-through experiments involving novel artificial soil aggregates made of sand and containing *Enterobacter cloacae* SLD1a-1 (Kausch et al., 2012). The experiments were carried out under a set of eight different chemical conditions (0.4 or 0.8 mM selenate and 0.3 or 1.2 mM pyruvate in the input solution under oxic and anoxic conditions). We used data on bacterial cell densities and concentrations of reduced selenium within three concentric sections of the aggregates, as well as data on temporal evolution of selenite and flow-tracer (bromide) concentrations in the reactor outflow. The flow-tracer data were used to establish that the physical flow model was representative of experimental flow and transport. The data on solution and solid phase selenium concentrations were used to parameterize the global expressions for chemical reaction rates and later to assess that the reactive transport model represented the experimentally observed spatial and temporal dynamics of the system under the full set of chemical conditions. The data on cell density were used constrain this biological factors in the reactive transport model by checking whether cell density varied between concentric sections of the aggregates and between the beginning and end of experiments.

2.2. Aggregate construction

Spherical (2.5 cm diameter) aggregates were constructed in the laboratory using the protocol developed by Pallud et al. (2010b). Aggregates were composed of pure quartz sand (IOTA 4 pure quartz powder, grain size of 150–250 μm, Unimin Corporation) homogenously inoculated with a suspension of *E. cloacae* to a density of approximately 10^8 cells/g dry aggregate mass. Right after the sand was inoculated with *E. cloacae*, is was mixed with hydrogel agarose to promote particle aggregation (150 g of 0.5 wt % agarose, 30 mL of bacterial suspension and 300 g of sand) and then molded into aggregates using a spherical press. The average pore diameter and porosity of aggregates thus constructed are 39 μm and 0.58, respectively (Pallud et al., 2010b). No carbon source or selenium was present in the aggregates at the time of synthesis. Pure quartz sand was chosen, since adsorption of selenium oxyanions is negligible under the

experimental conditions thus allowing the investigation of transport mechanisms independent of sorption.

2.3. Flow-through experiments

Flow-through systems consisted of individual artificial soil aggregates placed at the center of a polycarbonate reactor cell (5.1 cm diameter, length 3.7 cm). A constant flow rate of 1.0±0.1 mL/h were imposed at the lower boundary of the reactors using a peristaltic pump and effluent samples were collected in 8 hour increments for 192 hours. The input solution was a sterile, artificial groundwater medium (prepared in 10 mM PIPES and containing (in mg/L): NaCl, 30; NH_4Cl, 0.95; KCl, 5; $MgSO_4$, 50; KH_2PO_4, 0.950 and 1 mL/L mineral Wolfe's solution with pH adjusted to 7.2), with selenate concentrations of either 0.4 or 0.8 mM, and pyruvate concentrations of either 0.3 or 1.2 mM (added from a filtered-sterile stock solution). Bromide (2 mM, as KBr) was included in inflow solutions as an unreactive flow-tracer, but not in the solution used to fill the reactors initially. For each experiment, the composition of the input solution remained constant throughout.

Anoxic experiments were fully contained within an anaerobic chamber (Coy Laboratories, Inc., Grass Lake, MI), and the input solutions (single batches of 0.5 L) were made anoxic by sparging with O_2-free N_2 for 15 minutes. The efficacy of the chosen sparging procedure and time was ascertained through tests with the redox indicator die resazurin (0.5 mg/L). For oxic experiments, thorough aeration of the solution surrounding the aggregates was insured by using oxic input solutions and continuously bubbling air into the solution surrounding the aggregates throughout the experiment.

At the conclusion of experiments, aggregates were shaved into three concentric sections (core: radius 0-5 mm, mid-section: radius 5-9 mm, and exterior: radius 9-12.5 mm, corresponding to relative volumes of 6.4%, 30.9% and 62.7%, respectively) (Pallud et al., 2010b) for solid phase Se extractions and analysis as well as enumerations of *E. cloacae*.

2.4. Chemical analysis

Selenium extraction from the solid phase was performed with 12 M HNO_3 (Kausch et al., 2012) and analysis of solid extraction and elution samples were performed via hydride generation coupled to optical emission spectrometry (PerkinElmer 5300 DV) as previously described by Kausch et al. (2012). While the procedure allows for direct analysis of selenite concentrations in liquid samples, the extraction and analysis of solid phase samples yields a single experimental fraction of reduced selenium including both selenite and elemental selenium (Kausch et al., 2012). Additionally, for outflow samples from two oxic and two anoxic experiments each, bromide concentrations were determined on a Dionex ion chromatograph (ED40 electrochemical detector) with an AS23 column (Thermo Fisher Scientific Inc.) using 4.5 mM Na_2CO_3, 0.8 mM $NaHCO_3$ eluent. Bromide and selenite standards were prepared from certified stock (Spex CentriPrep Group L.L.C. and VHG Labs, respectively).

2.5. Bacterial cell counts

Counts of bacteria per gram of sand were obtained prior to and at the conclusion of experiments. Prior to experiments, the sand-agarose-cell mixture from which aggregates were shaped was sampled, whereas at the conclusion of experiments, separate samples from the exterior and mid sections of each individual aggregate were used. The volume of sand in core sections was too small to allow bacterial counts for that aggregate section. The 1 g (wet weight) samples were each transferred into 9 mL of sterile saline solution (NaCl, 8 g/L) and shaken thoroughly. A 10-fold dilution series in sterile NaCl (8 g/L) was prepared from each aggregate sample solution. Then, 100 μL aliquots of appropriate dilutions were plated in triplicate on solid medium (30 g/L tryptic soy broth, 15 g/L agar). Plates were incubated for 2-5 days at 25˚C before colony forming units (CFU) were counted.

2.6. Reactive Transport Model

The transport model and geometry used here are based on previous work modeling iron reduction in artificial aggregates (Pallud et al., 2010a). The experimental setup was emulated in a 2D axi-symmetric reactive transport model (**Fig. 2a**) describing physical solute transport by advection and molecular diffusion and the effect of kinetically driven redox reactions on mass balance expressions for pyruvate, oxygen, selenate, selenite, and elemental selenium.

The flow and pressure fields were computed using the stationary, incompressible Navier-Stokes equations in the free fluid surrounding the aggregate and the Brinkman equation inside the aggregate (see Appendix for an explicit account of the governing equations). The aggregate permeability was computed based on grain size and porosity measurements and a uniform flow velocity was imposed at the lower boundary of the reactor (inflow), with no slip conditions at the reactor walls (Pallud et al., 2010a).

Reactions of selenium species, pyruvate, and (in oxic simulations) oxygen were formulated by taking into account aerobic respiration and selenium reduction coupled with pyruvate oxidation by *E. cloacae* (Losi and Frankenberger, 1998). All reactions were implemented using kinetic rate expressions with a Monod type dependency on both electron acceptor (i = oxygen, selenate, or selenite) and electron donor (pyruvate) (Rittman and VanBriesen, 1996) as:

$$R_i = k_i \rho_{cells} \cdot \frac{[pyruvate]}{K_{mi}^{pyruvate} + [pyruvate]} \cdot \frac{[i]}{K_m^i + [i]} \cdot I_i([oxygen]) \qquad (1)$$

where R_i is the reaction rate and k_i the cell specific rate constant for the respective electron acceptor (i), ρ_{cells} denotes the cell density of *E. cloacae,* and $K_{mi}^{pyruvate}$ and K_m^i are the half-saturation constants for electron donor and acceptor, respectively. $I_i([oxygen])$ is the oxygen concentration dependent inhibition term (Van Capellen and Galliard, 1996) specific for selenate or selenite reduction ($I_i([oxygen])=1$ for aerobic respiration). $I_i([oxygen])$ was parameterized by fitting the data collected by Losi and

Frankenberger (1997b) on the inhibition of selenate and selenite reduction by *E. cloacae* at various oxygen concentrations (**Fig. A1** in the Appendix).

A cell death term was introduced that led to a linear decrease in cell density over time (see Appendix or details) based on our observations that the average cell density measured at the conclusion of anoxic experiments was an order of magnitude lower than the initial cell density (see below). This term was only used in fitting the model to experimental results and not in the predictive simulations. Other than those relating to cell density, model parameters were kept constant among all simulations (i.e. different chemical conditions). For the predictive simulations, the cell density was also held constant at 1×10^8 cells/g for all chemical conditions. The values of reaction parameters used in the model are listed in **Table 1**. A detailed description of the model is given in Appendix.

2.7. Model fitting

For all eight chemical scenarios in parallel, the reactive transport model was fitted to both temporal data of selenite breakthrough curves and spatial data of reduced selenium solid phase concentrations, by manually adjusting reaction rate and cell density parameters. Among the reaction rate parameters (**Table 1**), only the maximum cell-specific rate-constants, the electron donor half-saturation constant for selenate reduction, and the oxygen half-saturation constant were adjusted; all other parameters were taken from the literature. Whereas reaction rate parameters where kept constant between chemical scenarios, the initial cell density values were varied between $1\text{-}3\times10^8$ cells/g. See Appendix for a discussion of the cell death term.

2.8. Predictive simulations

Predictive simulations were performed by varying the aggregate diameter for chemical scenarios equivalent to those run experimentally (0.3 and 1.2 mM pyruvate, with 0.4 and 0.8 mM selenate input solutions under both oxic and anoxic conditions). Each predictive scenario consisted of a set of 9 simulations in which the aggregate diameter varied between 1 cm (which corresponds to the size of core sections in experiments) and 2.5 cm (which corresponds to the full size of experimental aggregates). Results were linearly interpolated between the 9 simulated diameters. Simulation time (192 h) and kinetic parameters (**Table 1**) were left unchanged and the cell density was constant at 1×10^8 cells/g.

3. Results

3.1. Experimental selenite breakthrough curves

Experimental selenite breakthrough curves from oxic and anoxic experiments are shown in **Figs. 1a** and **1b**, respectively. It can be seen that under both oxic and anoxic conditions, selenite outflow concentrations reached their highest value between 80 and 150 h. Selenite concentrations in the reactor outflow were 6-20 times higher under anoxic than oxic conditions, with peak selenite concentrations of respectively 40-70 μM and 2-

12 µM. The initially steeply increasing selenite concentrations plateaued as they approached their peak value; however a clear steady-state was not maintained under all experimental conditions. Selenite concentrations decreased after reaching the peak value in the oxic experiment with high pyruvate (1.2 mM) and selenate (0.8 mM) concentrations in the input solution and in all anoxic experiments, except the one with low pyruvate (0.3 mM) and selenate (0.4 mM) input concentrations.

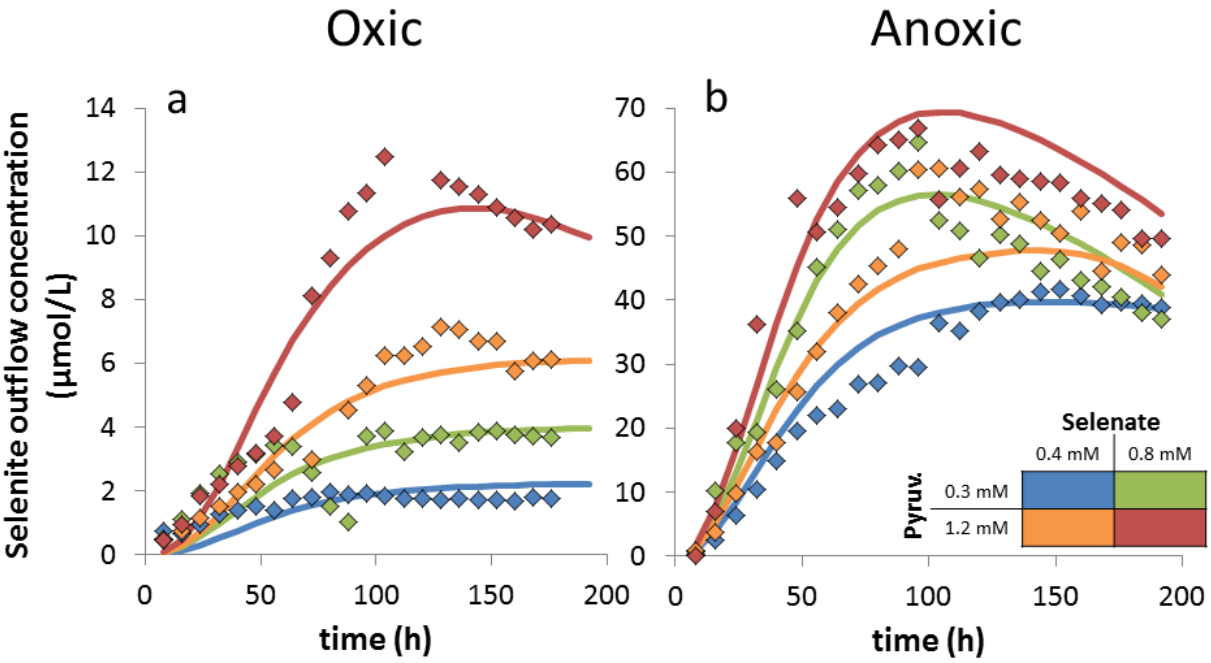

Figure 1. Measured (diamonds) and simulated (solid lines) selenite concentrations in the reactor outflow under oxic (a) and anoxic (b) conditions. Colors correspond to specific combinations of input selenate and pyruvate concentrations (see legend).

Higher concentrations of both pyruvate and selenate in the input solution led to higher concentrations of selenite in the outflow under both oxic and anoxic conditions (**Fig. 1**). Under oxic conditions, peak selenite concentrations approximately tripled with an increase of the pyruvate input concentration from 0.3 mM to 1.2 mM, whereas they approximately doubled with an increase of selenate input concentrations from 0.4 mM to 0.8 mM (**Fig. 1a**). In contrast, under anoxic conditions peak selenite concentrations increased by a factor of less than 1.5 with both an increase of the pyruvate input concentration from 0.3 mM to 1.2 mM, and an increase of selenate input concentrations from 0.4 mM to 0.8 mM (**Fig. 1b**).

3.2. Experimental solid phase distribution of reduced selenium

Reduced selenium, measured as the sum of selenite and elemental selenium, was detected in core, mid-, and exterior sections of all aggregates, with positive gradients in reduced selenium concentrations observed from the aggregate exterior towards the cores of aggregates under all investigated chemical conditions (**Fig. 2**). These gradients were

steeper under oxic than under anoxic conditions. Specifically, the ratio in solid phase concentrations of reduced selenium between core and exterior sections of aggregates was between 2.2-3.9 and 1.8-2.0 under oxic and anoxic conditions, respectively.

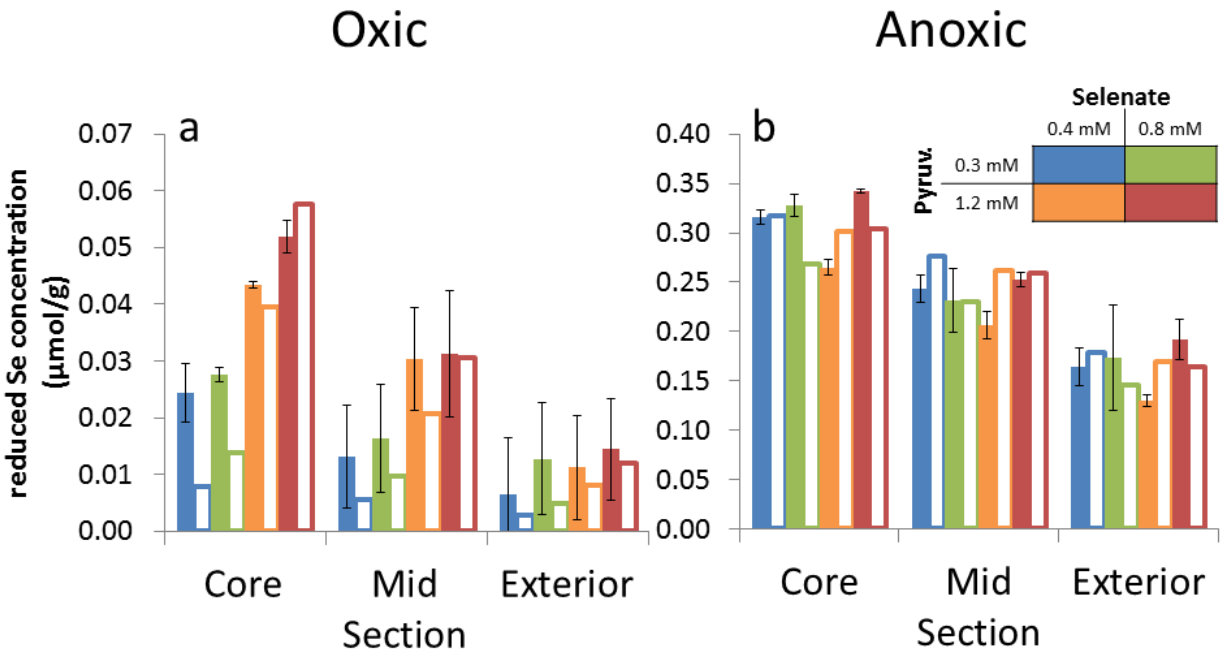

Figure 2. Measured (solid bars) and simulated (hollow bars) concentrations of reduced selenium (selenite + elemental Se) in the solid phase of concentric aggregate sections (core, mid-section, exterior) under oxic (a) and anoxic (b) conditions. Error bars correspond to the standard deviation of replicate measurements (N=2 for the core section and 3 otherwise). Colors correspond to specific combinations of input selenate and pyruvate concentrations (see legend).

Absolute concentration values of solid phase reduced selenium varied between 0.01-0.05 µmol/g and 0.16-0.34 µmol/g under oxic and anoxic conditions, respectively (**Fig. 2**). The differences within the oxic and anoxic sets of solid phase concentrations were not statistically significant (Kausch et al., 2012), but are here presented separately for the purpose of showing the fits of individual model scenarios. For example, under oxic conditions the concentrations of reduced solid phase selenium appear systematically higher for pyruvate input concentrations of 1.2 mM as compared to pyruvate input concentrations of 0.3 mM and while this difference in experimental results was not large enough to be statistically significant it was nevertheless reproduced by the simulated results.

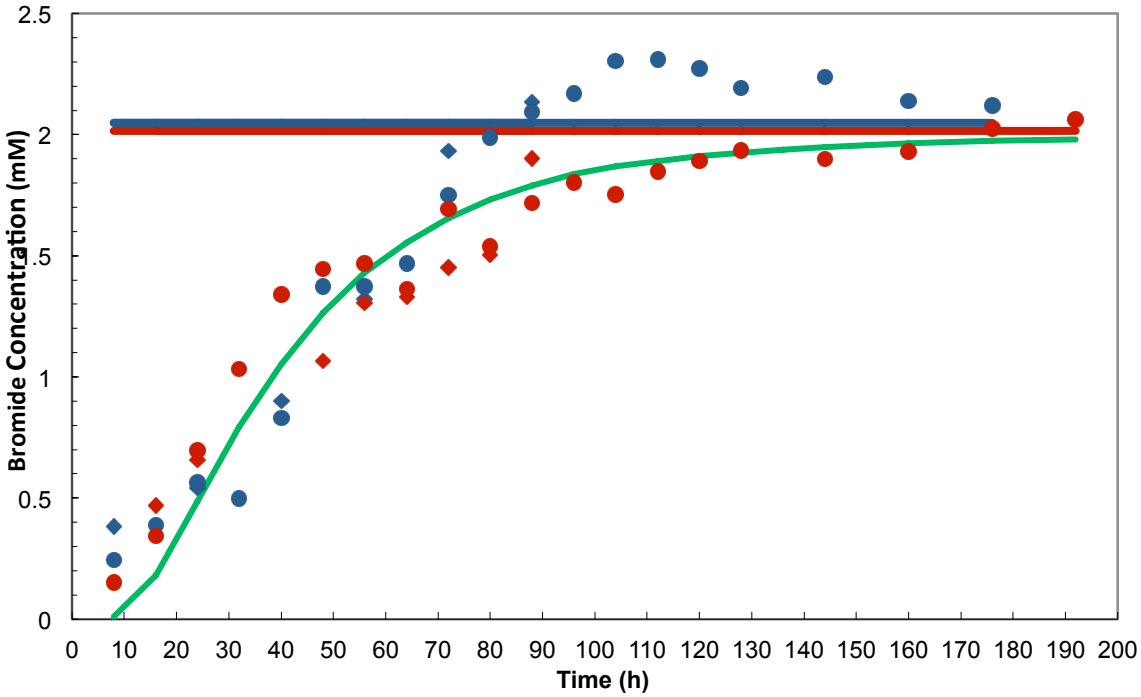

Figure 3. Breakthrough curves (points) and input solution concentrations (solid lines) of the flow tracer bromide measured from the two oxic (blue) and two anoxic (red) reactor with 0.3 mM pyruvate input concentrations. The two reactors labeled A and B here correspond to those with input selenate concentrations of 0.4 mM and 0.8 mM respectively. The green line corresponds to the breakthrough curve simulated by the transport model.

3.3. Flow-tracer (bromide) breakthrough curves and transport model

Steady-state concentrations of bromide (within 10% of the 2 mM input concentration) in the outflow from the four reactors tested were reached between 80 and 120 h (**Fig. 3**). This compares well with results from the transport model, which predicts that 90% of the input concentration of an unreactive tracer should be reached after 116 h in the outflow. Experimental data points scatter around the simulated curve with a maximum distance of 0.5 mM.

3.4. E. cloacae cell counts prior to and at termination of experiments

The density of *E. cloacae* (average ± standard deviation) determined in aggregate material prior to experiments was $(1.2\pm0.5)\times10^8$ CFU/g (N=3). Under anoxic conditions, cell densities decreased by an order of magnitude over the course of the experiments. In fact, the average value from replicates from all aggregate sections measured at the experiment conclusion was $(8\pm7)\times10^6$ CFU/g (N=25). However, under oxic conditions, cell densities remained relatively constant over time with an average cell density from replicates of all aggregate sections at the end of experiments of $(1.1\pm0.6)\times10^8$ CFU/g (N=26), one outlier aggregate section excluded. The only exception was the exterior section of the oxic aggregate run with high pyruvate (1.2 mM) and high selenate (0.8

mM) input concentrations, where *E. cloacae* density reached a value of $(1.4\pm0.9)\times10^9$ CFU/g at the conclusion of experiments (N=3), which is an order of magnitude higher than the initial value. Aside from this, no systematic differences in the cell density based on aggregate section or input solution composition were discerned.

3.5. Model fitting and validation

The temporal and spatial concentration data produced by the reactive transport model are compared to experimental observations in **Figs. 1** and **2**, respectively. The model accurately fitted both the breakthrough curves and solid phase data with a single kinetic parameterization (**Table 1**) for the full set of experiments. Similarly to what was observed in experiments, simulations showed quasi-steady state in selenite outflow concentrations being reached after around 100 h regardless of the chemical conditions (**Fig. 1**). The decrease in selenite outflow concentrations after 100 h in three of the anoxic and one of the oxic experiments was also reproduced as a result of a decrease in modeled cell densities (active cell death term). The reactive transport model also accurately reproduced the differences in outflow selenite concentrations observed experimentally for different chemical conditions. In fact, peak selenite concentrations in the modeled outflow ranged between 2-11 μM and 40-70 μM for oxic and anoxic conditions, respectively, compared to experimental values of 2-12 μM and 40-70 μM. The experimentally observed spatial trend of increasing concentrations of reduced selenium towards the core of aggregates was also reproduced by the model (**Fig. 2**). Comparing modeled and experimentally determined solid phase concentrations of reduced selenium individually based on aggregate section and chemical conditions (**Fig. 2**), it can be seen that the modeled results lie within one standard deviation of the experimental measurements in 8 out of 12 and 5 out of 12 sections for oxic and anoxic conditions, respectively. Furthermore, it is obvious that while absolute concentrations were not always reproduced, the spatial trend was reproduced for all chemical scenarios. Specifically, the modeled concentration ratio between the simulated core and exterior sections was 1.8 for anoxic conditions, and 2.8-4.9 for oxic conditions, compared to experimental values of 1.8-2.0 and 2.2-3.9.

3.6. Dynamics of concentration fields and reaction rates

The spatial and temporal behavior displayed by chemical species in our reactive transport model differed qualitatively based on whether they were reactants or products of reactions, whether they were solids or solutes, and based on the bulk oxidation conditions. Here, we use concentration and reaction rate maps from the oxic simulation with 0.3 mM pyruvate and 0.4 mM selenate as an example to illustrate spatial and temporal patterns that were consistent among the different chemical scenarios explored. **Fig. 4** shows the final concentration fields for pyruvate, oxygen, selenate, selenite, and elemental selenium at the termination of this simulation. Movies showing the dynamics of pyruvate, oxygen, selenate, selenite, and elemental selenium concentration fields (Movies S1-S5) and of reaction rate fields (Movies S6-S7) are included in the Supplementary Material.

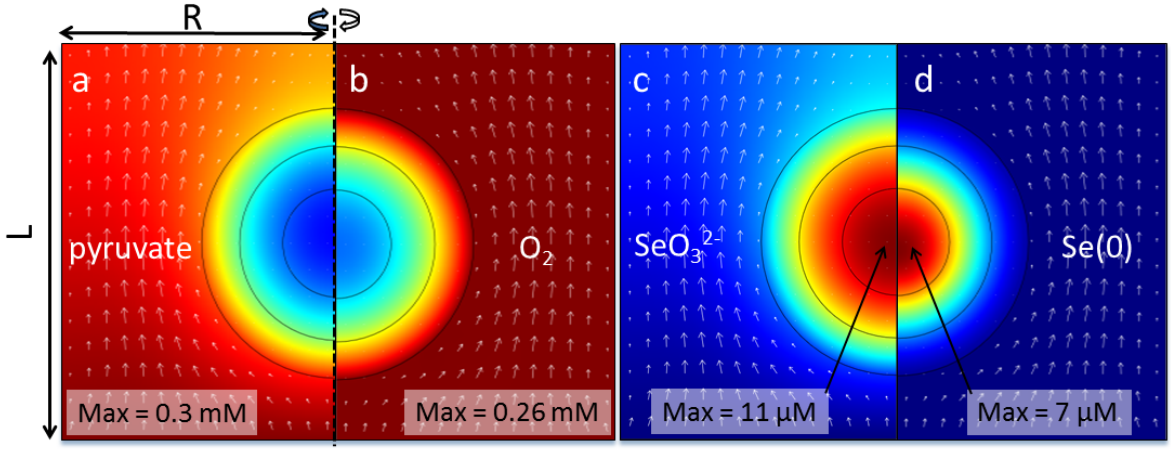

Figure 4. Modeled concentration fields of pyruvate (a), O2 (b), selenite (c), and Se(0) (d) within the aggregate (circle) and the surrounding solution after 192 h simulation time (steady-state) in an oxic simulation with 0.3 mM pyruvate and 0.8 mM selenate input concentrations. Cold colors denote the absence of the species (minimum concentration is zero in all panels), whereas warm colors represent high concentrations, with maximum values as indicated on the panels. Dimensions L and R correspond to the length and radius of experimental reactors (3.7 and 2.55 cm respectively) and the dotted line represents the axis of cylindrical symmetry. The black rings correspond to the boundaries between the exterior, mid-, and core sections that were experimentally sampled. Molarities are expressed with respect to the pore/solution volume. The white arrows represent the flow field.

Whereas the concentrations of pyruvate, selenate, and selenite approached steady-state between 64 and 192 h of simulation time (Movies S1, S3, S4), those of oxygen reach steady-state within 32 h (Movie S2). Concentrations of elemental selenium on the other hand kept increasing inside the aggregate domain throughout the simulation time (Movie S5). Over the course of simulations, all compounds developed smooth gradients of approximately radial symmetry within the aggregate domain (the symmetry is slightly shifted in the direction of flow). However, whereas concentrations of reactants (pyruvate, selenate, and when present, oxygen) decreased towards the core of the aggregate domain, those of products (selenite and elemental selenium) increased towards the core (**Fig. 4**). The gradients of selenite, elemental selenium and, except in the case of selenate, also of reactants, were steeper under oxic than under anoxic conditions (data not shown). The maximum concentrations of the reactants pyruvate, selenate, and oxygen found in the free fluid surrounding the aggregate at steady-state correspond to the input concentrations (**Fig. 4**, note: 0.26 mM correspond to atmospheric equilibrium oxygen concentration).

Diffusive and advective transport, respectively, dominated inside the aggregate and in the surrounding solution. This is illustrated for the case of selenite in **Fig. 5**. It can be seen that while the diffusive selenite flux was near zero at the core of the aggregate it increased towards the aggregate exterior and is 0.4 nmol/(m^2s) at the interface between the aggregate and the surrounding solution (**Fig. 5a**). In the surrounding solution the

diffusive flux decreased with increasing distance from the aggregate. This was however compensated by an increasing advective flux component downstream of the aggregate, where it lead to a maximal total selenite flux of 0.5 nmol/(m^2s) (**Fig. 5b**).

Similar to solute concentrations, reaction rates of selenate and selenite reduction reached a steady state after 60 and 150 h of simulation time, respectively (Movies S6-S7). The rates of selenate reduction approached a steady-state that is relatively homogenous throughout the aggregate (**Fig. 5c**). In contrast, the rates of selenite reduction approached a steady-state that mirrored the concentration field of selenite (with increasing values towards the core of the aggregate domain, **Fig. 5d**). In the example simulation the steady-state rates of selenate reduction were 130-190 nM/s everywhere in the aggregate domain (**Fig. 5c**), whereas those of selenite reduction smoothly increased from 0 at the aggregate exterior to 12 nM/s at the core (**Fig. 5d**).

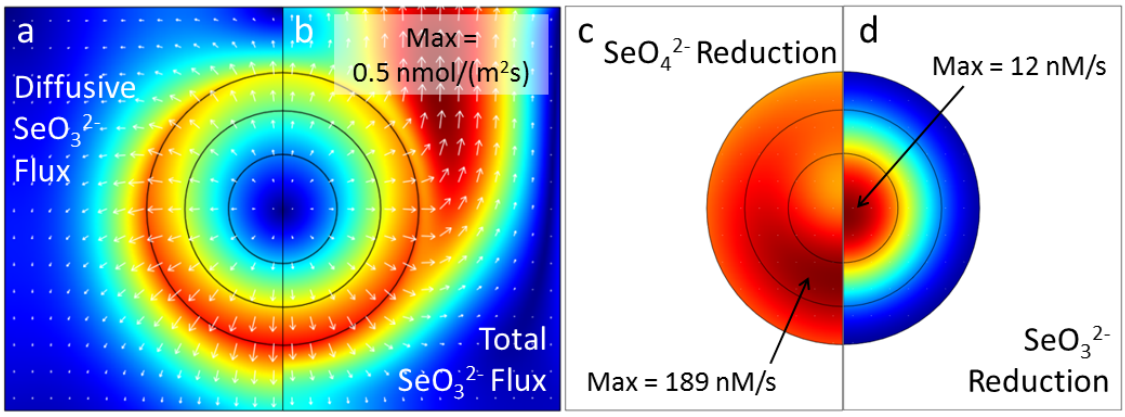

Figure 5. Modeled fields of diffusive selenite flux (a), total selenite flux (b), selenate reduction rates (c), and selenite reduction rates (d) within the aggregate (circle) and the surrounding solution after 192 h simulation time (steady-state) in an oxic simulation with 0.3 mM pyruvate and 0.8 mM selenate input concentrations. Cold colors denote low values (minimum concentration is zero in all panels), whereas warm colors represent high concentrations, with maximum values as indicated on the panels. The black rings correspond to the boundaries between the exterior, mid-, and core sections that were experimentally sampled. Molarities are expressed with respect to the pore/solution volume. The white arrows in panels a and b represent flux vectors.

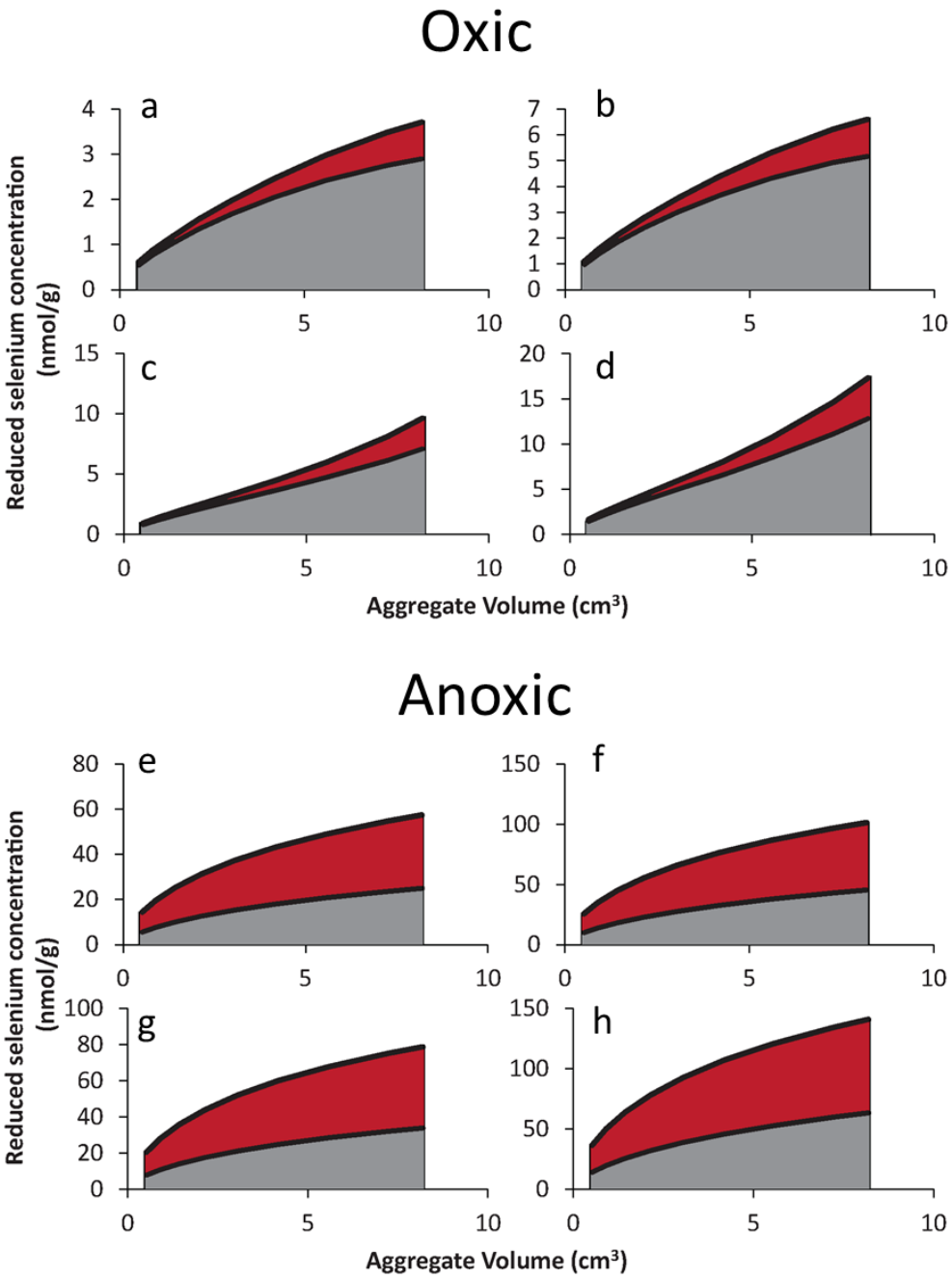

Figure 6. Results of oxic (a-d) and anoxic (e-h) simulation series evaluating the amount of reduced selenium per gram of the solid phase as a function of aggregate size for conditions with (a&e) 0.3 mM pyruvate/0.4 mM selenate, (b&f) 0.3 mM pyruvate/0.8 mM selenate,

(c&g) 1.2 mM pyruvate/0.4 mM selenate, and (d&h) 1.2 mM pyruvate/0.8 mM selenate. The amount of selenite in the solid phase is shown in grey, while the amount of elemental selenium in the solid phase is shown in red. Each panel shows the results of 9 simulations carried out at different aggregates sizes, the space between simulations was linearly interpolated.

3.7. Predictive simulations of aggregate size impact on selenium retention

Simulations in which the diameter of the spherical aggregate was varied between 1 and 2.5 cm (corresponding to volumes of 0.5 cm^3 and 8.2 cm^3, respectively) showed that the aggregate solid phase concentrations of reduced selenium scale with aggregates size under all chemical conditions investigated (**Fig. 6**). This effect was more pronounced under oxic conditions than under anoxic conditions. In fact, under oxic conditions the average solid phase concentrations of total reduced selenium were 0.6-1.6 nmol/g in aggregates of 1 cm diameter and 4-17 nmol/g in aggregates of 2.5 cm diameter, which corresponds to a difference by a factor of 6-11 between the two size extremes (**Fig. 6a-d**). On the other hand, under anoxic conditions the average solid phase concentrations of total reduced selenium were only about 4 times higher in 2.5 cm diameter aggregates than in 1 cm diameter aggregates, with values of 57-140 nmol/g and 14-36 nmol/g, respectively (**Fig. 6e-h**). Under oxic conditions, solid phase concentrations of elemental selenium in aggregates were particularly sensitive to aggregate size, scaling from 0.1-0.2 to 0.8-4.5 nmol/g over the investigated size range (factor 8-23). Thus the fraction of elemental selenium in aggregates varied greatly with aggregate size under oxic conditions (11-26% of reduced selenium). In contrast, under anoxic conditions elemental selenium makes up around 60% (55-61%) of reduced selenium in aggregates regardless of aggregate size and input solution concentrations.

Under anoxic conditions, the curves describing reduced selenium solid phase concentrations as a function of aggregate size displayed negative curvature throughout the different reactant concentration scenarios investigated (**Fig. 6e-h**). However, under oxic conditions the curves corresponding to high pyruvate (1.2 mM) concentration scenarios (**Fig. 6c-d**) were markedly steeper towards the larger end of the aggregate size spectrum (positive curvature) than those for low pyruvate (0.3 mM) concentration scenarios (negative curvature) (**Fig. 6a-b**).

4. Discussion

4.1. Model validity

The reactive transport model we developed in this work reproduces the general spatial and dynamic behavior observed in experiments across the full spectrum of chemical conditions investigated. More specifically, our model reproduces the time to reach quasi-steady-state, the impact of aeration conditions and input solution composition on outflow selenite concentrations (which are a proxy for experimental reaction rates (Kausch et al., 2012)), and the spatial distribution of reduced selenium inside the aggregates (i.e concentrations increase towards the core). For the solid phase data

however, when comparing individually for specific aggregate sections and chemical conditions the modeled results lie within one standard deviation of experimental measurements for only a little over half of all aggregate sections. Overall, the solid phase model fits are convincing when viewed in the context of the large uncertainty introduced by uncontrollable biological factors. Deviations between experimental and model results are likely due to the inability to perfectly control experimental conditions rather than a misinterpretation of the biogeochemistry and physics that occur in the idealized soil aggregates.

The greatest error source in simulating aggregate experiments is the variability in cell densities and microbial activity since they factor into every rate law, are difficult to control experimentally, and their temporal evolution is hard to measure. In fact, the random error in the solid phase determination of cell density, which was already large at the beginning of experiments (standard deviation was 42% of the average measurement), increased in the measurements conducted at the conclusion of experiments. Whereas some of the error in measuring cell densities is likely to have been corrected by using cell density as a fitting parameter in simulations, this does not include potential errors introduced by temporal variations in cell-specific reaction rates which could not be measured or controlled. Additionally, cell densities were modeled as spatially homogenous within aggregates whereas spatial variation is likely to have occurred, though eclipsed by the large uncertainty range of experimental observations. Based on the data collected for this work with *E. cloacae* and previous work with *Shewanella putrefaciens* CN-32 (Pallud et al., 2010a;Pallud et al., 2010b), we are confident that our procedure of aggregate construction leads to a distribution of cell density that is initially homogenous. However, spatial heterogeneity may occur over the course of experiments as cell populations grow or decay differentially in different sections of aggregates. For example, in our work with *S. putrefaciens* we found a trend at the conclusion of experiments indicating that cell densities may have been slightly higher (factor 2) at the exterior of aggregates (Pallud et al., 2010b), where elevated concentrations of electron donors may have led to more growth. Similarly, in the data presented here, the elevated CFU count value for the exterior section of the oxic aggregate run with high pyruvate (1.2 mM) and high selenate (0.8 mM) provides an indication of preferential growth in certain sections of the aggregate under certain chemical conditions. For example, our model shows that under oxic conditions concentrations of both pyruvate and oxygen are expected to decrease steeply towards the core of aggregates. Since these are the substrates for aerobic growth, it is plausible that *E. cloacae* may have grown preferentially at the aggregate-solution boundary where concentrations of pyruvate and oxygen were the highest.

The cell density values (including the cell death term) used in the model are similar to the experimentally obtained values from bacterial cell counts (see above). The maximum cell specific rate constants which were the result of our model fitting (13 and 0.9×10^{-17} mmol/s/cell for selenate and selenite reduction respectively) align well with what has previously been published for *E. cloacae*. Losi and Frankenberger (1997) found that the bacterium reduces 5 μmol/g of selenate over 30 minutes in a medium with 127

μM selenate and 2.8 mM pyruvate. Assuming a bacterial cell mass of 10^{-12} g (Davis et al., 1973) and the rate law (Eq. 1) and half-saturation constants (**Table 1**) given in the methods section, this would amount to a maximum cell specific rate of about 10^{-17} mmol/s/cell, which is within an order of magnitude from our value. Similarly, Ma et al. (2009) found that *E. cloacae* reduces 1 mM concentrations of selenate and selenite at rates of 1.6 and 0.17 μmol/s/g respectively, which following the same conversion as above amounts to maximum cell specific rates of 10 and 1×10^{-17} mmol/s/cell respectively. These values are nearly identical to the ones that resulted from our model fitting (13 and 0.9×10^{-17} mmol/s/cell for selenate and selenite reduction, respectively).

In summary, the simulations appear to capture the dynamics of the model aggregate system well and the kinetic parameters resulting from the model fitting represent the model organism (*E. cloacae*) in congruence with the literature. Thus, the reactive transport model presented here is a suitable framework for a theoretical exploration of aggregate scale impacts on selenium reduction.

4.2. Controls of aggregate-scale gradients in reduced selenium

Previous experimental work showed substantial mm-scale radial intra-aggregate variations in reduced selenium distribution, with concentrations that increase from the advection boundary towards the core of artificial, 2.5 cm diameter aggregates (Kausch et al., 2012). With the reactive transport model presented here, we can now provide a mechanistic explanation of how this accumulation of reduced selenium at the core of aggregates occurs.

The rates of selenate reduction to selenite are relatively homogenous throughout the aggregate, yet selenite accumulates at the core of aggregates because increasing distance from the advective boundary surrounding the aggregate increases mass transfer limitations (lower selenite flux). The diffusive selenite flux is directed away from the aggregate's core throughout the aggregate (since the aggregate is a selenite source), the local magnitude of the flux however depends on the steepness of the selenite concentration gradient. Consequently, the diffusive flux is fastest at the aggregate solution boundary, since it is the boundary between the source domain (aggregate) on the one hand and a domain of zero production (free solution) on the other. At the boundary, this gradient is maintained by fast advective transport of selenite away from the aggregate-solution interface. Inside the aggregate, the concentration gradient is smoothed out by the diffusive flux which decreases with increasing distance from the boundary along with the steepness of the gradient. The absolute steady-state selenite concentrations depend on the reduction rates, since faster reduction shifts the equilibrium between production and diffusive export of selenite to higher concentrations. However, the decrease in concentrations towards the advective boundary occurs across the full experimental spectrum of reduction rates. Additionally, in the presence of oxygen, reduction is increasingly inhibited as oxygen concentrations increase towards the exterior of the aggregate. This explains why the experimentally observed ratio between reduced selenium concentrations in the core and exterior aggregate sections was greater under oxic than under anoxic conditions. The effect of differential oxygen inhibition in the

exterior of aggregates is however secondary to the effect of diffusive mass transfer limitation in creating the observed gradients in reduced selenium. This is evidenced by the similarity in reduced selenium gradients observed under anoxic and oxic conditions. Another effect of oxygen is that by enabling aerobic respiration it increases the limitations imposed by the electron donor (pyruvate). Oxygen can thus indirectly inhibit selenium reduction at the aggregate core by limiting electron donor concentrations if the supply from the surrounding solution is small. In contrast to selenite concentrations, those of pyruvate decrease with increasing distance from the advective boundary. This explains why higher concentrations of pyruvate in the input solution lead to a much higher reduced selenium concentrations at the core of aggregates under oxic conditions, but not under anoxic conditions.

The concentrations of solid phase elemental selenium inside aggregates mirror those of selenite because selenite is the primary limiting factor in the production of elemental selenium (selenite reduction). The half saturation constant for selenite in selenite reduction by *E. cloacae* is 0.7 mM (Ma et al., 2007), thus at selenite concentrations representative of our experiments (~0.01 and 0.05 mM for oxic an anoxic conditions, respectively), selenite reduction rates depend almost linearly on selenite concentrations (Eq. 1). Consequently, the rates of selenite reduction are very heterogeneous inside aggregates with faster rates at the core where selenite accumulates. Once produced, elemental selenium will not move, and is thus not affected by transport, as selenite is. This also explains why elemental selenium concentrations in aggregates respond more strongly than selenite concentrations to conditions that promote the production of both forms of reduced selenium (i.e. for example, anoxic condition). Increasing selenite concentrations inside the aggregate will also lead to an increase of diffusive flux out of the aggregate. This negative feedback equilibrates concentrations of selenite in aggregates, which is why selenite distributions reached a steady-state in all simulations. This is not the case for elemental selenium, which is not affected by diffusive transport and can thus grow boundlessly while selenite reduction occurs. The rates of elemental selenium production (selenite reduction) reach a selenite concentration dependent steady-state, but the concentrations of elemental selenium keep increasing (at a steady rate) for as long as chemical input and microbial activity remain stable.

4.3. Impact of soil aggregate size on selenium retention

The same process that leads to the accumulation of reduced selenium at the core of aggregates causes the retention of reduced selenium to scale with aggregate size. Specifically, selenite (and consequently also elemental selenium) accumulates inside aggregates by virtue of diffusive mass transfer limitations that are more pronounced in larger aggregates. Smaller aggregates have a shorter average diffusion path length to the surrounding advective boundary (selenite sink) than larger aggregates. Consequently, selenite export from smaller aggregates to the surrounding solution is less limited than in the case of larger aggregates, and selenite will accumulate to a lesser extend at their cores. The impact of aggregate size is enhanced in the presence of oxygen, since oxygen inhibition of selenium reduction will be stronger in smaller aggregates (shorter average

diffusion path from the surrounding oxic solution). It is for this reason that under bulk oxic conditions the concentrations of reduced solid phase selenium scaled more strongly with aggregate size than under anoxic conditions. Additionally, under oxic conditions, the interaction between electron donor concentrations and aggregate size becomes more important. The electron donor is needed both for aerobic respiration, which reduces oxygen concentrations in aggregates, and for selenium reduction. Thus, rates of electron donor consumption are faster under oxic conditions and the electron donor concentrations inside the aggregate are lower than under anoxic conditions. At the core of aggregates, the electron donor can become limiting for selenium reduction, but less so in aggregates of smaller size where the average diffusion path to the advective boundary (electron donor supply) is shorter than for larger aggregates. As a result, there is an interactive effect of electron donor concentrations and aggregate size under conditions that are oxic in bulk: The concentrations of reduced selenium retained in the solid phase will scale more strongly with aggregate size if the supply of electron donor is larger. In summary, all other things equal, the amount of reduced selenium retained by a soil is expected to scale with increased aggregate size or electron donor concentrations, and with decreased aeration. Additionally, there are important interactive effects between these variables since, in the presence of oxygen, organic carbon (electron donor) concentrations increase the impact of aggregate size on reduced selenium concentrations.

With regards to selenium retention, the impact of aggregate size on elemental selenium concentrations is particularly relevant. Elemental selenium is insoluble and environmentally observed rates of oxidation are 3-4 orders of magnitude below those of reduction (Stolz et al., 2002; Stolz et al., 2006). Thus soil elemental selenium is a good pool for long-term selenium retention and the transformation of selenium oxyanions to solid elemental selenium has been suggested as a remedial strategy for contaminated sites (Darcheville et al., 2008; Dungan and Frankenberger, 1999; Oremland et al., 1991). Average concentrations of both solid phase selenite and elemental selenium scale with aggregate size, but the effect is particularly pronounced for the elemental selenium fraction. Furthermore, in contrast to selenite, elemental selenium concentrations are not expected to reach a steady-state according to our reactive transport model. It can therefore be expected that, as long as conditions are favorable to selenium reduction persist, the impact of aggregate size on elemental selenium content will keep increasing over time as the concentrations of elemental selenium build up. Increased soil aggregation may thus lead to a significant increase in long-term selenium retention.

Further studies are needed to establish whether the impact of aggregate size on selenium retention described here is significant at the field scale. A single, artificial aggregate surrounded by saturated flow cannot capture the full complexity of a structured soil and relevant processes are likely to have been excluded. For example, selenite diffusing from aggregates may build up in macropores along the diffusion path, thereby decreasing the concentration gradient at the aggregate-macropore interface and reducing the impact of aggregate size on intra-aggregate selenite concentrations. Furthermore, the trends here discussed were obtained with selenate supplied in excess, while diffusive limitations in selenate supply may reduce selenium reduction in larger aggregates under

field conditions. On the other hand, the dynamic saturation conditions in a natural surface soil may serve to increase the impact of aggregate size on selenium reduction through steeper redox gradients, as the macropores surrounding aggregates are expected to be filled with air rather than water part of the time. The advantage of simplified models in studying complex natural systems is that they allow for the isolation of individual processes that may be inextricable in nature. The results here described, point to general reactive transport mechanisms that may lead a soil with a larger mean aggregate size to retain more selenium. This would have implications for the management of irrigated seleniferous soils, since the fraction of macro-aggregates (>0.25 mm in diameter) in a soil is sensitive to agricultural management on time scales of 2 years or less (Degens, 1997). Notably, conservation tillage has been found to lead to significant increases in both mean soil aggregate size and organic matter content of surface soils (Angers et al., 1993; Carter, 1992). Similarly, the addition of manure can result in a rapid increase of mean aggregate size within the first two years of application (Whalen et al., 2003). It is particularly interesting to note that organic carbon input can increase aggregate size, since the concomitant increase in electron donor availability and aggregate size are expected to synergistically enhance selenium retention according to our model. The beneficial effects of soil aggregation for plant growth have long been established (Dexter, 1988). If there were to be additional external benefit to enhancing soil structure for seleniferous soils, in the form of reduced selenium exports, conservation tillage and organic amendments may prove to be an attractive management technique in regions prone to irrigation-induced selenium contamination. Viewed in this context, our results suggest that field studies investigating the effect of conservation tillage and organic matter applications on selenium retention are may be warranted in the search for management strategies to reduce selenium export.

In conclusion, our reactive transport model suggests that enhanced soil aggregation may increase the fraction of elemental selenium in aggregates and consequently increase the degree to which selenium is retained. This effect could be useful in the prevention of irrigation-induced selenium contamination. Managing seleniferous agricultural soils in a way that optimizes aggregation (i.e. reduced tillage and organic amendments) may reduce the amount of exported selenium and thus alleviate the impact of selenium pollution for aquatic ecosystems downstream of such soils.

5. Appendix: Detailed description of reactive transport model

The cylindrical reactor is represented by a rectangle of 3.70 cm height and 2.55 cm width, corresponding to the length and radius of the reactor, respectively, rotated around a central symmetry axis. In the free water surrounding the aggregate, the flow and pressure field is computed according to the stationary, incompressible Navier-Stokes equations:

$$\rho(\mathbf{u}\cdot\nabla)\mathbf{u} = \nabla\cdot\left[-p\mathbf{I} + \eta\left(\nabla\mathbf{u} + (\nabla\mathbf{u})^T\right)\right] \text{ and } \nabla\cdot\mathbf{u} = 0\,, \qquad \text{(A1)}$$

where **u** is a velocity vector, ρ is density (1kg L^{-1}), p is pressure and η is dynamic viscosity (0.001 Pa s), and **I** the identity matrix. Inside the aggregate, **u** and p are computed according to the Brinkman equations:

$$\rho\frac{\partial \mathbf{u}}{\partial t}+\frac{\eta}{\kappa}\mathbf{u}=\nabla\cdot\left[-p\mathbf{I}+\eta\left(\nabla\mathbf{u}+(\nabla\mathbf{u})^{T}\right)\right] \text{ and } \nabla\cdot\mathbf{u}=0, \tag{A2}$$

where t is time (s) and κ is permeability. Its value was computed based on grain size and porosity, using Kozeny-Carman's empirical relationship

$$\kappa = d^{2}\phi^{3}/\left(80(1-\phi)^{2}\right), \tag{A3}$$

where d is a representative grain diameter and ϕ is porosity (Bear, 1972) (d = 200 μm, ϕ = 0.58 as stated in the methods section).

A uniform flow velocity is imposed at inflow side of the reactor, a no slip condition is applied at the outer reactor wall (**u**=0), a neutral outflow condition is imposed at that top,

$$\left[-p\mathbf{I}+\eta\left(\nabla\mathbf{u}+(\nabla\mathbf{u})^{T}\right)\right]\mathbf{n}=0, \tag{A4}$$

where **n** is the normal vector, and axial symmetry is imposed at the reactor center. At the aggregate surface, internal and external pressure and velocities are set to match.

The following reactions are considered.

Selenate reduction ($R_{Se(VI)}$):

$$CH_3COCOO^- + 5SeO_4^{2-} + H^+ \rightarrow 5SeO_3^{2-} + 3CO_2 + 2H_2O \tag{A5}$$

Selenite reduction ($R_{Se(IV)}$):

$$2CH_3COCOO^- + 5SeO_3^{2-} + 12H^+ \rightarrow 5Se(0) + 6CO_2 + 9H_2O \tag{A6}$$

Aerobic respiration (R_O):

$$2CH_3COCOO^- + 5O_2 + 2H^+ \rightarrow 6CO_2 + 4H_2O \tag{A7}$$

Reaction rates are formulated with a Monod type dependency on both electron acceptor and donor (pyruvate) and with a term for oxygen inhibition for selenate and selenite reduction:

$$R_{Se(VI)} = k_{Se(VI)}\rho_{cells}\cdot\frac{[pyruvate]}{K_{mSe(VI)}^{pyruvate}+[pyruvate]}\cdot\frac{[SeO_4^{2-}]}{K_m^{Se(VI)}+[SeO_4^{2-}]}\cdot Inh_{Se(VI)}([O_2]) \tag{A8}$$

$$R_{Se(IV)} = k_{Se(IV)}\rho_{cells}\cdot\frac{[pyruvate]}{K_{mSe(IV)}^{pyruvate}+[pyruvate]}\cdot\frac{[SeO_3^{2-}]}{K_m^{Se(IV)}+[SeO_3^{2-}]}\cdot Inh_{Se(IV)}([O_2]) \tag{A9}$$

$$R_O = k_O \rho_{cells} \cdot \frac{[pyruvate]}{K_{mO}^{pyruvate} + [pyruvate]} \cdot \frac{[O_2]}{K_m^O + [O_2]} \quad \text{(A10)}$$

k_i are cell specific rate constant for the respective electron acceptor and K_{mi} are the half-saturation constants for the specific reaction (Rittman and VanBriesen, 1996). **Table A1** shows the values used for these parameters in this model. The density of *E. cloacae* cells, ρ_{cells}, was set to 1×10^8 cells/g in predictive simulations, but expressed as a function of time in fitting experimental data:

$$\rho_{cells}(t) = \rho_{cells}(0) \cdot \left(1 - \delta_{t>t_d} \alpha \frac{t - t_d}{t_f - t_d}\right) \quad \text{(A11)}$$

with t_f being the end of the simulation (192 h = 691200 s) and δ being 1 if $t>t_d$, 0 else. $\rho_{cells}(0)$, α, and t_d were used as fitting parameters to achieve modeled breakthrough curves and solid concentrations that closely match the experimentally observed ones. $\rho_{cells}(0)$ was varied between $1\text{-}3\times10^8$ cells/g, while α and t_d were varied (between 0.2-0.7 and between $1\text{-}5\times10^5$ s respectively) for anoxic simulations and the oxic simulation with 1.2 mM pyruvate and 0.8 mM selenate input solution and set to 0 otherwise.

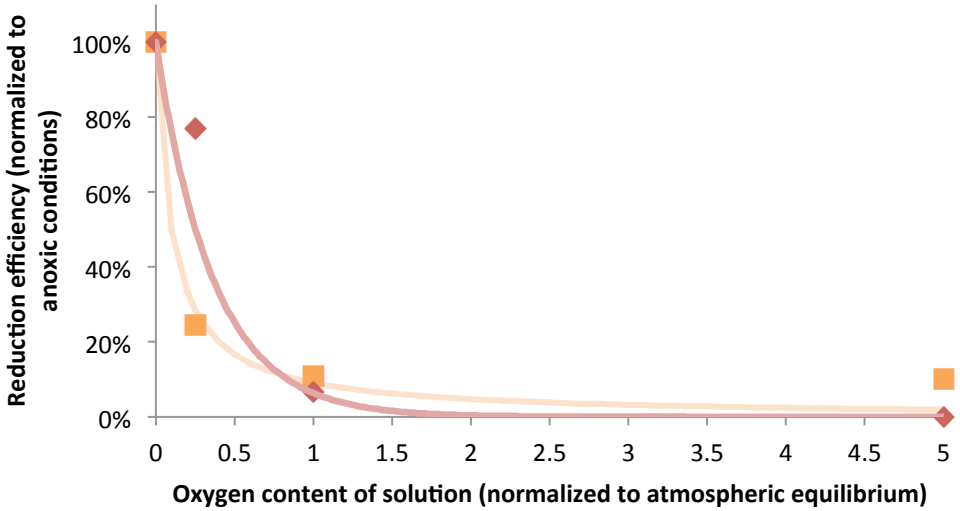

Figure A1. Selenate (red) and selenite (orange) inhibition models (solid lines) fitted to the data collected by Losi and Frankenberger (1997b) for *E. cloacae* reducing selenate (diamonds) and selenite (squares) at various oxygen concentrations. The inhibition of selenate reduction was fitted with a reverse Monod type inhibition term (Van Cappellen and Gaillard, 1996) and that of selenite reduction with an exponential function (see Eqs. A12 & A13 in the Appendix of the main manuscript). The R^2 of these fits are 0.985 and 0.999 for the inhibition of selenate and selenite reduction respectively.

Finally, for oxidation of pyruvate with selenate or selenite as electron acceptor, an oxygen concentration dependent inhibition term, $Inh_i([oxygen])$, was introduced (Van Cappellen and Gaillard, 1996) parameterized by fitting the data on the inhibition of selenate and selenite reduction by *E. cloacae* at various oxygen concentrations collected by Losi and Frankenberger (1997b). Assuming that the oxygen concentration of an aqueous solution in equilibrium with atmospheric air (20% oxygen) is 0.26 mM their data is best described by:

$$Inh_{Se(VI)}([oxygen]) = 1 - \frac{[oxygen]}{[oxygen] + K_{inh}} \tag{A12}$$

$$Inh_{Se(IV)}([oxygen]) = \exp(-a_{inh} \cdot [oxygen]) \tag{A13}$$

with K_{inh} = 0.026 mM and a = 10.6 mM^{-1}. These inhibition models fit Losi and Frankenberger's (1997b) data with R^2 of 0.985 and 0.999 for $Inh_{Se(VI)}$ and $Inh_{Se(IV)}$, respectively (**Fig. A1**).

These reactions are combined with expressions for the transport of dissolved constituents by advection and diffusion in an expression for the conservation of mass:

$$\varepsilon \frac{\partial C}{\partial t} = \nabla \cdot \left(- \varepsilon D \nabla C \right) - \mathbf{u} \cdot \nabla C + \varepsilon R \tag{A14}$$

where flow velocity **u** is obtained from solving the above Navier-Stokes and Brinkman equations. D is the molecular diffusion coefficient (D_{mol}), estimated based on (Haynes, 2011), which inside the aggregate is corrected for tortuosity:

$$D = D_{mol} \cdot \frac{1}{1 - \ln(\phi^2)} \tag{A15}$$

At the slow flow velocities used, hydrodynamic dispersion is assumed negligible and size exclusion is ignored. ε is 1 in the free fluid and ϕ inside the aggregate. For oxic simulations oxygen concentrations were fixed at 0.26 mM (water saturated with atmospheric concentrations) in the free fluid surrounding the aggregate (to represent air flushing) and allowed to vary according to the mass conservation expressions on the interior of the aggregate. For anoxic simulations oxygen concentrations were set to zero throughout. The rate terms are assembled using the above rate laws and reaction stoichiometries (Eqs. A5-A10).

6. Supplementary Material

Movie S1 – Dynamics of pyruvate concentrations [mM]*

Movie S2 – Dynamics of oxygen concentrations [mM]*

Movie S3 – Dynamics of selenate concentrations [mM]*

Movie S4 – Dynamics of selenite concentrations [mM]*

Movie S5 – Dynamics of elemental selenium concentrations [mM]*

Movie S6 – Dynamics of selenate reduction [mM/s]*

Movie S7 – Dynamics of selenite reduction [mM/s]*

*Note: in all movies time is in s and dimensions in m. Input concentrations of selenate and pyruvate in this scenario were set to 0.4 and 0.3 mM, respectively. The supplementary material is avaialable for download on the Biogeosciences server on which a previous version of this chapter has been published: http://www.biogeosciences.net/10/1323/2013/bg-10-1323-2013-supplement.zip.

7. Acknowledgements

I thank Chandra Richards and Vu Ngo for running the analysis of bromide concentrations in outflow samples, and Walter Mayeda, Eduardo Ruiz, Hoai Ngo, and Peter Ng for help in the laboratory. I thank Sharon Bone, Gavin McNicol, and Steven Hall for commentary during manuscript preparation. I also thank Christof Meile for teaching me the art of reactive transport modeling. Finally, I thank anonymous referees as well as the editors at Biogeosciences, where a prior version of this manuscript was published.

8. References

Angers, D.A., N. Samson, et al. 1993. Early changes in water-stable agregation induced by rotation and tillage in a soil under barley production. Canadian Journal of Soil Science 73:51-59.

Arah, J.R.M., and A.J.A. Vinten. 1995. Simplified models of anoxia and denitrification in aggregated and simple-structured soils. Eur. J. Soil Sci. 46:507-517.

Bear, J. 1972. Dynamics of fluids in porous media. Dover, New York.

Brady, N.C., and R.R. Weil. 2002. The nature and properties of soils. 13th ed. Prentice Hall, Upper Saddle River, NJ.

Carter, M.R. 1992. Influence of reduced tillage systems on organic matter, microbial biomass, macro-aggregate distribution and structural stability of the surface soil in a humid climate. Soil and Tillage Research 23:361-372.

Darcheville, O., L. Fevrier, et al. 2008. Aqueous, solid and gaseous partitioning of selenium in an oxic sandy soil under different microbiological states. Journal of Environmental Radioactivity 99:981-992.

Davis, B., R. Dulbecco, et al. 1973. Bacterial physiology: Microbiology. 2nd ed. Harper and Row, Maryland.

Degens, B.P. 1997. Macro-aggregation of soils by biological bonding and binding mechanisms and the factors affecting these: A review. Aust. J. Soil Res. 35:431-459.

Dexter, A.R. 1988. Advances in characterization of soil structure. Soil and Tillage Research 11:199-238.

Dungan, R.S., and W.T. Frankenberger, Jr. 1999. Microbial transformations of selenium and the bioremediation of seleniferous environments. Bioremediation Journal 3:171–188.

Hamilton, S.J. 2004. Review of selenium toxicity in the aquatic food chain. Science of the Total Environment 326:1-31.

Haynes, W.M. 2011. Crc handbook of chemistry & physics (internet version). [Online] CRC Press/Taylor & Francis Group, Boca Raton.

Kaurichev, I.S., and L.F. Tararina. 1972. Oxidation-reduction conditions within and outside aggregates of grey forest soil. Pochvovedenie 10:39-42.

Kausch, M., P. Ng, et al. 2012. Soil-aggregate-scale heterogeneity in microbial selenium reduction. Vadose Zone Journal DOI:10.2136/vzj2011.0101.

Lemly, A.D. 2004. Aquatic selenium pollution is a global environmental safety issue. Ecotoxicology and Environmental Safety 59:44-56.

Lenz, M., and P.N.L. Lens. 2009. The essential toxin: The changing perception of selenium in environmental sciences. Science of The Total Environment 407:3620-3633.

Losi, M.E., and W.T. Frankenberger. 1997. Reduction of selenium oxyanions by *enterobacter cloacae* sld1a-1: Isolation and growth of the bacterium and its expulsion of selenium particles. Applied and Environmental Microbiology 63:3079-3084.

Losi, M.E., and W.T. Frankenberger. 1997. Reduction of selenium oxyanions by *enterobacter cloacae* strain sld1a-1: Reduction of selenate to selenite. Environmental Toxicology and Chemistry 16:1851-1858.

Losi, M.E., and W.T. Frankenberger. 1998. Reduction of selenium oxyanions by *enterobacter cloacae* strain sld1a-1. p. 515–544. *In* W.T. Frankenberger, and R.A. Engberg (ed.) Environmental chemistry of selenium. Marcel Dekker, New York.

Luoma, S.N., and T.S. Presser. 2009. Emerging opportunities in management of selenium contamination. Environmental Science & Technology 43:8483–8487.

Ma, J., D.Y. Kobayashi, et al. 2007. Chemical kinetic and molecular genetic study of selenium oxyanion reduction by *enterobacter cloacae* sld1a-1. Environmental Science & Technology 41:7795-7801.

Ma, J.C., D.Y. Kobayashi, et al. 2009. Role of menaquinone biosynthesis genes in selenate reduction by enterobacter cloacae sld1a-1 and escherichia coli k12. Environmental Microbiology 11:149-158.

Masue-Slowey, Y., B.D. Kocar, et al. 2011. Transport implications resulting from internal redistribution of arsenic and iron within constructed soil aggregates. Environmental Science & Technology 45:582-588.

Oremland, R.S., J.T. Hollibaugh, et al. 1989. Selenate reduction to elemental selenium by anaerobic bacteria in sediments and culture - biogeochemical significance of a novel, sulfate-indipendant respiration. Applied and Environmental Microbiology 55:2333-2343.

Oremland, R.S., N.A. Steinberg, et al. 1991. Insitu bacterial selenate reduction in the agricultural drainage systems of western nevada. Applied and Environmental Microbiology 57:615-617.

Pallud, C., M. Kausch, et al. 2010. Spatial patterns and modeling of reductive ferrihydrite transformation observed in artificial soil aggregates. Environmental Science & Technology 44:74–79.

Pallud, C., Y. Masue-Slowey, et al. 2010. Aggregate-scale spatial heterogeneity in reductive transformation of ferrihydrite resulting from coupled biogeochemical and physical processes. Geochimica et Cosmochimica Acta 74:2811-2825.

Pirt, S.J. 1975. Principles of microbe and cell cultivation. John Wiley & Sons, NYC.

Presser, T.S. 1994. "the kesterson effect". Environmental Management 18:437-454.

Ridley, H., C.A. Watts, et al. 2006. Resolution of distinct membrane-bound enzymes from *enterobacter cloacae* sld1a-1 that are responsible for selective reduction of nitrate and selenate oxyanions. Applied and Environmental Microbiology 72:5173-5180.

Rittman, B.E., and J.M. VanBriesen. 1996. Microbial processes in reactive modeling. p. 311-332. *In* P.C. Lichtner, C.I. Steefel, and E.H. Oelkers (ed.) Reactive transport in porous media. Mineralogical Society of America, Washington, D.C.

Seiler, R.L., J.P. Skorupa, et al. 1999. Areas susceptible to irrigation-induced selenium contamination of water and biota in the western united states p. 36. U.S. Geological Survey Circular. U.S. Department of the Interior.

Sexstone, A.J., N.P. Revsbech, et al. 1985. Direct measurement of oxygen profiles and denitrification rates in soil aggregates. Soil Sci. Soc. Am. J. 49:645-651.

Sposito, G., A. Yang, et al. 1991. Selenate reduction in an alluvial soil. Soil Sci Soc Am J 55:1597-1602.

Steinberg, N.A., and R.S. Oremland. 1990. Dissimilatory selenate reduction potentials in a diversity of sediment types. Applied and Environmental Microbiology 56:3550-3557.

Stolz, J.F., P. Basu, et al. 2002. Microbial transformation of elements: The case of arsenic and selenium. Int Microbiol 5:201–207.

Stolz, J.F., P. Basu, et al. 2006. Arsenic and selenium in microbial metabolism. Annual Review of Microbiology 60:107-130.

Stolz, J.F., and R.S. Oremland. 1999. Bacterial respiration of arsenic and selenium. FEMS Microbiology Reviews 23:615-627.

Strawn, D., H. Doner, et al. 2002. Microscale investigation into the geochemistry of arsenic, selenium, and iron in soil developed in pyritic shale materials. Geoderma 108:237-257.

Tokunaga, T.K., S.R. Sutton, et al. 1994. Mapping of selenium concentration in soil aggregates with synchrotron x-ray fluorescence microprobe. Soil Sci. 158:421-434.

Tokunaga, T.K., J. Wan, et al. 2003. Distribution of chromium contamination and microbial activity in soil aggregates. Journal of Environmental Quality 32:541-549.

Van Capellen, P., and J.-F. Galliard. 1996. Biogeochemical dynamics in aquatic sediments. *In* P.C. Lichtner, C.I. Steefel, and E.H. Oelkers (ed.) Reactive transport in porous media. Mineralogical Society of America, Washington, D.C.

Watts, C.A., H. Ridley, et al. 2003. Selenate reduction by *enterobacter cloacae* sld1a-1 is catalysed by a molybdenum-dependent membrane-bound enzyme that is distinct from the membrane-bound nitrate reductase. FEMS Microbiology Letters 228:273-279.

Whalen, J.K., Q.C. Hu, et al. 2003. Compost applications increase water-stable aggregates in conventional and no-tillage systems. Soil Sci. Soc. Am. J. 67:1842-1847.

WHO. 1996. Chapter 6 - selenium p. 105-122. Trace elements in human nutrition and health. World Health Organization, Geneva.

Yee, N., and D.Y. Kobayashi. 2008. Molecular genetics of selenate reduction by *enterobacter cloacae* sld1a-1. Advances in Applied Microbiology 64:107-123.

Yee, N., J. Ma, et al. 2007. Se(vi) reduction and the precipitation of se(0) by the facultative bacterium *enterobacter cloacae* sld1a-1 are regulated by fnr. Applied and Environmental Microbiology 73:1914-1920.

Chapter 4 – A diagenetic model for selenium distribution in Salton Sea sediment

Abstract – The Salton Sea, California's largest inland water body, is an essential stopover for migratory birds along the Pacific Flyway. Reported concentrations of selenium in the tissues of Salton Sea fish are high enough to threaten the reproductive and immune health of piscivorous birds. Most selenium entering the Salton Sea is sequestered in its sediment through microbial reduction, yet without information on the speciation and distribution of this selenium within the sediment, the threat of this selenium pool to Salton Sea wildlife is difficult to assert. To predict the likely distribution profiles of selenium within the sediment and evaluate likely factors driving variability in near surface sediment selenium concentrations, we constructed a diagenetic model for selenium in Salton Sea sediment. Depending on local reduction kinetics, and dissolved concentrations in the water column, our model predicts near surface (2 cm) sediment concentrations of solid phase selenium between 0.024 and 0.272 μmol/g, which is in good agreement with the literature if the potential impact of bioturbation in lowering near surface concentrations by ~25% is considered. The range of modeled selenium concentrations in surface sediment crosses threshold values for which negative impacts on fish and waterfowl have been predicted (0.025-0.030 μmol/g) or observed (0.050 μmol/g) at other sites, suggesting that ecological impacts of selenium in the Salton Sea may depend locally on variation in the diagenetic factors here explored.

1. Introduction

Selenium (Se) contamination represents an acute threat to aquatic ecosystems in the Western United States (Presser et al., 1994; Seiler et al., 1999) and around the world (Lemly, 2004). The trace element is an unusual contaminant, since its toxic effects on fish and waterfowl are not predictable solely based on dissolved concentrations (Stewart et al., 2010). It has for example been argued that concentrations in fish tissue or sediments may be a better indicator of ecosystem contamination (Canton and Van Derveer, 1997; Luoma and Presser, 2009; Renner, 2003; Van Derveer and Canton, 1997). While current US regulatory levels are still based on a dissolved concentrations (US.EPA, 1987), efforts are underway to transition to site specific criteria that would account for partitioning between the dissolved phase and suspended particulates, as well as trophic transfer in the local food web (Presser and Luoma, 2010a). Such an approach also has the potential to lead to greater harmonization in international guidelines for selenium, as regulatory levels based on dissolved concentrations differ dramatically (from 2 μg L^{-1} to no legal limit) between countries (Luoma and Presser, 2009). In this context it is worthwhile to evaluate the threat to aquatic ecosystems arising from selenium reservoirs other than the dissolved phase, such as the selenium in aquatic sediments.

Selenium occurs naturally in four oxidation states (-II, 0, IV, and VI), with its bioavailability, solubility, and sorptive behavior depending critically on its speciation. In its highest oxidation states (IV and VI), selenium takes the form of the highly soluble and bioavailable oxyanions selenate (SeO_4^{2-}) and selenite (SeO_3^{2-}) (Dungan and Frankenberger, 1999). Selenate sorbs weakly to soil solid particles (Neal and Sposito, 1989), while selenite forms strong stable complexes on the surfaces of Al-, Fe- and Mn-oxy-hydroxides (Balistrieri and Chao, 1990; Catalano et al., 2006; Mandal et al., 2009; Saha and Huang, 2010; Su and

Suarez, 2000) and of clays (Balistrieri and Chao, 1987; Baryosef and Meek, 1987; Duc et al., 2003), reducing its mobility. Elemental selenium, Se(0), is solid and immobile, whereas the most reduced form of selenium (-II) occurs in soluble and bioavailable organo-selenides, solid metal-selenides, or in gaseous methylated forms (Hamilton, 2004; Stolz and Oremland, 1999). Transformations between these various species are kinetically hindered and thus the speciation of selenium is poorly predicted by thermodynamic models (Luoma and Presser, 2009) and key redox reactions are catalyzed primarily by microorganisms (Stolz and Oremland, 1999; Stolz et al., 2006). The microbial reduction of selenate *via* selenite to elemental selenium is an important attenuation pathway for selenium in soils and sediments (Darcheville et al., 2008; Dungan and Frankenberger, 1999; Oremland et al., 1991; Steinberg and Oremland, 1990; Strawn et al., 2002). Recent work showed that microbial reduction of selenium can go beyond elemental selenium and that selenide can be produced by selenite-reducing bacteria during incubation of estuarine sediment slurries containing elemental selenium (Herbel et al., 2003). Selenides may then form insoluble precipitates with metallic cations (Fe^{2+}, Pb^{2+}, Zn^{2+}, Cu^{2+}) under highly reducing conditions (Elrashidi et al., 1989; Masscheleyn et al., 1990). Knowledge regarding the speciation composition of reduced selenium in sediments is limited, since most published information has been obtained through extraction procedures that can yield ambiguous results (Herbel et al., 2003; Oram et al., 2008; Tokunaga et al., 1998). There is evidence suggesting elemental selenium is the major species in sediment upon reduction (Tokunaga et al., 1998; Wiramanaden et al., 2010), however organic species and metal selenides (Se(-II)) have also been observed together with elemental selenium (Wiramanaden et al., 2010). Due to limits in the current understanding of the formation rates and processes for these species in natural sediments, as well as the analytical challenges associated with their detection, elemental selenium and solid selenium in the –II oxidation state are frequently undistinguishable in natural samples (Oram et al., 2008). As a result, they are often considered as a single selenium pool in describing aquatic ecosystems.

Of the 66 water bodies listed on California's 303(d) list of impaired waters for concerns regarding selenium pollution, the Salton Sea is by far the largest (US.EPA, 2010) and arguably the one of greatest ecological significance. The Salton Sea is California's largest inland water body (974 km^2) (Krants et al., 2002). It is shallow (maximum depth: 16 m, average depth: 8 m), moderately hypersaline (currently 48 g/L total dissolved solids), and has an uncertain ecological future (Cohen and Hyun, 2006; Krants et al., 2002; Schroeder et al., 2002; VillaRomero et al., 2013). It has been labeled one of the most important bird habitats in the American Southwest, since it is used by more than 100,000 waterfowl pertaining to resident and migratory bird species, including endangered ones like the brown pelican (*Pelecanus occidentalis* Linnaeus) (Moreau et al., 2007a). Since the Salton Sea's creation in 1906, more than 90% of California's natural wetland habitat has been converted to agricultural or urban uses making the artificial lake an essential stopover for migratory waterfowl on the Pacific Flyway (Krants et al., 2002).

Selenium concentrations in the agricultural runoff entering the Salton Sea (2.4-8.0 $\mu g\ L^{-1}$) frequently exceed the 5 $\mu g\ L^{-1}$ national water quality criterion for the protection of aquatic life (Holdren and Montano, 2002; Schroeder et al., 2002; Setmire and Schroeder, 1998; US.EPA, 1987). Despite the steady influx, the dissolved selenium concentrations in the Salton Sea water column are consistently low between 0.5 and 2.0 $\mu g\ L^{-1}$ (Holdren and Montano, 2002; Schroeder et al., 2002) – 99% of selenium entering the lake is sequestered within its sediment (Schroeder et al., 2002). In a previous study we demonstrated that microbial reduction in Salton Sea sediment

is the most likely mechanism for this sequestration (VillaRomero et al., 2013). Despite the effective removal of selenium from solution, the selenium concentrations measured in the tissues of four Salton Sea fish species including the dominant tilapia (*Oreochromis mossambicus* x *O. urolepis hornorum* hybrid) were elevated enough (~2 μg g^{-1}) to potentially impact viability of the fish themselves as well as the reproductive and immune health of piscivorous birds consuming them (Moreau et al., 2007a; Moreau et al., 2007b). This suggests the existence of pathways for sedimentary selenium to enter the food chain.

Here we present a diagenetic model, based on the current understanding of selenium cycling in the Salton Sea and similar environments. Using this model we derive plausible distribution profiles for selenate and solid phase selenium in littoral Salton Sea sediments and explore the significance of variation in the reduction kinetics, sedimentation rates, dissolved concentrations, and bioturbation on predicted selenium concentrations in near surface sediment.

2. Materials and Methods

2.1. Study site

The Salton Sea was formed accidentally during multiple flood events in 1905/1906, when the destruction of levees, dams, and flood gates near the U.S.-Mexican border changed the Colorado River's course. For a one-year period, the river's entire water load was brought into the Imperial Valley thus forming the Salton Sea (Krants et al., 2002). The lake has no outflows or groundwater interactions, and has since been maintained solely through input of irrigation drainage, while the arid climate and high evaporation rates (~1.8 m yr^{-1} (Setmire and Schroeder, 1998)) have led to a steady increase in salinity.

Selenium is imported to the Salton Sea through its tributaries, the Alamo, New and Whitewater Rivers that carry concentrations between 2.4 and 8 μg L^{-1} (Holdren and Montano, 2002; Schroeder et al., 2002; Setmire and Schroeder, 1998). This selenium originates from soils in the Upper Colorado River Basin where it is mobilized through irrigation and is essentially all in its most oxidized state, selenate (Schroeder et al., 2002). In the closed Salton Sea basin, selenium volatilization is negligible (Schroeder and Orem, 2000; Schroeder et al., 2002; Setmire and Schroeder, 1998; Vogl and Henry, 2002) and virtually all selenium entering the lake is thought to be sequestered in its sediment (Schroeder et al., 2002) through microbial reduction (VillaRomero et al., 2013). A wide range of surface sediment selenium concentrations (0.58 up to 15 μg g^{-1}) have been reported for the Salton Sea (Byron and Ohlendorf, 2007; Schroeder and Orem, 2000; Schroeder et al., 2002). These concentrations are about 30 times larger than those found in the soils of the surrounding areas (Schroeder et al., 1993). Generally selenium concentrations appear to be elevated at deep sediment locations compared to littoral ones and in the northern part of the lake compared to the southern part (Krants et al., 2002; Vogl and Henry, 2002).

For the past 70 years or more, the Salton Sea's benthos has been dominated by the polychaete *Neanthes (Nereis) succinea* (Carpelan and Linsley, 1961; Detwiler et al., 2002; Dexter et al., 2007; Hartman, 1939). While there is evidence that the pileworm's population density has been decreasing over time (Detwiler et al., 2002), it is still the lake's most abundant macroinvertebrate (Dexter et al., 2007). The estimated standing stock of *N. succinea* in the Salton Sea fluctuates between $1.5 \cdot 10^{10}$ kg in March and $6.7 \cdot 10^{7}$ kg in September. Spring and

summer anoxia leads to a drastic decline in abundance, with *N. succinea* completely absent at water depths below 2 m between July and November (Detwiler et al., 2002). The yearly average lake-wide density in 1999 was 927 m^{-2}, with local maximal densities as high as 81,000 in littoral and 21,000 m^{-2} in offshore sediments. These densities are high compared to those typically observed for *N. succinea* in brackish and marine sites (maximum reported values between 90 and 3,200 m^{-2}) (Detwiler et al., 2002). This high abundance make it necessary to consider the potential impact of bioturbation in the distribution of chemical species in Salton Sea sediments (Swan et al., 2007), even though bioturbation is usually minimal in hypersaline environments (Jaglarz and Uchman, 2010).

2.1. Modeling selenium reduction in Salton Sea sediments

We considered selenate as the dominant dissolved species, since it is documented that it is the main form of selenium entering the Salton Sea (Schroeder et al., 2002). The rate of microbial selenate reduction in sediments follows Monod kinetics with respect to selenate concentration as described by Steinberg and Oremland (1990):

$$R = \frac{v_{\max} C_{SeVI}}{K_m + C_{SeVI}} \quad (1)$$

where v_{max} is the maximum rate of selenate reduction [μmol/L_{tot}/day], C_{SeVI} is the dissolved selenate concentration [μM], and K_m is the selenate half-saturation constant [μM]. Steinberg and Oremland (1990) determined potential selenate reduction rates using core incubations on a variety of sediments sampled from freshwater, saline, and hypersaline sites. They found that apparent K_m ranged between 7.9 to 720 μM independent of salinity, pH, or ambient selenate concentrations. This was thus deemed a plausible range of values for model. Our choice of v_{max} values was informed by a previous study (VillaRomero et al., 2013) in which we determined apparent v_{max} values ranging between 30 and 300 μmol/L_{tot}/h in surface sediment slurries from 7 Salton Sea littoral sites. Selenate adsorption is negligible on Salton Sea sediments (VillaRomero et al., 2013) and dissolved selenite is only a temporary phase during reduction in sediments (Dungan and Frankenberger, 1999; Oremland et al., 1991; Oremland et al., 1990; Steinberg and Oremland, 1990) thus obviating the need for consideration of a separate adsorbed phase in our model. The solid phase is assumed to contain all selenium that has been microbially reduced from selenate in solution. Neither the solid phase speciation of selenium in Salton Sea sediment nor that of the products of microbial selenate reduction in sedimentary environments has conclusively been determined in the literature. However, it is expected that any form of reduced selenium is immobilized in the sediment – either through adsorption in the case of selenite, or by virtue of being a solid in the case of Se(0) and Se(-II) – it is thus unnecessary to further define the chemical speciation of the modeled solid phase.

2.2. Implementation of diagenetic model

Since selenate adsorption is negligible and there is no selenate solid phase, the only way for selenium to enter the solid phase is through reduction. The reduction reaction (Eq. 1) is combined with standard constitutive equations for molecular diffusion, sedimentation as well as bioturbation (Boudreau, 1997) – the latter one being considered only in the second part of our modeling efforts – to yield the following set of coupled partial differential equations for the mass balance in dissolved selenate (Eq. 2) and solid phase selenium (Eq. 3):

$$\frac{\partial}{\partial t}\left(\phi C_{SeVI}\right) = \frac{\partial}{\partial z}\left(D\phi \frac{\partial (C_{SeVI})}{\partial z}\right) - \frac{v_{\max} C_{SeVI}}{K_m + C_{SeVI}} \quad (2)$$

$$\frac{\partial}{\partial t}\left(\rho_d S_{Se}\right) = \frac{\partial}{\partial z}\left(D_b \frac{\partial \left(\rho_d S_{Se}\right)}{\partial z}\right) - \frac{\partial}{\partial z}\left(u_{sed} \rho_d S_{Se}\right) + \frac{v_{\max} C_{SeVI}}{K_m + C_{SeVI}} \quad (3)$$

where t is time [days], Φ is porosity [L/L_{tot}][1], C_{SeVI} is the dissolved selenate concentration in pore water [µM], z is depth from the sediment-water interface [cm], u_{sed} is the sedimentation rate [cm/day], D_b is the bioturbation rate [cm^2/day] (set equal zero unless otherwise specified, i.e. section 2.4), ρ_d is the dry bulk density of the sediment [g/L_{tot}], S_{Se} is the solid phase selenium concentration [µmol/g], and D [cm^2/day] is the apparent diffusion coefficient, which is the molecular diffusion of selenate in pure water (D_{mol} = $1.0 \cdot 10^{-5}$ cm^2/s) (Haynes, 2011), corrected for tortuosity as described by (Boudreau, 1997):

$$D = D_{mol} \cdot \frac{1}{1 - \ln(\phi^2)} \quad (4)$$

The porosity and bulk density used correspond to the mean values we previously determined for littoral Salton Sea sediments (Φ = 0.5±0.05 L/L_{tot}, ρ_d = 1350±100 g/L_{tot}) (VillaRomero et al., 2013). Note that concentrations in the dissolved phase are expressed with respect to the volume of the solute phase (L), while the mass balance equations are expressed with respect to the total volume (L_{tot}) which includes the volume of both solute and solid phase. The sedimentation rate was chosen as 0.127 cm/year which was the average sedimentation rate estimated for the Salton Sea for the period after 1935 by (Arnal, 1961).

We used initial conditions of C_{SeVI} (t=0) = S_{Se} (t=0) = 0, and boundary conditions of C_{SeVI} (z=0) = $C_{SeVI\text{-}water}$, $\partial C_{SeVI}/\partial z(z=L) = 0$; $[u_{sed} S_{Se} - D_b \partial S_{Se}/\partial z](z=0) = \partial S_{Se}/\partial z(z=L) = 0$, where L is the length of the model domain considered (L = 20 cm). $C_{SeVI\text{-}water}$ was informed by the reported range of dissolved water column concentrations measured in the Salton Sea: 0.5-2 µg/L (Holdren and Montano, 2002; Schroeder et al., 2002).

The model was implemented in Python using the FiPi package (Jonathan et al., 2009) to solve the partial differential equations (the code is attached in the Appendix). Assuming constant parameters and boundary conditions and a finite model domain, the system will approach a steady-state. However Eq. 1 reaches steady-state in less than 2 days for parameter ranges as specified in **Table 1**, while the time for Eq. 2 to reach steady-state is of the order of L/u_{sed} (~100 years for the top 10 cm). The equations were thus solved sequentially, by first determining the steady-state solution for selenate concentrations across the sediment profile (Eq. 1) and then iterating the equation for solid phase selenium concentrations (Eq. 2) in time for 100 years. For selenate, steady-state was defined as a rate of change in the average selenate concentration across the profile of less than 10^{-5} µM/day.

[1] We distinguish here between the total volume measured in L_{tot} and the volume of the pore-space measured in L.

2.3. Assessing the impact of reaction kinetics, sedimentation rates, and water column selenate concentrations on near surface sediment concentrations of solid phase selenium

Of the parameters used in the model v_{max}, K_m, u_{sed}, and $C_{SeVI\text{-}water}$ are relatively unconstrained by the literature or expected to vary significantly within the Salton Sea (**Table 1**). To explore the impact of these parameters on the near surface concentrations of solid phase selenium, simulations were run across the full value range for each parameter with the other parameters at default values. The default values and parameter ranges explored are shown in **Table 1**. For v_{max}, the default value is the site mean of the 7 sites measured by VillaRomero et al. (2013). For K_m the median value of the 7 from the Steinberg and Oremland (1990) study was chosen, since the highest measured value (K_m = 700 µM) is an order of magnitude larger than the second highest (K_m = 60 µM). Only a single basin wide estimate (Arnal, 1961) was available for u_{sed} (0.127 cm/year) so this was chosen as the default value. Finally, for $C_{SeVI\text{-}water}$ 1 µg/L was deemed to be a characteristic value based on the small range reported in the literature (Holdren and Montano, 2002; Schroeder et al., 2002). Regarding the uncertainty ranges of parameters tested, for v_{max}, K_m, and $C_{SeVI\text{-}water}$ these correspond to the full ranges of reported values in the referenced studies. For u_{sed}, no range of measurements was available since the default value is based on a single estimate derived from planimeter measurements, and a rough estimate of the amount of sediment that was initially contributed by the Colorado River before this flux started to be retained by the Hoover Dam in 1935. Given the approximate nature of this estimate and the fact that sedimentation in the Salton Sea is likely to vary by location and water depth (Anderson et al., 2008) we assigned an uncertainty factor of 4 and used a parameter range of 0.03 to 0.5 cm/year. Confidence that average sedimentation values lie within this range is increased by an estimated sedimentation rate based on a single deep-water core from the Salton Sea of 0.23 cm/year by Schroeder et al. (2002).

In conducting this sensitivity analysis, the solid phase selenium concentration at a sediment depth of 2 cm was chosen as the target variable representing the response to parameter variations.

Table 1. Default parameter values and explored parameter ranges for v_{max}, K_m, u_{sed}, and $C_{SeVI\text{-}water}$. The literature sources used to inform the values chosen for each parameter are listed in the final column.

Parameter		Value			Unit	Reference
full name	notation	default	min.	max.		
Maximum selenate reduction rate	v_{max}	130	30	300	µmol/L_{tot}/h	VillaRomero 2013
Selenate half-saturation constant	K_m	22	10	700	µM	Steinberg and Oremland 1990
Salton sea sedimentation rate	u_{sed}	0.127	0.03	0.5	cm/year	Arnal 1961; Schroeder et al. 2002
Water column selenate concentration	$C_{SeVI\text{-}water}$	1	0.5	2	µg/L	Holdren & Montano 2002; Schroeder et al. 2002

2.4. Assessing the potential impact of bioturbation on the distribution of solid phase selenium

To obtain a first-order understanding of the potential impact bioturbation may have on the distribution of selenium in Salton Sea sediment we used an estimate for D_b based on an empirical relationship with u_{sed} derived for marine sediments by Boudreau (1994), and ran simulations in which mixing at this rate occurred to a typical mixing depth of 10 cm. D_b was thus set to 0.012 cm^2/day for $z \leq 10$ cm and to zero otherwise.

3. Results

3.1. Depth profiles of selenate concentrations, selenate reduction rates, and solid phase selenium concentrations

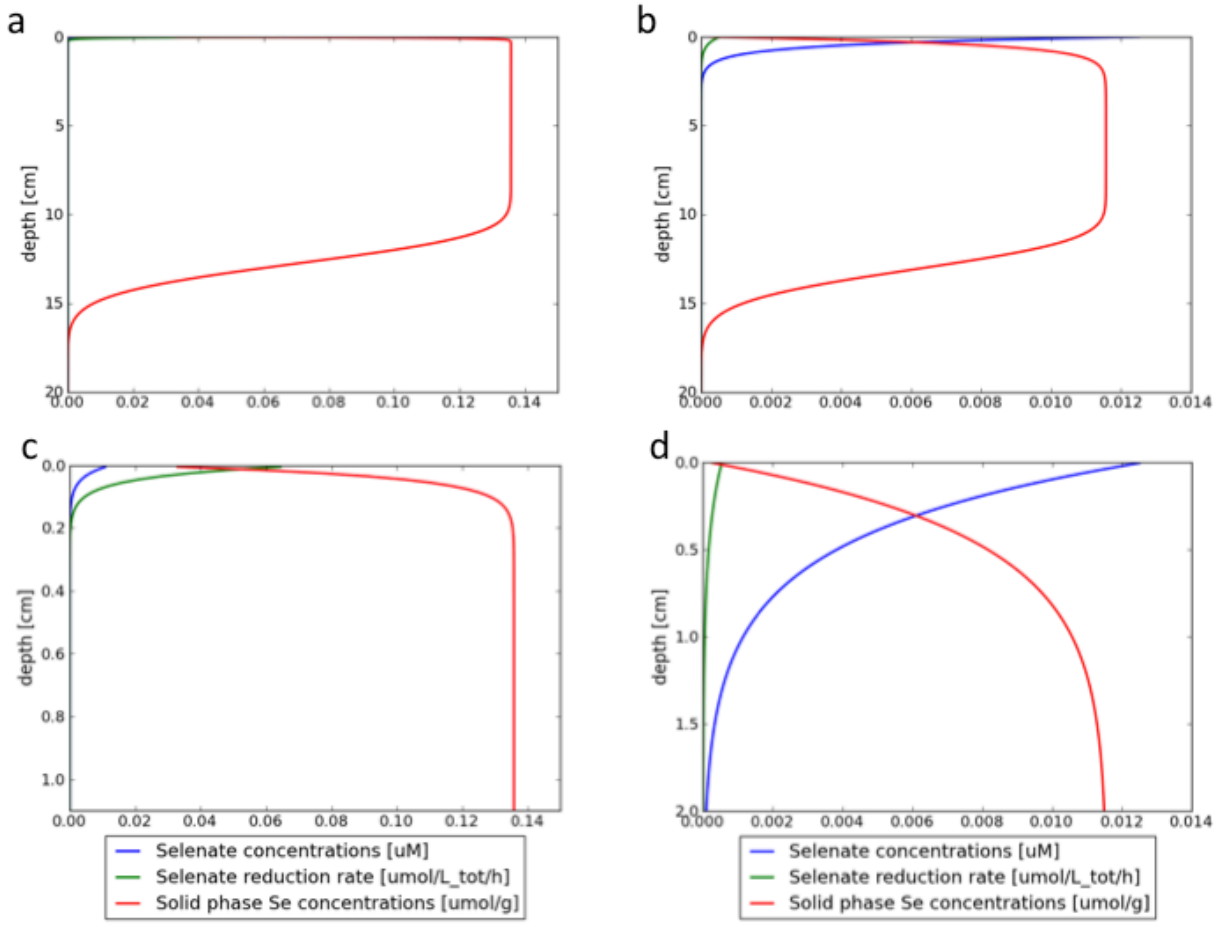

Figure 1. Sediment depth profiles of selenate concentration (blue), selenate reduction rate (green), and solid phase selenium concentration (red). Panels a and b show the profiles across a sediment depth of 20 cm for default parameter values and for minimal selenate reduction rates (v_{max}= 30 µmol/L_{tot}/h; K_m= 700 µM) respectively. Panels c and d show the detailed view of the first centimeters at the sediment surface for the same profiles as in a and b respectively. Note that while the three profiles are shown on the same axis, they differ in their units (x-axis labels shown in legend).

The depth profiles of selenate concentrations, selenate reduction rates, and solid phase selenium concentrations after 100 years of simulation time are shown in **Fig. 1a** and **c** for default parameter values, and in **Fig. 1b** and d for the smallest possible reaction rates (minimal value for v_{max}= 30 µmol/L_{tot}/h, and maximal value for K_m= 700 µM). As can be seen in **Fig. 1a** for default parameter values (**Table 1**), solid phase selenium concentrations increase rapidly within the first centimeter below the sediment surface and reach a constant maximum value. For the smallest possible reaction rates (**Fig. 1b**) this area of increasing solid phase selenium concentrations is larger, but the maximum solid phase selenium concentration is still reached within the to 2 cm of the sediment. For default parameter values (**Fig. 1a**), the maximum solid phase selenium concentration is 0.136 µmol/g, while for the smallest possible reaction rates (**Fig. 1b**) it is more than an order of magnitude lower (0.011 µmol/g). In both cases the maximal solid phase selenium concentrations propagate downwards in the sediment, as fresh sediment is added at the top. The propagating front reaches a depth between 10 and 15 cm in the sediment after 100 years of simulation time with default sedimentation rates, regardless of the selenate reduction rate (**Fig. 1a** and **1b**). The detailed views in **Fig. 1c** and **1d**, reveal that selenate concentrations decrease rapidly within the first cm of the sediment. For default parameter choices virtually all selenate is consumed in this region (**Fig. 1c**), while for the smallest possible reaction rates the remaining concentration of selenate is 9% of the water column concentrations at a sediment depth of 1 cm (**Fig. 1d**). The selenate reduction rates follow the same pattern as selenate concentrations, since they are nearly proportional to C_{SeVI}, when $C_{SeVI} << K_m$ (Eq. 1). Selenate concentrations drop to essentially zero across the same area in which solid phase selenium concentrations increase with depth.

Figure 2 illustrates the dependence of the depth to which the maximum solid phase selenium concentrations propagate within 100 years on the sedimentation rate. The greater the rate of sedimentation, the faster solid phase selenium is transported downwards in the sediment and the greater the depth at which maximal solid phase selenium concentrations are attained. For the lowest sedimentation rate value in the explored parameter range (u_{sed} = 0.03 cm/year), maximum solid phase selenium concentrations reach a depth of just under 5 cm. For sedimentation rate values at the high end of the parameter range explored (u_{sed} = 0.3-0.5 cm/year) the depth of maximum solid phase selenium concentrations extends to below the modeled domain of 20 cm. It should be noted that the depth of maximum solid phase selenium concentrations extends to below 2 cm – the depth chosen as characteristic solid phase selenium concentration for the sensitivity analysis – across the full range of sedimentation rates investigated in this paper (**Fig. 2**). The dependence of the maximum solid phase selenium concentrations themselves on sedimentation rates is described in section 3.3.

3.2. Impact of reaction kinetics on sediment selenate concentration profiles

Figure 3 shows the steady-state sediment selenate concentration profiles for a series of v_{max} and K_m values. Selenate concentrations drop below 1% of the water column concentrations at shallow depths, more specifically between 0.2 and 1 cm for the range of K_m values investigated and between 0.2 and 0.4 cm for the range of v_{max} values investigated. The depth across which selenate is consumed decreases with increasing values of v_{max} and decreasing values of K_m. Selenate profiles are more sensitive to variations in v_{max} at the low end of the explored range, where the sediment depth at which concentrations drop below 1% of water column concentrations decreases from 0.4 cm for v_{max} = 30 µmol/L_{tot}/h to 0.2 cm for v_{max} = 120 µmol/L_{tot}/h. Similarly, selenate profiles are also more sensitive to variations in K_m at the low end

of the explored range, where the sediment depth at which concentrations drop below 1% of the water column concentrations increases from below 0.2 cm for K_m = 10 µM to 0.4 cm for K_m = 125 µM.

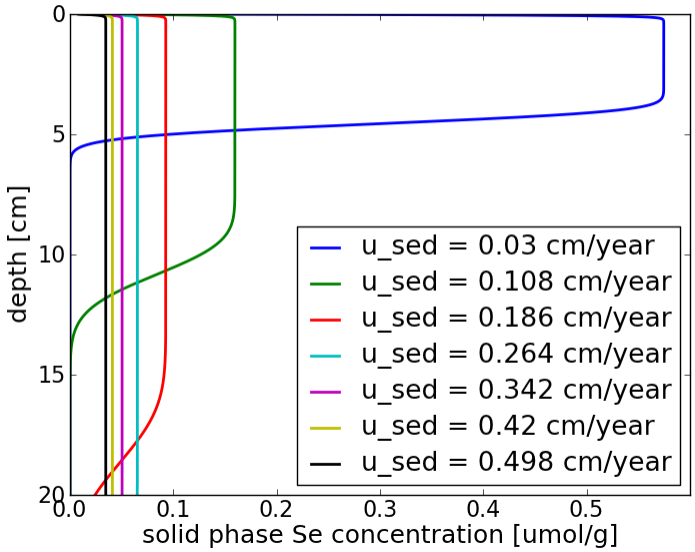

Figure 2. Solid phase selenium concentration profiles after 100 years of simulation for various sedimentation rates (u_{sed}). Values of u_{sed} were equally spaced across the investigated uncertainty range, while all other parameters are at default values (Table 1).

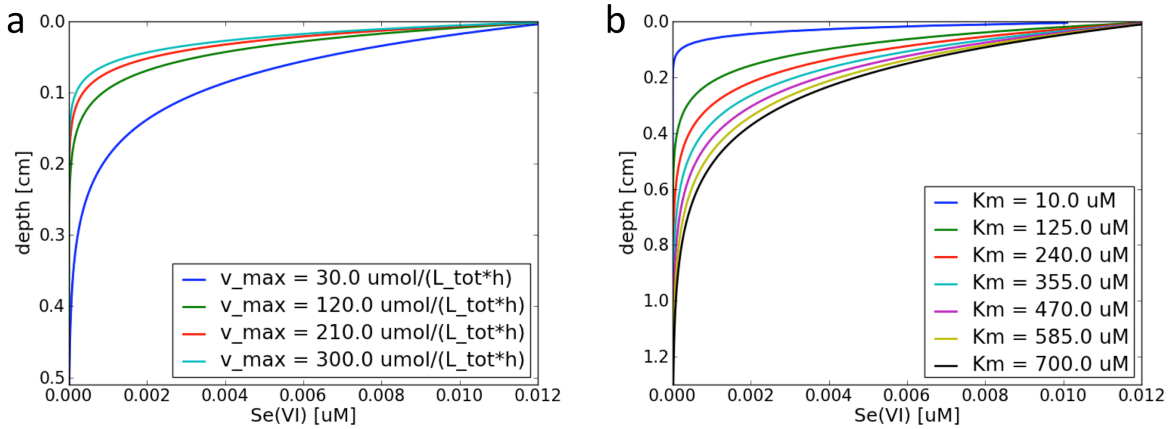

Figure 3. Sediment depth profiles of selenate concentration at 100 years of simulation time for a range of values of v_{max} (a) and K_m (b). Parameters not shown in the legend are at default values (see Table 1).

3.3. Impact of reaction kinetics, sedimentation rates, and water column selenate concentrations on near surface sediment concentrations of solid phase selenium

We used the solid phase selenium concentration at 2 cm sediment depth as a characteristic measure for the entire equilibrium profile of solid phase selenium because the 2 cm depth is representative of maximal equilibrium concentrations (**Fig. 1** and **2**). It is both deep enough to be beyond the zone of decreasing selenate and increasing solid phase selenium concentrations regardless of selenate reduction rates (**Fig. 3**) and shallow enough to assure that the propagating front of solid phase selenium concentrations will have moved well past this depth after 100 years regardless of the sedimentation rates (**Fig. 2**).

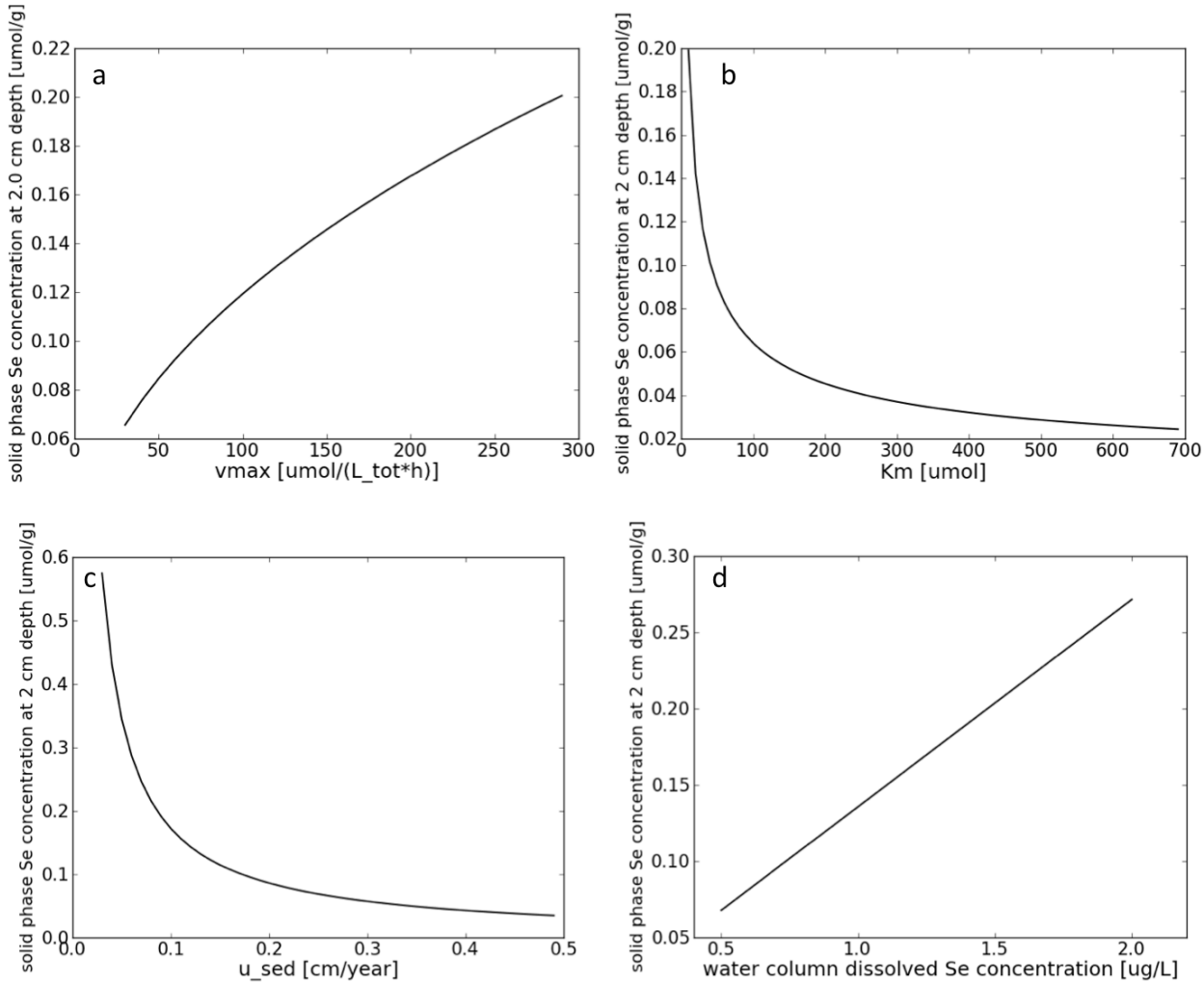

Figure 4. Concentrations of solid phase selenium at 2 cm sediment depth after 100 years simulation time as a function of v_{max} (a), K_m (b), u_{sed} (c), and $C_{SeVI\text{-}water}$ (d). Non-plotted parameters are at default values (Table 1) and bioturbation was not simulated.

Figure 4 shows the solid phase selenium concentration at 2 cm sediment depth as a function of v_{max} and K_m, u_{sed}, and $C_{SeVI\text{-}water}$. It can be seen that except for $C_{SeVI\text{-}water}$, the impact of these parameters on solid phase selenium concentrations is non-linear. For values of v_{max} between 30 and 300 µmol/L_{tot}/h, the concentration of solid phase selenium at 2 cm depth increases from 0.066 to 0.204 µmol/g (factor 3.0). The incremental increase in equilibrium

concentrations per increase in v_{max} (i.e. the slope) decreases with higher values of v_{max} (**Fig. 4a**). For values of K_m between 10 and 700 µM, the concentration of solid phase selenium at 2 cm depth decreases from 0.199 to 0.024 µmol/g (factor 8.2). The incremental decrease in equilibrium concentrations per increase in K_m lessens for greater values of K_m (**Fig. 4b**). For values of u_{sed} between 0.03 and 0.5 cm/year, the concentration of solid phase selenium at 2 cm depth decreases from 0.575 to 0.034 µmol/g (factor 17). The incremental decrease in equilibrium concentrations per increase in u_{sed} lessens for greater values of u_{sed} (**Fig. 4c**). Finally, for values of $C_{SeVI\text{-}water}$ between 0.5 and 2.0 µg/L, the concentration of solid phase selenium at 2 cm depth increases linearly from 0.068 to 0.272 µmol/g (factor 4.0) (**Fig. 4d**).

3.4. Impact of bioturbation

The solid phase selenium concentration profile from a simulation with active bioturbation and with default parameters of v_{max}, K_m, u_{sed}, and $C_{SeVI\text{-}water}$, is compared to an equivalent profile without bioturbation in **Fig. 5**. Note that the non-bioturbated profile is equivalent to that shown in **Fig. 1b**, since in both cases the default parameter values were used (**Table 1**). Bioturbation rapidly distributes the solid phase selenium produced near the sediment surface across the sediment profile, thus decreasing the solid phase selenium concentrations at shallow to intermediate (1-10 cm) depths and increasing the time needed to reach equilibrium concentrations. It should be noted that the equilibrium concentration itself remains unaffected (0.136 µmol/g for default parameters). However this concentration is not reached after 100 years with bioturbation and maximum solid phase selenium concentrations are still below 0.103 µmol/g throughout the profile at this time (**Fig. 5**). After 200 years with default parameters (**Table 1**) and bioturbation the solid phase selenium concentration across the mixing zone (top 10 cm of sediment in the model) is 0.127 µmol/g and equilibrium concentrations are reached only after 365 years, which is significantly greater than the age of the Salton Sea (~100 years).

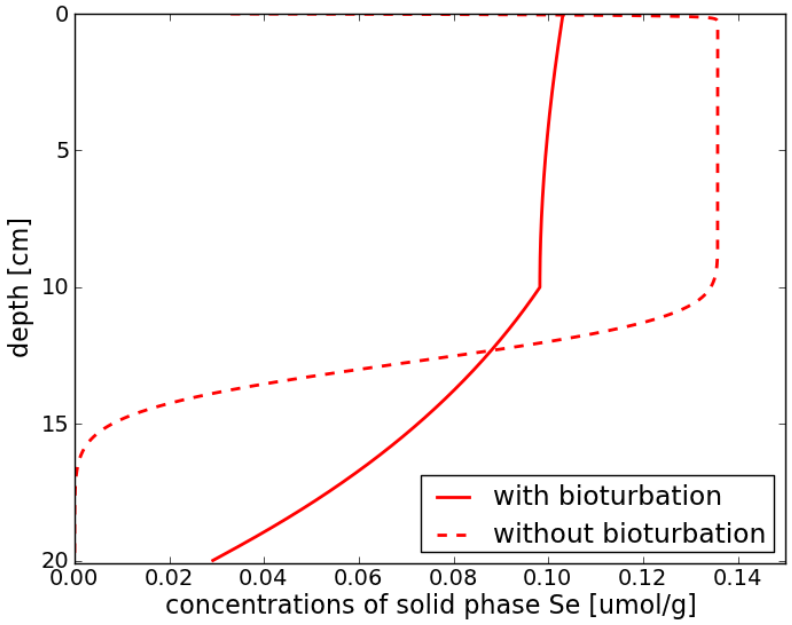

Figure 5. Sediment depth profiles at 100 years of simulation time for solid phase selenium concentrations with (solid line) and without (dashed line) bioturbation enabled as described in section 2.4. All parameters are at default values (see Table 1).

4. Discussion

4.1. Selenium concentrations in the surface sediment of the Salton Sea

Excluding uncertainty in sedimentation rates, the solid phase selenium concentration modeled in this paper varied between 0.024 and 0.272 μmol/g within the space of plausible parameters explored. The range of total selenium concentrations in Salton Sea surface sediment reported in the literature (0.007 to 0.190 μmol/g) is 30% lower than the modeled range at its upper end (Byron and Ohlendorf, 2007; Schroeder and Orem, 2000; Schroeder et al., 2002). The modeled surface sediment solid phase selenium concentration for default parameter values (0.136 μmol/g) falls within the reported range, albeit at the upper end. Considering that the bioturbation mixing in the surface layer of the sediment (discussed in section 4.3) has likely led to lower surface sediment solid phase selenium concentrations of the order of 25% at the Salton Sea, the modeled solid phase selenium concentrations are in good agreement with the reported values.

The depth profiles predicted by our model also match the available field observations and reproduce the decrease in concentrations at sediment depths below 10 cm (Schroeder, 2004; Schroeder and Orem, 2000; Schroeder et al., 2002; Vogl and Henry, 2002). Furthermore the model prediction that selenate reduction is constrained to the top cm at the water sediment interface matches previous observations at other sites in the Western USA (Oremland et al. 1990). The authors investigated *in situ* selenate reduction in sediments from Big Soda Lake (a saline/alkaline environment) as well as from an agricultural drain, both located in Western Nevada, and observed that 85% of selenate reduction activity was constrained to the top 4-8 cm of sediment profiles. Overall it thus appears that the diagenetic model here presented accurately reflects the dynamics of selenium incorporation into the Salton Sea sediment.

4.2. Key factors impacting the solid phase selenium concentrations of Salton Sea surface sediment

Of the factors investigated in this paper, simulated surface sediment solid phase selenium concentrations varied most (by a factor of 17) across the uncertainty range of the sedimentation rate. This is mainly due to the large uncertainty range of the sedimentation rate estimate itself, but also indicates that variation in local sedimentation rates may have a strong impact on the local surface concentrations of sedimentary solid phase selenium at the Salton Sea. Reports show that sediment selenium concentrations are in fact lower in the river delta areas of the southern basin (Schroeder et al., 2002) where high sedimentation rates can be expected based on the sediment load contributed by the rivers and the decrease in flow velocities from channel to lake. This suggests that it may be possible to obtain a first-order estimate of the cross-basin variation in solid phase selenium concentrations in surface sediments based on a physical sedimentation model for the Salton Sea and the response curve here presented.

Solid phase selenium concentrations were also sensitive across the ranges explored for the kinetic parameters of selenate reduction v_{max} and K_m, which affected them by a factor of 3.2 and 8.0 respectively. The explored range of v_{max} was directly derived from site-specific variations determined in Salton Sea sediment (VillaRomero et al., 2013) and is thus expected to be highly reflective of the kind of impact this factor can have on solid phase selenium concentrations across the Salton Sea. While the overall impact across the investigated range of K_ms was more than twice as strong, the range for K_ms was derived from multiple locations that

did not include the Salton Sea and was greatly extended by a single high value (K_m = 700 μM) that was more than an order of magnitude above the 6 other reported values (Steinberg and Oremland, 1990). It is thus uncertain whether variation in the affinity of the local microbial community to selenate has a significant impact on the variation of surface sediment solid phase selenium concentrations across the Salton Sea.

It should be noted, that microbial reduction rates are likely affected by factors not explicitly accounted for in this model, such as the amount of organic matter (VillaRomero et al., 2013) or the local redox level (Oremland et al., 1989) in the sediment. As such, the kinetic parameters here employed (v_{max} and K_m) should be seen as an aggregation of factors impacting microbial selenate reduction: they are apparent reaction constants. Organic matter content and redox level are expected to vary spatially, across the lake, but also with sediment depth. The extreme shallowness (<1cm) of simulated selenate reduction zone in Salton Sea sediment indicates that changes in apparent reaction rates with depth may however be negligible. Cross-lake variation in organic matter concentrations on the other hand, may drive variation in the solid phase selenium concentrations of surface sediment. Schroeder et al. (2002) measured selenium and organic matter concentrations across 11 sites at the Salton Sea and an analysis of their published data set reveals a strong correlation (Pearson's r = 0.89) between the two variables. Within the context of our model this correlation could be explained through the impact of organic matter concentrations on apparent selenate reduction rate constants. If this impact were quantified under laboratory conditions, it would be possible to amend the model with an additional term that would account for organic matter concentrations and further improve the models predictive power for potential applications investigating cross-lake variation in surface sediment solid phase selenium concentrations.

In summary the model reveals the following competing drivers that have shaped present day concentrations of solid phase selenium in Salton Sea surface sediment: High rates of selenate reduction can lead to increase concentrations of solid phase selenium in surface sediment, while rapid sedimentation can submerge solid phase selenium produced at the sediment surface and thus decrease near surface concentration. Cross-lake variation in both local reduction and sedimentation rates may explain the current variability in near surface sediment selenium concentrations at the Salton Sea. The impact of these drivers is independent from the potential impact of bioturbation discussed in the next section.

4.3. Potential impact of bioturbation mixing on the solid phase selenium concentrations of Salton Sea surface sediment

Using a constant first-order estimate for D_b, the simulation with active bioturbation showed that differences in current surface selenium concentrations of ~25% may have been caused by bioturbation over the last 100 years. Bioturbation has likely contributed to a lowering of surface sediment solid phase selenium concentrations at the Salton Sea by transporting reduced selenium downwards in the sediment. The effect operates by impacting the dynamics of solid phase selenium concentrations in surface sediment, increasing the time needed to achieve steady state at the surface and thus also slowing down the response of surface selenium concentrations to changes in selenium loading or sedimentation. Since the equilibrium concentrations themselves are not altered, this also means that the solid phase selenium concentrations in the surface sediment of the Salton Sea would continue to increase over the next 100 years if conditions were to remain the same. The concentration ranges here presented for

simulations without bioturbation (0.024 and 0.272 μmol/g) may be indicative of the equilibrium concentrations that would eventually be attained. Additionally, the rise in surface sediment solid phase selenium concentrations would be expected to accelerate if the salinity in the Salton Sea were to rise to the point at which the agents of bioturbation (most likely *N. succinea*) are no longer viable. *N. succinea* populations have long been observed to be in decline (Detwiler et al., 2002) and will likely become extinct due to the inability to reproduce once salinity reaches 50 g/L (Kuhl and Oglesby, 1979). Current lake salinity is at 48 g/L and rapidly rising (Hurlbert, 2008; VillaRomero et al., 2013).

4.4. Implications for Salton Sea wildlife

Selenium exposure for multicellular organisms is dominated by dietary intake, since concentrations generally increase with each trophic level as selenium bioaccumulates and biomagnifies. In aquatic environments, the greatest accumulation step occurs from the dissolved phase to the base of the food chain (algae and other planktonic microorganisms) where, depending on the site, concentrations usually increase by a factor of 10^2-10^6 compared to the dissolved phase (Stewart et al., 2010). Obtaining information about the concentrations of selenium at the base of the food chain is the most crucial step in modeling the risk of selenium contamination in aquatic ecosystems due to the large site specific variation in the intensity of bioaccumulation (Stewart et al., 2010). Given the difficulties in physically separating planktonic microorganisms from inorganic suspended particles, the selenium concentration in the total suspended particulate fraction is often used as a measure of selenium concentrations at the base of the food chain (Luoma and Presser, 2009; Presser and Luoma, 2010b; Stewart et al., 2010). Alternatively, the selenium concentration in surface sediment can also be used as it may more accurately reflect the dietary exposure of benthic invertebrates (Stewart et al., 2010). Selenium accumulation in benthic macroinvertabrates occurs predominantly from sedimentary uptake (Wiramanaden et al., 2010). In the Salton Sea, *N. succinea* may drive the uptake of selenium from the sediment into the food chain, as the pileworm is the primary food source for Salton Sea fish (Detwiler et al., 2002; Dexter et al., 2007; Kuhl and Oglesby, 1979) and some waterfowl species (Anderson et al., 2007; Detwiler et al., 2002; Dexter et al., 2007).

The concentration range for solid phase selenium in Salton Sea surface sediment here simulated (0.012-0.24 μmol/g) cuts across concentration thresholds thought to represent potential threats for top-level predators (fish and waterfowl). Lemly (2002) recommended toxic effects thresholds for sediment selenium concentrations of 0.025 μmol/g (2 μg/g, lowest concentration at which sensitive fish and waterfowl may show effects) (Lemly, 2002). From a compilation of field data from irrigation drainage studies conducted throughout the western United States and studies on coal-fired power plant reservoirs receiving Se-laden effluents, Van Derveer and Canton (1997) concluded that tissue concentrations in fish and wildlife can exceed levels of concern in locations with 0.03 μmol/g (2.5 μg/g) of selenium in their sediment and that toxic effects, such as deformities in fish or birds, can be visible in the field at locations with 0.05 μmol/g (4.0 μg/g) of selenium in their sediment. Selenium concentrations in the surface sediments of the Salton Sea are thus likely to pose a threat to local fish and wildlife. The magnitude of this threat may depend locally on the diagenetic factors discussed in this paper. Regions of high sedimentation, such as the deltas of the Salton Sea's tributaries, may be fairly safe for local wildlife, while other regions may not. Conversely, hotspots of high surface sediment concentrations and high threat to local wildlife may occur in areas where fast reduction (for example due to an abundance of organic matter) has concentrated solid phase selenium.

This information could be used in the selection and management of habitat restoration areas along the Salton Sea's shoreline. Current plans for habitat restoration are driven by salinity considerations and largely ignore sedimentary selenium (CDG, 2012). Without restoration efforts, increasing salinities would likely make the Salton Sea uninhabitable for fish and most waterfowl by 2017 (Cohen and Hyun, 2006). To address this near-term loss of habitat the California Department of Fish and Game was recently given authority to create or enhance habitat at the Salton Sea's receding perimeter – constructing shallow, lower-salinity ponds that would be separated from the main water body (CDG, 2012). Considerations of selenium loads in the surface sediments may be crucial in the selection of appropriate project areas in the Salton Sea littoral and in the management of created habitat, since habitat restored from a salinity standpoint may still poison its inhabitants with selenium. The acute lack of state funding for these projects (Clarke, 2012) may however make extended monitoring of sediment selenium levels impossible. A mechanistic model for surface sediment selenium concentrations, based on the approach here presented may provide a low cost tool to support these efforts.

5. Conclusion

The diagenetic model here presented accurately reproduces the observed range of Salton Sea surface sediment selenium concentrations based on plausible ranges of selenate reduction kinetics, and water column dissolved selenate concentrations. Given the large amount of spatial variation in sediment selenium concentrations measured in the field (Krants et al., 2002; Vogl and Henry, 2002) and the analytical challenge of determining these values, our model could be used to provide first-order estimates of local sediment selenium concentrations based on knowledge of the variation in sedimentation rates across the Salton Sea. Additionally, the model illustrates the sensitivity of surface sediment selenium concentrations to selenium reduction kinetics and sedimentation rates over timescales of decades to centuries and that current near surface concentrations are likely to have been significantly impacted by bioturbation over the last 100 years. While additional research is necessary to constrain the uncertainty ranges of key parameters, in particular the rates of sedimentation and bioturbation mixing of Salton Sea sediment, the approach here presented may yield a low-cost alternative to extended field sampling and monitoring campaigns. To preserve essential habitat at the Salton Sea swift interventions are necessary. However, without an improved understanding of the dynamic transfer between the lake's pools of selenium – of which the sediment is the largest – such interventions may backfire: Habitat preserved from a salinity standpoint may still poison its inhabitants with excess selenium from its sediments.

6. Acknowledgements

I thank Christof Meile for providing valuable feedback during manuscript preparation, Chloe Lewis and Elliot Cuzzilo for critical support in implementing the diagenetic model in Python, Nick Neuer for advice regarding the feasibility of analytical approaches to find steady-state solutions to my PDEs, and Juan-Fernando VillaRomero for providing valuable insights from the field.

7. Appendix: Model Code

```
'''
SeRed.py
Created on Oct 24, 2012

@author: Matteo Kausch
'''
from fipy import Grid1D, CellVariable, TransientTerm, DiffusionTerm, PowerLawConvectionTerm,
Viewer, TSVViewer
import matplotlib.pyplot as plt

#DEFINE FUNCTIONS & CONSTANTS

dx = 0.01       # [cm] cell length in model grid

def steadySe(por=0.5,
             # [L_por/L_tot] 0.46 +/- 0.13 for site F and 0.51 +/- 0.04 for site G
             rho=1.35*1000,
             # [g/L_tot] 1.4 for site F and  1.3 for site G
             DmolSeVI =  1.01e-5*60*60*24,
             # [cm^2/day] molecular diffusivity of selenate; CRC Handb. of Chem. & Phys., 91st
Ed., Internet version 2011, Ed. W.M. Haynes: 1.008e-5 cm^2/s
             u_sed=0.127/365,
             # [cm/day]R! sedimentation rate; estimated to be 0.2 inch/year on average between
1905-1955, 0.05 inch/year (=0.127 cm/year) after 1935 (Arnal, 1961)
             Km= 22.0,
             # [uM]R!(8-700) half-saturation constant for selenate reduction; Steinberg &
Oremland (1990): 7.9-720 uM
             vmax= 130.0*24,
             # [umol/(L_tot*day)]R!(30-300)*24 from JF paper (see below)
             WSeVI = 1.0/79,
             # [uM]R!(0.5-2)/79 concentration of SeVI at the water-column-sediment interface,
0.5-2 ug/L  (Holdren & Montano, 2002; Schroeder et al., 2002)
             Lx = 20.0,
             # [cm] length/depth of simulated sediment
             T =None,
             # [years] duration of simulation
             Db=None,
             Lm=None,
             bioturb=False,
             plot=False):


    def tort(Dmol, por):
        '''correct molecular diffusion value for tortuosity based on Boudreau, 1997: Diagenetic
models and their implementation. Springer, New York.'''
        import numpy as np
        D = Dmol * 1/(1-np.log(por**2))
        return D

    DSeVI = tort(DmolSeVI, por)
        # """""""" effective diffusivity of selenate in sediment

    if Db is None:
        if bioturb:
            Db = 15.7*(u_sed*365)**0.6/365
            # [cm^2/day] bioturbation rate; based on Boudreau's empirical relation with u_sed;
            #alternatively: Middelburg et al. (1997) compiled a large selection (n = 132) of
210Pb tracer measurements and found a mean DB value for shallow marine sediments (<100 m) between
```

```
3e-7 and 6e-7 cm2/s
        else:
            Db = 0.0

    if bioturb and Lm is None:
        Lm = 10.0
        # [cm] mixing depth; 10 cm is a typical value based on the data summarized by Boudreau
(1994), though there is a lot of variation and this is no perfect metric

    #simulation parameters
    if bioturb and Lx<2*Lm: Lx=2*Lm
    nx = Lx/dx     # number of cells

    #initialize mesh/grid

    m = Grid1D(nx=nx, Lx=Lx)

    #set Db_var to Db between the second cell and Lm
    #Note: bioturbation must be 0 at the surface, since otherwise solid phase Se would diffuse
into the water column, which doesn't make sense
    Db_var = CellVariable(name='Bioturbation rate [cm^2/day]', mesh=m, value=0.0)
    if bioturb:
        Db_var[0:int(Lm/dx)]=Db
    else: Db_var = 0


    #define variables and initial conditions

    SeVI = CellVariable(name='Selenate concentrations [uM]', mesh=m, hasOld=True, value=0.0)
    Se_solid = CellVariable(name='Solid phase Se concentrations [umol/g]',mesh=m, hasOld=True,
value=0.0)

    #define boundary conditions

    SeVI.constrain(WSeVI, m.facesLeft)
    SeVI.faceGrad.constrain(0, m.facesRight)

    #no facesLeft constrain means no flux of solid phase Se across the water-sediment boundary
    Se_solid.faceGrad.constrain(0, m.facesRight)

    #define reactive transport PDEs

    eqSeVI = (TransientTerm(coeff=por, var=SeVI) ==
              (DiffusionTerm(coeff=por*(DSeVI), var=SeVI) -   SeVI*vmax/(Km+SeVI)))
    #UNITS:   1/day(  L_por/L_tot  * umol/L_por) ==
    #          1/cm^2(L_por/L_tot * cm^2/day * umol/L_por) -   umol/(L_tot*day)
    eqSe_solid = (TransientTerm(coeff=rho, var=Se_solid) ==
             (DiffusionTerm(coeff=rho*Db_var, var=Se_solid)       -
PowerLawConvectionTerm(coeff=[rho*u_sed,], var=Se_solid) + SeVI*vmax/(Km+SeVI)))
    #UNITS:        1/day(  g/L_tot  * umol/g)  ==
    #              1/cm^2(g/L_tot * cm^2/day * umol/g)      -           1/cm(g/L_tot * cm/day  *
umol/g)              +  umol/(L_tot*day)


    #initialize viewer
    if plot:
        vi = Viewer((SeVI, Se_solid),title='Se concentration profile', datamin=0)
        plt.axis([0.0, 1.0, 0.0, 0.01])
    #update variables, solve equations, and plot for each time step, count the time steps
```

```
    #First we find the steady state selenate profile
    toll = 1.e-5 #[uM/day] setting tolerance to 10^-7 uM/day

    time_passed = 0
    diff = 1.0
    SeVI_av = 0.0

    dt = (WSeVI + Km)/vmax * 0.1

    while abs(diff) > toll*dt:
        SeVI.updateOld()
        eqSeVI.solve(dt=dt)
        diff = float(SeVI.cellVolumeAverage) - SeVI_av
        SeVI_av = float(SeVI.cellVolumeAverage)
        if plot:
            vi.plot()
        time_passed = time_passed + dt
        print time_passed, 'days passed and diff/dt is ', diff/dt


    #after selenate has reached the steady state
    #we can take much bigger time steps and only march solid phase Se forward

    if T is None:
        Tmax = 1.5/u_sed *3 + 366
        if Tmax < 100.0*365: Tmax = 100.0*365

    else: Tmax = T*365

    print 'Se_solid simulation will be run for ', Tmax/365, ' years.'

    time_passed = 0

    while time_passed <= Tmax:
        Se_solid.updateOld()
        eqSe_solid.solve(dt=365.0)
        if plot:
            vi.plot()
        time_passed = time_passed + 365.0

    print 'The solid phase Se concentration at 2.0 cm sediment depth is ', Se_solid[int(2.0/dx)],
' umol/g.'


    return ([dx/2, Lx+dx/2, dx], SeVI, Se_solid, m, Km, vmax)


if __name__=='__main__':

    WcolumnSeVI = 1.0/79    #[uM]R!(0.5-2)/79 concentration of SeVI at the water-column-sediment
interface, 0.5-2 ug/L  (Holdren & Montano, 2002; Schroeder et al., 2002)

    (nums, SeVI, Se_solid, m, Km, vmax) = steadySe(bioturb=True, plot=True)#Km=125.0,
vmax=130.0*24, u_sed=0.127/365, WSeVI = 1.0/79)


    #make final plot (with SeRedRate)
    SeRedRate = CellVariable(name='Selenate reduction rate [umol/L_tot/day]', mesh=m,
value=SeVI*vmax/(Km+SeVI))
    vii = Viewer((SeVI, SeRedRate, Se_solid),title='Se concentration and reduction rate profile',
```

```
datamin=0)
    vii.plot()

    #plotting using matplotlib directly
    plt.xlabel('depth [cm]')
    plt.show(block=True)


    #compute & print average Se_solid concentration
    Se_solid_av = float(Se_solid.cellVolumeAverage)
    print('The average solid phase Se concentration is '+str(Se_solid_av)+' umol/g.')
    print('The solid phase Se concentration at 2 cm is '+str(Se_solid[int(2.0/dx)])+' umol/g.')
    print('The selenate concentration at 0.4 cm is '+str(SeVI[int(0.4/dx)]/WcolumnSeVI*100)+' %
of the dissolved concentrations.')
    print('The selenate reduction rate at 0.4 cm is
'+str(SeRedRate[int(0.4/dx)]/SeRedRate[0]*100)+' % of the surface rate.')

    # export the final value of all variables to an output file

    TSVViewer(vars=(SeVI, Se_solid)).plot(filename="output.txt")


'''
paramSpaces.py
Created on Feb 7, 2013

@author: Matteo Kausch
'''
import matplotlib.pyplot as plt, numpy
from SeRed import steadySe, dx

#param space explorations
if __name__=='__main__':

    #exploration of vmax
    if 0:
        vmaxes = numpy.arange(30.0*24, 300.0*24, 10.0*24)
        # [umol/(L_tot*day)]R!(30-300)*24 from JF paper (see below)

        if 1:
            vals = [float(steadySe(vmax=vmax)[2][int(2.0/dx)]) for vmax in vmaxes]
        else:       #alternative way of doing the same thing
            vals = []
            for vmax in vmaxes:
                (m, SeVI, Se_solid) = steadySe(vmax=vmax)
                vals.append(Se_solid[float(Se_solid[int(1.5/dx)])])

        x_vals = vmaxes/24
        x_label = 'vmax [umol/(L_tot*h)]'
        y_label = 'solid phase Se concentration at 2.0 cm depth [umol/g]'


    #exploration of Km
    elif 1:
        Kms = numpy.arange(10.0, 700.0, 10.0)
        # [uM]R!(8-700) half-saturation constant for selenate reduction; Steinberg & Oremland
(1990): 7.9-720 uM

        vals = [float(steadySe(Km=Km)[2][int(2.0/dx)]) for Km in Kms]
```

```
        x_vals = Kms
        x_label = 'Km [umol]'
        y_label = 'solid phase Se concentration at 2 cm depth [umol/g]'

    #exploration of u_sed
    elif 1:
        u_seds = numpy.arange(0.03/365, 0.5/365, 0.01/365)
        # [cm/day] sedimentation rate; estimated to be 0.2 inch/year on average between 1905-
1955,
        # 0.05 inch/year (=0.127 cm/year) after 1935 (Arnal, 1961), factor 4 uncertainty is
plausible: 0.03 to 0.5 cm/year

        vals = [float(steadySe(u_sed=u_sed)[2][int(2.0/dx)]) for u_sed in u_seds]

        x_vals = u_seds*365
        x_label = 'u_sed [cm/year]'
        y_label = 'solid phase Se concentration at 2 cm depth [umol/g]'

    #exploration of WSeVI
    else:
        WSeVIs = numpy.arange(0.5/79, 2.01/79, 0.5/79)
        #[uM]R!(0.5-2)/79 concentration of SeVI at the water-column-sediment interface,
        # 0.5-2 ug/L  (Holdren & Montano, 2002; Schroeder et al., 2002)


        vals = [float(steadySe(WSeVI=WSeVI)[2][int(2.0/dx)]) for WSeVI in WSeVIs]

        plt.axis([0.4, 2.2, 0.05, 0.3])
        x_vals = WSeVIs*79
        x_label = 'water column dissolved Se concentration [ug/L]'
        y_label = 'solid phase Se concentration at 2 cm depth [umol/g]'

    # Produce Plot
    plt.plot(x_vals, vals, linewidth=1.5, color='k')#, linestyle='_')
    plt.xlabel(x_label, fontsize = 18)
    plt.ylabel(y_label, fontsize = 15.5)


    font = {#'family' : 'normal',
            #'weight' : 'bold',
            'size'   : 16}
    plt.rc('font', **font)

    plt.show(block=True)
```

8. References

Anderson, M.A., L. Whiteaker, E. Wakefield, and C. Amrhein. 2008. Properties and distribution of sediment in the Salton Sea, California: an assessment of predictive models. Hydrobiologia 604:97-110.

Anderson, T.W., M.A. Tiffany, and S.H. Hurlbert. 2007. Stratification, sulfide, worms, and decline of the Eared Grebe (Podiceps nigricollis) at the Salton Sea, California. Lake and Reservoir Management 23:500-517.

Arnal, R.E. 1961. Limnology, Sedimentation, and Microorganisms of the Salton Sea, California. Geological Society of America Bulletin 72:427-478.

Balistrieri, L.S., and T.T. Chao. 1987. Selenium adsorption by goethite. Soil Science Society of America Journal 51:1145-1151.
Balistrieri, L.S., and T.T. Chao. 1990. Adsorption of selenium by amorphous iron oxyhydroxide and manganese-dioxide. Geochimica et Cosmochimica Acta 54:739-751.
Baryosef, B., and D. Meek. 1987. Selenium sorption by kaolinite and montmorillonite. Soil Science 144:11-19.
Boudreau, B.P. 1994. Is burial velocity a master parameter for bioturbation? Geochimica et Cosmochimica Acta 58:1243-1249.
Boudreau, B.P. 1997. Diagenetic models and their implementation Springer, New York.
Byron, E.R., and H.M. Ohlendorf. 2007. Diffusive flux of selenium between lake sediment and overlying water: Assessing restoration alternatives for the Salton Sea. Lake and Reservoir Management 23:630-636.
Canton, S.P., and W.D. Van Derveer. 1997. Selenium toxicity to aquatic life: An argument for sediment-based water quality criteria. Environmental Toxicology and Chemistry 16:1255-1259.
Carpelan, L.H., and R.H. Linsley. 1961. The Spawning of Neanthes Succinea in the Salton Sea. Ecology 42:189-190.
Catalano, J.G., Z. Zhang, P. Fenter, and M.J. Bedzyk. 2006. Inner-sphere adsorption geometry of Se(IV) at the hematite (100)-water interface. Journal of Colloid and Interface Science 297:665-671.
CDG. 2012. Salton Sea Financial Assistance Program Guidelines, pp. 17. California Natural Resource Agency, Ontario.
Clarke, C. 2012. Governor Cuts Salton Sea Agency, Enviros Shrug KCET. Community Television of Southern California, Burbank.
Cohen, M., and K. Hyun. 2006. Hazard – The future of the Salton Sea with no restoration project. Pacific Institute, Oakland, California.
Darcheville, O., L. Fevrier, F.Z. Haichar, O. Berge, A. Martin-Garin, and P. Renault. 2008. Aqueous, solid and gaseous partitioning of selenium in an oxic sandy soil under different microbiological states. Journal of Environmental Radioactivity 99:981-992.
Detwiler, P.M., M.F. Coe, and D.M. Dexter. 2002. The benthic invertebrates of the Salton Sea: distribution and seasonal dynamics. Hydrobiologia 473:139-160.
Dexter, D.M., J.S. Dainer, P.M. Detwiler, M.F. Moreau, and S.H. Hurlbert. 2007. Decline of springtime abundance of the pileworm Neanthes succinea in relation to hydrographic conditions at the Salton Sea, California. Lake and Reservoir Management 23:570-581.
Duc, M., G. Lefevre, F. Fedoroff, J. Jeanjean, J.C. Rouchaud, F. Monteil-Riviera, J. Dumonceau, and S. Milonjic. 2003. Sorption of selenium anionic species on apatites and iron oxides from aqueous solutions. Journal of Environmental Radioactivity 70:61-72.
Dungan, R.S., and W.T. Frankenberger, Jr. 1999. Microbial transformations of selenium and the bioremediation of seleniferous environments. Bioremediation Journal 3:171–188.
Elrashidi, M.A., D.C. Adriano, and W.L. Lindsay. 1989. Solubility speciation and transformations of slenium in soils. SSSA Special Publication:51-64.
Hamilton, S.J. 2004. Review of selenium toxicity in the aquatic food chain. Science of the Total Environment 326:1-31.
Hartman, O. 1939. New Species of Polychaetous Annelids from Southern California University of Southern California Press.

Haynes, W.M., (ed.) 2011. CRC Handbook of Chemistry & Physics (Internet version). CRC Press/Taylor & Francis Group, Boca Raton.
Herbel, M.J., J.S. Blum, R.S. Oremland, and S.E. Borglin. 2003. Reduction of elemental selenium to selenide: Experiments with anoxic sediments and bacteria that respire Se-oxyanions. Geomicrobiology Journal 20:587-602.
Holdren, G.C., and A. Montano. 2002. Chemical and physical characteristics of the Salton Sea, California. Hydrobiologia 473:1-21.
Hurlbert, S.H. 2008. The Salton Sea Centennial Symposium - Proceedings of symposium celebrating a century of symbiosis among agriculture, wildlife and people, 1905-2005 - San Diego, USA, March 2005 - Preface. Hydrobiologia 604:1-3.
Jaglarz, P., and A. Uchman. 2010. A hypersaline ichnoassemblage from the Middle Triassic carbonate ramp of the Tatricum domain in the Tatra Mountains, Southern Poland. Palaeogeography, Palaeoclimatology, Palaeoecology 292:71-81.
Jonathan, E.G., W. Daniel, and A.W. James. 2009. FiPy: Partial Differential Equations with Python. Computing in Science & Engineering 11:6-15.
Krants, T., S. Hoover, M. Diederich, M. Brenneman, K. Althiser, P. Egle, D. Guthrie, S. Huynen, E. Kena, D. Kreske, M. Karman, J. Lensch, L. Lewis, and M. Sorensen. 2002. Salton Sea Atlas Redlands Institute / ESRI Press, Redlands, California.
Kuhl, D.L., and L.C. Oglesby. 1979. Reproduction and survival of the pileworm Nereis-succinea in higher Salton Sea salinities. Biological Bulletin 157:153-165.
Lemly, A.D. 2004. Aquatic selenium pollution is a global environmental safety issue. Ecotoxicology and Environmental Safety 59:44-56.
Lemly, D.A. 2002. Selenium Assessment in Aquatic Ecosystems: A Guide for Hazard Evaluation and Water Quality Criteria. Springer-Verlag, New York.
Luoma, S.N., and T.S. Presser. 2009. Emerging Opportunities in Management of Selenium Contamination. Environmental Science & Technology 43:8483–8487.
Mandal, S., S. Mayadevi, and B.D. Kulkarni. 2009. Adsorption of Aqueous Selenite [Se(IV)] Species on Synthetic Layered Double Hydroxide Materials. Industrial & Engineering Chemistry Research 48:7893-7898.
Masscheleyn, P.H., R.D. Delaune, and W.H. Patrick. 1990. Transformations of selenium as affected by sediment oxidation-reduction potential and pH. Environmental Science & Technology 24:91-96.
Moreau, M.F., J. Surico-Bennett, M. Vicario-Fisher, R. Gerads, R.M. Gersberg, and S.H. Hurlbert. 2007a. Selenium, arsenic, DDT and other contaminants in four fish species in the Salton Sea, California, their temporal trends, and their potential impact on human consumers and wildlife. Lake and Reservoir Management 23:536-569.
Moreau, M.F., J. Surico-Bennett, M. Vicario-Fisher, D. Crane, R. Gerads, R.M. Gersberg, and S.H. Hurlbert. 2007b. Contaminants in tilapia (Oreochromis mossambicus) from the Salton Sea, California, in relation to human health, piscivorous birds and fish meal production. Hydrobiologia 576:127-165.
Neal, R.H., and G. Sposito. 1989. Selenate adsorption in alluvial soils. Soil Science Society of America Journal 53:70-74.
Oram, L.L., D.G. Strawn, M.A. Marcus, S.C. Fakra, and G. Möller. 2008. Macro- and microscale investigation of selenium speciation in Blackfoot River, Idaho sediments. Environmental Science & Technology 42:6830–6836.

Oremland, R.S., N.A. Steinberg, T.S. Presser, and L.G. Miller. 1991. Insitu bacterial selenate reduction in the agricultural drainage systems of Western Nevada. Applied and Environmental Microbiology 57:615-617.

Oremland, R.S., N.A. Steinberg, A.S. Maest, L.G. Miller, and J.T. Hollibaugh. 1990. Measurement of insitu rates of selenate removal by dissimilatory bacterial reduction in sediments. Environmental Science & Technology 24:1157-1164.

Oremland, R.S., J.T. Hollibaugh, A.S. Maest, T.S. Presser, L.G. Miller, and C.W. Culbertson. 1989. Selenate reduction to elemental selenium by anaerobic bacteria in sediments and culture - Biogeochemical significance of a novel, sulfate-indipendant respiration. Applied and Environmental Microbiology 55:2333-2343.

Presser, T.S., and S.N. Luoma. 2010a. Ecosystem-Scale Selenium Modeling in Support of Fish and Wildlife Criteria Development for the San Francisco Bay-Delta Estuary U.S. Geological Survey, Menlo Park, California.

Presser, T.S., and S.N. Luoma. 2010b. A Methodology for Ecosystem-Scale Modeling of Selenium. Integrated Environmental Assessment and Management 6:685–710.

Presser, T.S., M.A. Sylwester, and W.H. Low. 1994. Bioaccumulation of selenium from natural geologic sources in western states and its potential consequences. Environmental Management 18:423-436.

Renner, R. 2003. California to develop selenium standard for wildlife. Environmental Science & Technology 37:274A–275A.

Saha, U.K., and P.M. Huang. 2010. Surface coverage effects on the desorption kinetics of selenite from a hydroxyaluminum-montmorillonite complex. Journal of Colloid and Interface Science 350:320-329.

Schroeder, R. 2004. Chemical Data for Detailed Studies of Irrigation Drainage in the Salton Sea Area, California, 1995–2001. U.S. Geological Survey, Sacramento.

Schroeder, R., and W.H. Orem. 2000. Nutrient dynamics in the Salton Basin-implications from calcium, uranium, molybdenum, and selenium Annual Meeting of American Geophysical Union, Vol. H31B-02, Washington, DC.

Schroeder, R.A., W.H. Orem, and Y.K. Kharaka. 2002. Chemical evolution of the Salton Sea, California: nutrient and selenium dynamics. Hydrobiologia 473:23-45.

Schroeder, R.A., M. Rivera, B.J. Redfield, J.N. Densmore, R.L. Michel, D.R. Norton, D.J. Audet, J.G. Setmire, and S.L. Goodbred. 1993. Physical, chemical, and biological data for detailed study of irrigation drainage in the Salton Sea area, California,1988–90. U.S. Geological Survey Open-File Report 93–83:179.

Seiler, R.L., J.P. Skorupa, and L.A. Peltz. 1999. Areas susceptible to irrigation-induced selenium contamination of water and biota in the western United States U.S. Department of the Interior.

Setmire, J., and R. Schroeder. 1998. Selenium and salinity concerns in the Salton Sea area of California, *In* W. T. Frankenberger and R. A. Engberg, eds. Environmental Chemistry of Selenium. Marcel Dekker Inc., New York.

Steinberg, N.A., and R.S. Oremland. 1990. Dissimilatory selenate reduction potentials in a diversity of sediment types. Applied and Environmental Microbiology 56:3550-3557.

Stewart, R., M. Grosell, D. Buchwalter, N. Fisher, S. Luoma, T. Mathews, P. Orr, and W.-X. Wang. 2010. Bioaccumulation and Trophic Transfer of Selenium, p. 93-139, *In* P. M. Chapman, et al., eds. Ecological Assessment of Selenium in the Aquatic Environment. CRC Press.

Stolz, J.F., and R.S. Oremland. 1999. Bacterial respiration of arsenic and selenium. FEMS Microbiology Reviews 23:615-627.
Stolz, J.F., P. Basu, J.M. Santini, and R.S. Oremland. 2006. Arsenic and selenium in microbial metabolism. Annual Review of Microbiology 60:107-130.
Strawn, D., H. Doner, M. Zavarin, and S. McHugo. 2002. Microscale investigation into the geochemistry of arsenic, selenium, and iron in soil developed in pyritic shale materials. Geoderma 108:237-257.
Su, C.M., and D.L. Suarez. 2000. Selenate and selenite sorption on iron oxides: An infrared and electrophoretic study. Soil Science Society of America Journal 64:101-111.
Swan, B.K., J.M. Watts, K.M. Reifel, and S.H. Hurlbert. 2007. Role of the polychaete Neanthes succinea in phosphorus regeneration from sediments in the Salton Sea, California. Hydrobiologia 576:111-125.
Tokunaga, T.K., S.R. Sutton, S. Bajt, P. Nuessle, and G. Shea-McCarthy. 1998. Selenium diffusion and reduction at the water-sediment boundary: Micro-XANES spectroscopy of reactive transport. Environmental Science & Technology 32:1092-1098.
US.EPA. 1987. Ambient Water Quality Criteria for Selenium, Vol. EPA-440/5-87-006. US Environmental Protection Agency, Washington, DC.
US.EPA. 2010. California's 2008-2010 Section 303(d) list of impaired waters. California State Water Resources Control Board, Sacramento.
Van Derveer, W.D., and S.P. Canton. 1997. Selenium sediment toxicity thresholds and derivation of water quality criteria for freshwater biota of western streams. Environmental Toxicology and Chemistry 16:1260-1268.
VillaRomero, J., M. Kausch, and C. Pallud. 2013. Selenate reduction and adsorption in littoral sediments from a hypersaline California lake, the Salton Sea. Hydrobiologia:1-14.
Vogl, R.A., and R.N. Henry. 2002. Characteristics and contaminants of the Salton Sea sediments. Hydrobiologia 473:47-54.
Wiramanaden, C.I.E., K. Liber, and I.J. Pickering. 2010. Selenium Speciation in Whole Sediment using X-ray Absorption Spectroscopy and Micro X-ray Fluorescence Imaging. Environmental Science & Technology 44:5389-5394.

Conclusion

Irrigation-induced selenium contamination of aquatic ecosystems is a problem in seleniferous regions across the world (Lemly, 2004). However, nowhere have the impacts been clearer or more dramatic, nowhere are the current stakes in terms of economic impact and conservation higher, and nowhere has there been more research on the matter than in California. In my first chapter, I showed that the last three decades have seen significant progress with respect to the management and regulation of irrigation-induced selenium contamination in California. Given that a majority of selenium load reductions to date have been achieved by reducing the volume of drainage water rather than the selenium concentrations in the drainage, there appear to be opportunities for additional reductions through management practices that enhance selenium retention in source soils. Recent research for example, suggests that organic matter amendments may enhance reduction, retention, and volatilization of selenium (Darcheville et al., 2008; Dhillon et al., 2010). Furthermore, improved understanding of the reactive transport of selenium in surface soils may yield additional approaches to reduce agricultural selenium emissions.

My second and third chapter showed that aggregate scale (mm-cm) heterogeneity in microbial selenium reduction arises in simple, initially homogenous model systems and that the reactive transport of selenium needs to be resolved on the aggregate scale to accurately represent the reality of structured soils. Experimentally, this was evidenced by observed selenium reduction under conditions that are unfavorable (oxic) in bulk and by measured increases in the concentrations of reduced selenium towards the core of aggregates. While reduction rates at the aggregate scale were shown to depend on the same controlling factors that have been found to be important in bulk (i.e. aeration conditions, reactant concentrations, etc.), a simple bulk model, ignoring intra-aggregate concentration gradients, misrepresents aggregate scale dynamics of selenium reduction under oxic conditions. In addition, the experiments showed that metabolic differences (enzyme kinetics) between different selenium reducing bacteria are reflected at the aggregate scale. Mathematical modeling revealed that the coupling of microbial reactions and slow diffusive transport at the interior of aggregates, leads to the accumulation of reduced selenium at the core of aggregates. A reactive transport model which accounted for this processes, accurately reproduced experimental results and through a logical extension of this mechanism, the retention of reduced selenium is predicted to scale with aggregate size. Specifically, the reactive transport model showed that selenite and indirectly also elemental selenium accumulate inside aggregates by virtue of diffusive mass transfer limitations that are more pronounced in larger aggregates. Additionally, there are important interactive effects between aggregate size, aeration condition, and organic carbon concentrations, since in the presence of oxygen, organic carbon concentrations increase the impact of aggregate size on reduced selenium concentrations.

These aggregate-scale results point to general reactive transport mechanisms that may lead a soil with a larger mean aggregate size to retain more selenium. These insights could be used in the development of engineered dual porosity flow-through treatment systems. Biological treatment systems to remove selenium from agricultural drainage water are currently being tested at the pilot scale and may find use in areas where selenium concentrations and agricultural drainage loads are exceptionally high (Presser and Schwartzbach, 2008). Based on our results, a dual porosity approach may yield improvements over traditional bioreactors. Regarding natural

systems, field studies investigating the effect of aggregate size on selenium retention are warranted in the search for new management strategies to reduce selenium export from agricultural soils. If the effect proves relevant at the field scale, this would have implications for the management of irrigated seleniferous soils, since the fraction of macro-aggregates (>0.25 mm in diameter) in a soil is sensitive to agricultural management on time scales of 2 years or less (Degens, 1997). Both conservation tillage (Angers et al., 1993; Carter, 1992) and the application of manure (Whalen et al., 2003) can significantly increase the mean aggregate size of a soil in a matter of years. The beneficial effects of soil aggregation for plant growth have long been established (Dexter, 1988). Conservation tillage and organic amendments may thus prove to be attractive management techniques in agricultural regions prone to irrigation-induced selenium contamination, such as California's Central Valley. At the same time, to enable effective management, greater clarity is needed on the regulatory targets for selenium loads in aquatic ecosystems that are on the receiving end of agricultural contamination.

The site-specific regulation currently under development for the San Francisco Bay and Delta represents an appropriate and timely update to federal selenium water quality criteria, which have proven inadequate in light of scientific findings over the last two decades. In this context, scientists and resource managers should think ahead about the needs that will arise as the approach is expanded to other sites of concern with respect to selenium contamination. California's 303(d) list of impaired waters currently includes more than 66 water bodies polluted by selenium of which the largest is the Salton Sea. Like the Kesterson Reservoir in the 1980s, the Salton Sea has long been the receiving body of seleniferous irrigation drainage (May et al., 2007). Whereas the Salton Sea is an obvious target for the expansion of the site-specific regulatory approach, an appropriate site-specific regulatory model of this shallow lake ecosystem may need to include an explicit representation of the sedimentary selenium pool, which is not part of the current approach.

The diagenetic model presented in my final chapter describes the mechanics of selenium incorporation in Salton Sea sediment and illustrates the main factors driving near-surface sediment selenium concentrations. Sedimentation rates and bioturbation were shown to have a large potential impact on near-surface selenium concentrations that is difficult to constrain based on the rough current estimates of these rates for the Salton Sea. This model could be used to provide first-order estimates of local sediment selenium concentrations based on knowledge of the variation in sedimentation rates across the Salton Sea or in similar environments with sufficient available data. While additional research is necessary to constrain the uncertainty ranges of key parameters, this may yield a low-cost alternative to extended field sampling and monitoring campaigns. To preserve essential habitat at the Salton Sea swift interventions are necessary. Current conservation plans are driven mostly by the threat of increasing salinity, rather than concerns of selenium contamination. However, without an improved understanding of the dynamic transfer between the lake's pools of selenium – of which the sediment is the largest – such interventions may backfire: Habitats preserved from a salinity standpoint may still poison their inhabitants with excess selenium from their sediments.

Agricultural selenium contamination is a difficult subject, because the non-point soil sources of selenium are separated in time and space from the locations at which site-specific ecological effects develop. From a scientific perspective, this separation plays out across differences in interactions between biogeochemistry and ecology, as well as spatial and temporal scales. Due to differences in ecological setting, microbial selenium reduction, which may reduce

selenium emissions form a soil, may also concentrate selenium in the bioavailable surface sediment of an aquatic environment. Across spatial scales, the aggregate-scale heterogeneity controlling the retention of selenium within soils may provide ways to manage regional heterogeneity in soil selenium concentrations due to geology. Across temporal scales, the microbial reduction rates that equilibrate in a matter of days with ambient dissolved selenium concentrations and diffusive transport, may lead to sedimentary selenium profiles that are fundamentally shaped by sedimentation and bioturbation operating over decades. Conversely, from a policy and management perspective, the separation between selenium sources and contaminated areas plays out across differences in intended land use and the choice between pollution prevention and clean-up. The agricultural lands that produce seleniferous drainage are used for the production of food, while the aquatic environments that receive it are to be preserved as habitat for fish and waterfowl. Preserving sensitive habitat while meeting agricultural drainage needs and maintaining productivity is a difficult challenge. Sustainable solutions will only be found if we continue to improve our mechanistic understanding of selenium cycling and bridge the gaps between ecosystems, scales, and disciplines.

References

Angers, D.A., N. Samson, and A. Legere. 1993. Early changes in water-stable agregation induced by rotation and tillage in a soil under barley production. Canadian Journal of Soil Science 73:51-59.

Carter, M.R. 1992. Influence of reduced tillage systems on organic matter, microbial biomass, macro-aggregate distribution and structural stability of the surface soil in a humid climate. Soil and Tillage Research 23:361-372.

Darcheville, O., L. Fevrier, F.Z. Haichar, O. Berge, A. Martin-Garin, and P. Renault. 2008. Aqueous, solid and gaseous partitioning of selenium in an oxic sandy soil under different microbiological states. Journal of Environmental Radioactivity 99:981-992.

Degens, B.P. 1997. Macro-aggregation of soils by biological bonding and binding mechanisms and the factors affecting these: A review. Australian Journal of Soil Research 35:431-459.

Dexter, A.R. 1988. Advances in characterization of soil structure. Soil and Tillage Research 11:199-238.

Dhillon, K.S., S.K. Dhillon, and R. Dogra. 2010. Selenium accumulation by forage and grain crops and volatilization from seleniferous soils amended with different organic materials. Chemosphere 78:548–556.

Lemly, A.D. 2004. Aquatic selenium pollution is a global environmental safety issue. Ecotoxicology and Environmental Safety 59:44-56.

May, T.W., M.J. Walther, and W.G. Brumbaugh. 2007. Selenium concentrations in irrigation drain inflows to the Salton Sea, California, October 2006 and January 2007. U.S. Geological Survey.

Presser, T.S., and S.E. Schwartzbach. 2008. Technical analysis of in-valley drainage management strategies for the western San Joaquin Valley, California *In* US.DOI, (ed.), Vol. Open-File Report 2008-1210. U.S. Geological Survey, Reston, Virginia.

Whalen, J.K., Q.C. Hu, and A.G. Liu. 2003. Compost applications increase water-stable aggregates in conventional and no-tillage systems. Soil Science Society of America Journal 67:1842-1847.